Dynamic Adaptation of Brain Networks from Rest to Task and Application to Stroke Research

A Thesis

Submitted to the Faculty

of

Drexel University

by

Lin Cheng

in partial fulfillment of the

requirements for the degree

of

Doctor of Philosophy

August 2017

Acknowledgement

First and foremost I want to thank my advisor Dr. Shanbao Tong. It has been an honor to be his Ph.D. student. He has taught me, both consciously and unconsciously, how good research is done. I appreciate all his contributions of time, ideas, and funding to make my Ph.D. experience productive and stimulating. The joy and enthusiasm he has for his research was contagious and motivational for me, even during tough time in the Ph.D. pursuit. I am also thankful for the example he has provided as a successful scientist and professor.

I would like to deeply thank my co-advisor in Drexel University Dr. Hasan Ayaz. I have spent two joyful and excellent years in Drexel University, which would be impossible without his help and support. His vision in combining engineering and medicine has taught me how to be a good researcher in biomedical engineering.

I am grateful to Dr. Junfeng Sun, the mentor of my academic life. He introduced me to the world of neuroimaging. Without his help, it would be impossible for me to complete the thesis. His diligence showed me that nothing achieved without hard work.

Thanks are due also to Dr. Banu Onaral who made the dual-Ph.D. program possible, and to Dr. Yao Li, Dr. Xiaoli Guo, Dr. Jijun Wang, Dr. Guo-Yuan Yang who have helped me a lot in the Ph.D. pursuit.

In addition, thanks go to friends in neural engineering lab, Dr. Peng Miao, Dr. Minheng Li, Dr. Xiangfei Hong, Dr. Hongyang Lu, Qi Liu, Hangdao Li, and etc. They made my seven years in neural engineering lab joyful and colorful.

Last but not the least, I would like to thank my family for all their love and encouragement. For my parents who raised me with a love of science and supported me in all my pursuits. And most of all for my loving, supportive, encouraging, and patient wife Yifan Xie whose faithful support during the final stages of this Ph.D. is also appreciated. Thank you.

Table of Contents

List of Tables

List of Figures

Abstract

Dynamic Adaptation of Brain Networks from Rest to Task and Application to Stroke Research
Lin Cheng
Hasan Ayaz Supervisor, PhD
Shanbao Tong Supervisor, PhD

Examining how motor task modulates brain activity plays a critical role of understanding how cerebral motor system works and could further be applied in the research of motor disability due to neurological diseases. Recent advances in neuroimaging have resulted in numerous studies focusing on motor-induced modulation of brain activity and most widely used strategy of these studies was identifying activated brain regions during motor task through event-related/block-design experiment paradigms. Despite progress obtained, motor-related activation analysis mainly focused on modulation of brain activities for individual brain regions. However, human brain is known to be an integrated network, and the adaptation of brain in response to motor task could be reflected by the modulation of brain networks. Thus, investigating the spatiotemporal modulation of task-state brain networks during motor task would provide system-level information regarding the underlying adaptation of cerebral motor system in response to the motor task and could be further applied in the research of motor disability due to neurological diseases.

Although the task-state functional connectivity (FC) and networks have been examined by previous studies, there are still several aspects needed to be explored: (1) Previous task-state FC studies were mainly based on functional magnetic resonance imaging (fMRI) and potential of applying functional near-infrared spectroscopy (fNIRS), which is a promising complementary modality to fMRI because of its low cost and relatively high temporal resolution (10 Hz in sampling rate compared with less than 1Hz in sampling rate for fMRI), in task-state FC studies should be explored. (2) In the fMRI studies, the task-state brain network was mainly investigated from the perspective of static FC, which focuses on the spatial pattern of the task-state brain networks. However, brain activities and cognitive processes are known to be dynamic and adaptive and the newly emerging dynamic FC analysis could further provide temporal patterns of the task-state brain networks. Thus, the spatiotemporal pattern of task-state brain network during motor task is still needed to be investigated by dynamic FC analysis based on fMRI; (3) Task-state brain network analysis has not been applied in the research of stroke, and the relationship between task-state brain network and stroke recovery has not been investigated; Therefore, in this thesis, we aim to investigate the task-state brain networks during motor task using both static and dynamic FC analysis based on fNIRS and fMRI to reveal the motor task-

specific spatiotemporal changes of brain networks compared with resting conditions, and further applied the task-state brain network analysis in the research of stroke recovery

In this thesis, fMRI and fNIRS were employed to record the brain hemodynamic signals, and static FC and dynamic FC were used to investigate spatiotemporal pattern of task-state brain network during motor task. In addition, the fMRI data of stroke patients were recorded at four time points post stroke, and the reorganization of task-state brain network as well as its relationship to stroke recovery were examined. Specific results are described as follow:

(1) Through static FC analysis of fNIRS during rest and motor preparation, increased FC were identified during motor preparation, especially the FC connecting right dorsolateral prefrontal cortex (DLPFC) with contralateral primary somatosensory cortex (S1) and primary motor cortex (M1) as well as the FC connecting contralateral S1 with ipsilateral S1 and M1. Channels located in sensorimotor networks and right DLPFC were also found activated during motor preparation. Our findings demonstrated that the sensorimotor network was interacting with high-level cognitive brain network to maintain the motor preparation state.

(2) Through dynamic FC analysis of fNIRS during rest and motor execution, increased variability of FC connecting contralateral premotor and supplementary motor cortex (PMSMC) and M1 was identified, and the nodal strength variability of these two brain regions were also increased during motor execution. Our findings demonstrated that contralateral M1 and PMSMC were interacting with each other actively and dynamically to facilitate the fist opening and closing.

(3) Through dynamic FC analysis on fMRI data, two principal FC states during rest and one principal FC state during motor task were identified. The 1st principal FC state in rest was similar to that in task, which likely represented intrinsic network architecture and validated the broadly similar spatial patterns between rest and task. However, the presence of a 2nd principal FC state with increased FC between default-mode network (DMN) and motor network (MN) in rest with shorter “dwell time” could imply the transient functional relationship between DMN and MN to establish the “default mode” for motor system. In addition, the more frequent shifting between two principal FC states in rest indicated that the brain networks dynamically maintained the “default mode” for the motor system. In contrast, during task, the presence of a single principal FC state and reduced FC variability implied a more temporally stable connectivity, validating the distinct temporal patterns between rest and task. Our findings suggested that the principal states could show a link between the rest and task states, and verified our hypothesis on overall spatial similarity but distinct temporal patterns of dynamic brain networks between rest and task states.

(4) Task-state motor network was applied in the research of motor disability due to stroke and topological reorganization of task-state motor network was identified during sub-acute phase post stroke. In addition, for the first time, our study found the topological configuration of task-state motor network at the early recovery stage were capable of predicting the motor function restoration during sub-acute phase. In general, the findings demonstrated the reorganization and potential prognostic value of task-state brain network after stroke, which provided new insights into understanding the brain reorganization and stroke rehabilitation.

In summary, this thesis used two neuroimaging modalities (fMRI and fNIRS) to investigate how brain networks, especially the motor network and high-level cognitive network, would reorganize spatiotemporally from resting-state to motor tasks through both static and dynamic FC analysis, and further applied the task-state brain network analysis in the research of motor disability due to stroke. Our findings revealed the underlying spatiotemporal adaptation of brain networks in response to motor task and demonstrated the potential clinical prognostic value of task-state motor network during stroke recovery. The novelties of this thesis are as follow: (1) dynamic FC was innovatively applied in revealing the motor task-specific spatiotemporal changes of brain networks compared with resting conditions; (2) task-state motor network was applied in the research of stroke recovery; (3) static and dynamic FC analysis were innovatively applied in fNIRS data.

KEY WORDS: Cerebral motor system, fMRI, fNIRS, functional connectivity, functional brain networks, stroke.

Chapter 1: Introduction

1.1 Background and motivation

Cerebral motor system has been one of the most important topics in neuroscience for decades. The study of cerebral motor system began in the late 19th century and earliest experiments were performed on animals, such as dogs [1] and nonhuman primates [2]. By electrical stimulation on patients during surgery for the removal of tumors and epileptic foci, studies on human cerebral motor system were also performed around mid-20th century [3, 4]. However, the early studies mainly focused on the mapping of cerebral motor system and it was difficult to research how cerebral motor system worked at that time.

Recent advances in neuroimaging techniques, such as functional magnetic resonance imaging (fMRI), positron emission tomography (PET), and functional near-infrared spectroscopy (fNIRS), have benefitted studies of cerebral motor system tremendously. Most widely used approach of these studies was identifying cerebral activation during motor tasks through event-related/block-design experiment paradigms. Activations were identified in several brain regions during motor tasks, which contributed to the understanding of how cerebral motor system works during motor tasks. For example, increased activity in both ipsilateral and contralateral primary sensorimotor cortex has been identified during finger movements through PET [5] and fMRI [6-9] (Please see Fig. 1.1 for example). Local increases of the oxy-hemoglobin concentration (HbO_2) and decreases of the deoxy-hemoglobin concentration (Hb) in the motor cortex during motor stimulation have also been demonstrated in several fNIRS studies [10-13]. In addition to the sensorimotor cortex, several adjacent cortical regions, such as supplementary motor area, premotor cortex, posterior parietal cortex, and the secondary somatosensory cortex, also showed increased activities induced by motor tasks [14, 15].

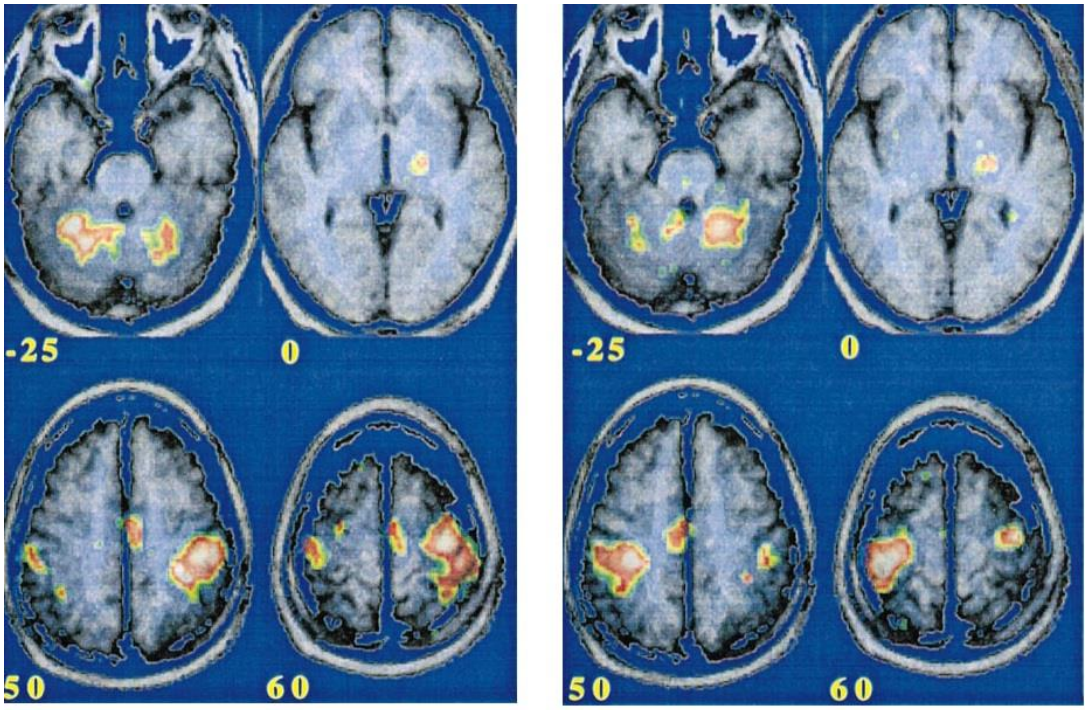

Figure 1.1 PET/MRI superimposition. PET data for t-values during right finger movements and left finger movements displayed on a color scale (white > 10, red > 5.41, yellow > 4.79, and green > 3.50) superimposed onto the averaged transformed MRI data. This figure is edited based on the figures adopted from [5] with courtesy.

In addition to the study of cerebral motor system, activation analysis was also applied in the research of stroke as well as the treatments of stroke. fMRI data of stroke patients showed hyper-activation in contralesional motor regions and secondary motor regions which were not normally involved in motor tasks for health subjects [16-20]. Based on activation analysis, previous studies found that the contralesional activation was also related to the severity of the motor function impairment. For example, patients with severe motor deficits exhibited higher activation in contralesional primary motor and premotor area, which was not found in the patients with mild motor deficits [21] (Fig. 1.2). Activation analysis was also applied in the longitudinal studies of stroke recovery, which found that the initial hyper-activation in contralesional and secondary motor regions gradually diminished and shifted to ipsilesional sensorimotor areas [16, 22, 23].

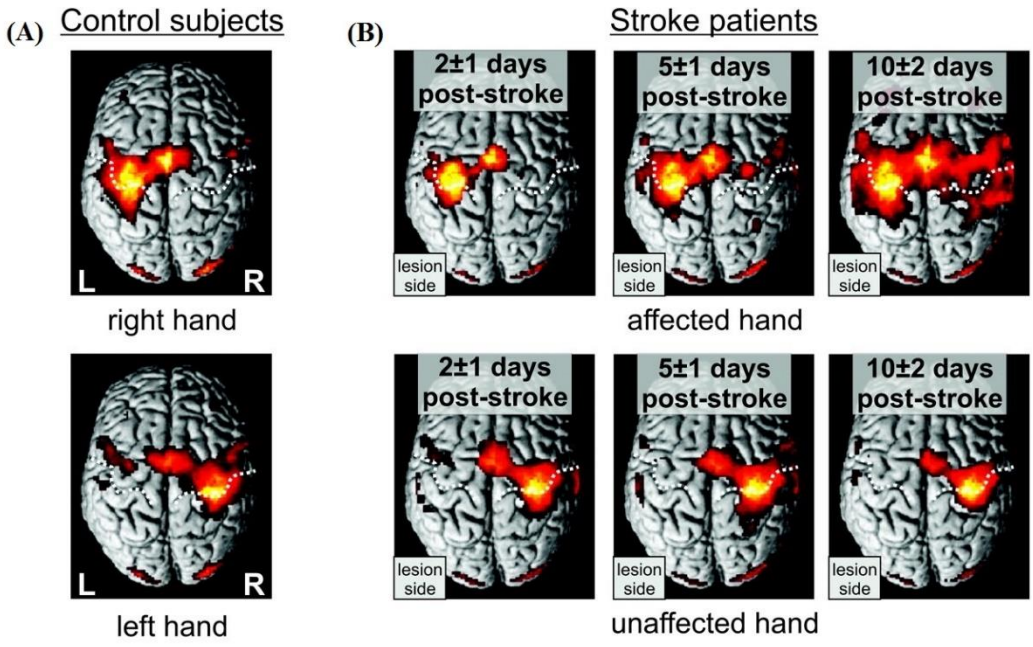

Figure 1.2 BOLD signal changes for hand movements of (A) healthy subjects and (B) stroke patients. The central sulcus is marked with dashed lines. This figure is adopted from [24] with courtesy.

In spite of the progresses obtained through activation analysis, it generally focused on illustrating cerebral regions of activation under motor task, rather than characterizing the integrated cerebral motor system involved in the motor tasks. Brain has been demonstrated to consist of discrete, large-scale networks with widely spaced nodal regions, which have highly correlated activity across time and such correlation was interpreted as functional connectivity (FC) [25-29]. FC estimated from resting state (i.e., no task engagement) is dominating this field [30-32]. The first resting-state fMRI study demonstrated that BOLD time courses of left sensorimotor cortex were correlated with the BOLD time courses of right sensorimotor cortex under resting condition [33]. Recently, the most studied resting-state network is the default-mode network (DMN), which is consisted of the precuneus/posterior cingulate, the lateral parietal area and mesial prefrontal cortex, and has been reported to be actively engaged under resting conditions but relatively de-activated during tasks [34]. Because previous studies have reported that resting-state FC is able to indicate the intrinsic brain network architecture, the resting-state FC, especially the activity of DMN, has been widely used in a lot of research studies [35] to reveal the functional organization of a variety of cerebral functional systems [36] and the modulation of brain organization induced by neurological/psychological disorders [37]. For example, with respect to the application of resting-state FC/brain networks in stroke research, previous studies found significant

alteration of inter-hemispheric FC between the bilateral motor areas [38], and modulated topological configuration of motor network based on resting-state fMRI post stroke [39] (see Fig. 1.3 for example).

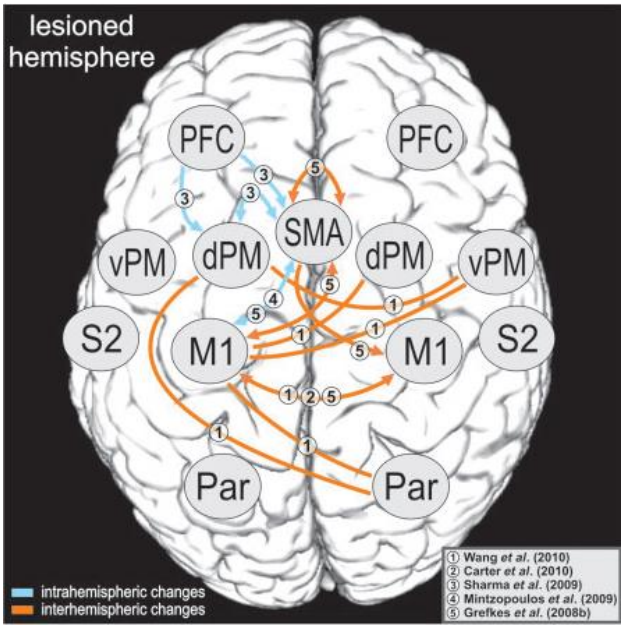

Figure 1.3 Synopsis of changed FC between brain regions post stroke. Among these brain regions, a number of intra-hemispheric (blue) and inter-hemispheric (orange) FC are identified to be changed in stroke patients. Numbers on FC indicate the publication in which a change in FC is reported. Arrow heads indicate the available directional information of the FC. This figure is adopted from [40] with courtesy.

Nevertheless, since there is no task engagement under resting conditions, resting-state FC is not capable of revealing the task-specific changes of FC/brain networks, which play critical roles in understanding how the brain achieve different functions. Therefore, task-state FC is a promising approach to reveal the task-specific changes of brain organization and has been used to investigate how task loads modulate functional brain organization to further understand the working mechanisms of a variety of cerebral functional systems [41-44]. For example, in working memory system, increasingly negative correlations emerged in the dorsal region of the posterior cingulate cortex during steady-state N-back task [45].In addition, regions engaged in auditory [46] and visual [47, 48] functions also demonstrated modulated FC during corresponding tasks. For cerebral motor system, motor-related network was

reported to be modulated during voluntary movements based on fMRI [41] and MEG [49]. In addition, the FC strength was related with the rate of finger tapping in key regions of the motor network [50].

However, previous studies on task-state FC/brain network, especially for the motor tasks, are relatively rare and not very comprehensive. Most of the studies only adopted conventional static FC analysis, which focuses on the spatial pattern but ignores the temporal patterns of task-state brain networks. In addition, most of the studies are performed based on fMRI, and fNIRS, which also measures the hemodynamic signals but with lower cost, has rarely been applied in the task-state FC/brain network studies. Finally, though task-state FC/brain network might provide extra information about underlying mechanism of neural response under specific task state, no studies have tried to investigate it in the research of stroke to the best of our knowledge.

Therefore, based on above considerations, the purpose of this thesis is to investigate the task-state brain networks under motor tasks using both static and dynamic FC analysis based on fNIRS and fMRI to reveal the motor task-specific spatiotemporal changes of brain networks compared with resting conditions, and further applied the task-state brain network analysis in the research of stroke recovery.

1.2 Approach and contribution

In order to achieve the purpose of this thesis, two neuroimaging modalities, i.e., fMRI and fNIRS, are adopted to record the brain hemodynamic signals. In addition, static FC analysis, static network analysis based on graph theory, and dynamic analysis are employed to investigate the task-state brain networks under motor task. Therefore, in this section, introduction of above approaches are provided. Furthermore, contributions of this thesis is also highlighted in this section.

1.2.1 Neuroimaging techniques

1.2.1.1 Principles of fMRI

fMRI is a functional neuroimaging procedure using MRI technique which measures brain activity by detecting hemodynamic changes associated with blood flow [51]. The most widely used form of fMRI is blood-oxygen-level dependent (BOLD) contrast, which was discovered by Ogawa and colleagues [52].

In normal clinical application, the MRI signal comes mostly from the protons of water in tissue, which depends on the density of these protons. Under the large static magnetic field produced by the MRI magnet, the proton magnetic moments is parallel to static magnetic field. After applying a pulse of radiofrequency magnetic field, the alignment of the proton magnetic moments is changed and then recovers to the original alignment in several tenths

of a second to seconds. During the recovery, the magnetization generated in the direction transverse to the static magnetic field induces a signal in a coil surrounding the scanned object. The recovery rate is described by relaxation time T1, which depends on the relevant water molecules contained in different tissues. In addition, another type of relaxation is also able to distinguish tissue types, such as the time constants associated with loss of signal once the magnetization has been sampled (T2 and T2*).

For BOLD-fMRI, the BOLD-contrast is based on the fact that paramagnetic deoxy-hemoglobin, comparing with diamagnetic oxy-hemoglobin, possesses a strong magnetic moment. Therefore, the local field variations in and around blood vessels generated by interaction of the bulk magnetization of deoxygenated blood with the external field lead to destructive interference from signal within the tissue voxel, resulting in shorter T2* relaxation time [52, 53]. During activated neuronal activity, increased energy consumption induced by neuronal activity results in increased blood flow. However, blood flow actually increases to a greater extent than what is necessary for simply providing oxygen and glucose for the increased energy consumption. As a result, oxygen extraction decreases with greater neuronal activity and the T2* becomes longer and the MRI signal intensity increases relative to the baseline state [54] (Fig. 1.4).

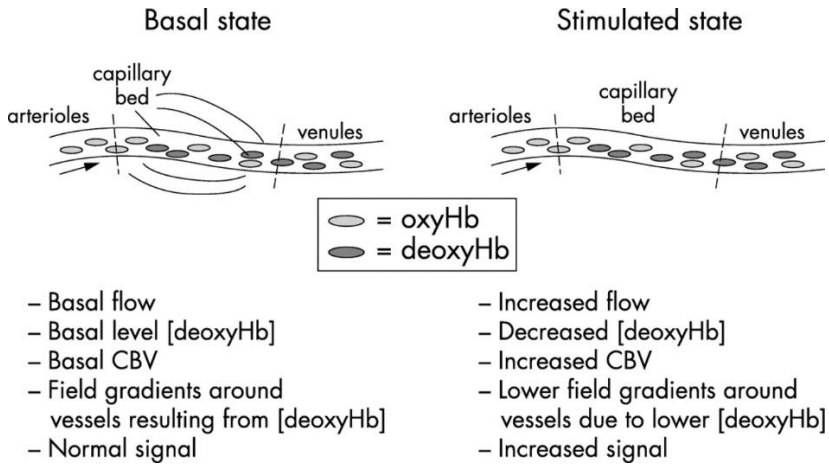

Figure 1.4 Schematic diagram showing the hemodynamic variables that change during neuronal activity. In the basal state, deoxy-hemoglobin in the capillaries and venules causes microscopic field gradients to the established field around the blood vessels. This in turn leads to a decreased signal in a gradient echo magnetic resonance imaging sequence. In the activated state, there is a significant increase in blood flow, but only a modest increase in oxygen consumption. This results in a lower deoxy-hemoglobin

concentration in the capillaries and venules and thus results in a reduction in the microscopic field gradients and an increase in the signal intensity. CBV = cerebral blood volume; deoxyHb = deoxy-hemoglobin. This figure is edited based on the figure adopted from [54] with courtesy.

1.2.1.2 Applications of fMRI

Since fMRI is entirely non-invasive and possesses excellent spatial resolution and quite good temporal resolution, it has had a major impact in cognitive neuroscience and played a growing role in translational medicine and clinical practice [55].

In the past two decades, fMRI covers all domains of cognitive neuroscience. All kinds of fMRI-based experiments have been designed to investigate how brain works to realize different cognitive functions, such as motor (Fig. 1.5) [56-58], auditory [59-61], visual [62-64], memory [65, 66], learning [67, 68] and etc.

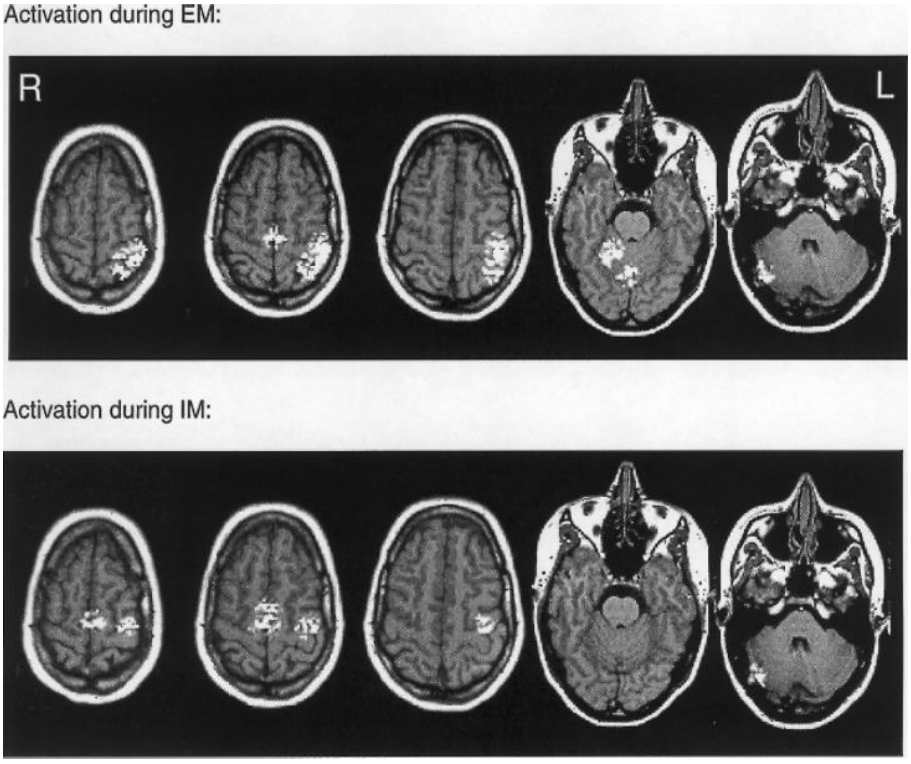

Figure 1.5 Top row: Activation in one subject during executed movements (EM) of the right hand in five slices. Bottom row: Activation of the same subject during imagined movements of the right hand for the same slices. This figure is edited based on the figure adopted from [56] with courtesy.

Though the application of fMRI in clinical practice is still developing, it has already started to make some clinically meaningful contributions to clinical neuroimaging, such as neurosurgical planning [69, 70], the research of clinical syndromes [71] and the development of new therapies [72, 73]. Especially for the research of clinical syndromes, fMRI is adopted to functionally characterize both neurophysiological and psychological disorders, such as schizophrenia [74, 75], stroke (Fig. 1.3) [24], Parkinson's disease [76], and Alzheimer's disease [77], and investigate the underlying pathological mechanism from a systemic view.

1.2.1.3 Principles of fNIRS

Like fMRI, fNIRS is to capture the hemodynamic change induced by neuronal activity. During activated neuronal activity, increased energy consumption induced by neuronal activity results in increased blood flow. However, blood flow actually increases to a greater extent than what is necessary for simply providing oxygen and glucose for the increased energy consumption. As a result, oxygen extraction decreases with greater neuronal activity. Since oxy-hemoglobin and deoxy-hemoglobin possess characteristic optical properties in the visual and near-infrared light range, the change in concentrations of these molecules can be captured using optical techniques [78]. Under the near-infrared light range between 700-900 nm, the major component of most tissue, water, absorbs very little energy, while the oxy-hemoglobin and deoxy-hemoglobin absorb a considerable amount of energy at these wavelengths (Fig. 1.6) [79]. Therefore, through measuring absorption changes at two wavelengths (one for oxy-hemoglobin and the other for deoxy-hemoglobin) based on the modified Beer-Lambert law [80], changes in the relative concentrations of these two hemoglobin can be calculated, which can be further used to assess brain activity in the specific region [81-83].

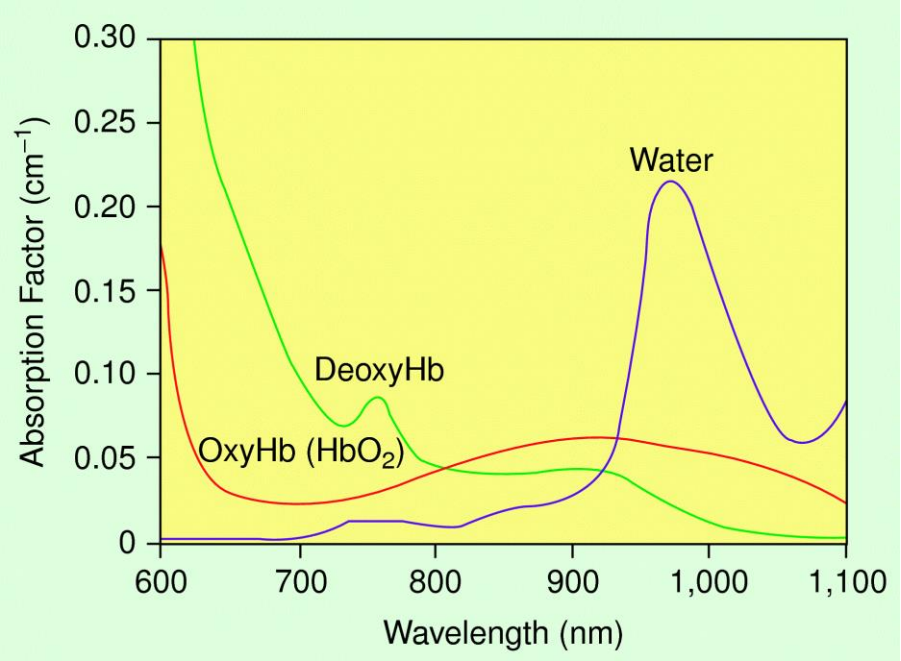

Figure 1.6 Absorption characteristics of oxy-hemoglobin, deoxy-hemoglobin, and water according to the light wavelength. This figure is adopted from [79] with courtesy.

1.2.1.4 Applications of fNIRS

As fNIRS is a safe, portable and very affordable neuroimaging modality, it has been applied in different fields. For basic research, fNIRS has been applied in brain computer interface [84], neuroergonomics [85], pain research [86], and sleep research [87]. With respect to cognitive neuroscience, applications of fNIRS have been reported in the research of attention [88], emotion [89], language [90], memory [91], and etc. In addition, fNIRS has also been adopted to investigate neurological and psychological disorders, such as Alzheimer's disease [92], stroke [93], schizophrenia [94], and etc.

1.2.2 Static FC analysis

In order to understand how multiple brain regions interact with one another, FC was introduced in the functional neuroimaging. FC represents a novel approach, which is capable of examining the neural activities of brain regions that are functionally connected no matter whether they are anatomically distant [25]. FC is usually defined as the synchrony of neural activities among brain regions and can be studied during both active tasks and resting state [35].

Since the conventional FC analysis is based on the whole time courses of signal under the assumption that the brain network would be relatively stable during the recording, it is also named static FC analysis [95].

Several analysis methods are used to estimate the static FC. The most widely used methods are seed-based analysis, region-of-interest (ROI) based analysis, and independent component analysis (ICA). For seed-based analysis, the representative signal of a predefined seed is extracted and then its synchronies with other voxels are calculated to identify the regions which are significantly correlated with the seed [35]. The most commonly employed approach to estimate the synchrony is Pearson's correlation. Please see the Fig. 1.7 for the details of seed-based analysis [96]. Seed-based FC analysis has been employed in numerous studies, including cognitive neuroscience studies [97, 98] and studies of neurological and psychological disorders [99, 100]. With respect to the ROI-based analysis, it is similar with the seed-based analysis. The ROI-based analysis does not only predefine one seed, but predefine several ROIs and the synchrony is estimated between each pair of ROIs. Since the ROI-based analysis is able to construct a network among ROIs, it is commonly employed in brain network analysis [101, 102].

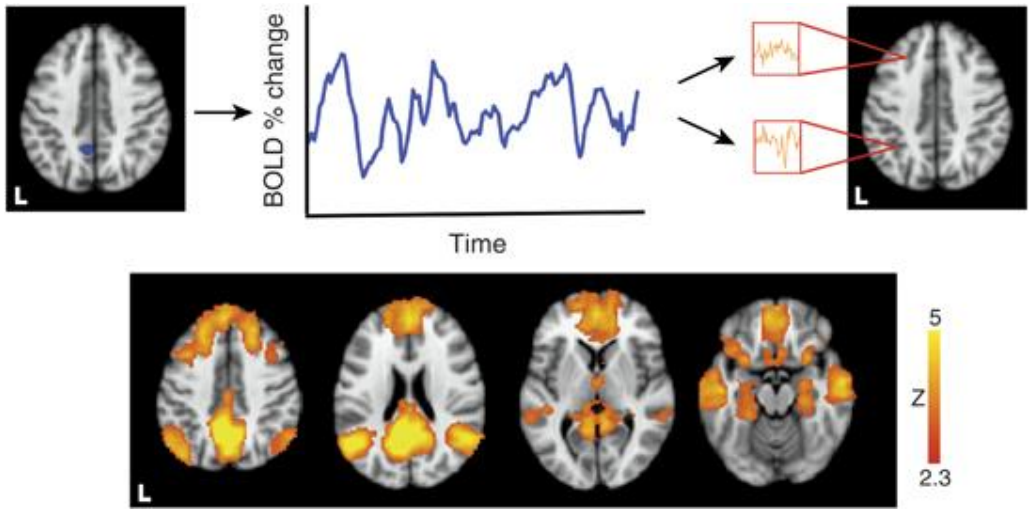

Figure 1.7 Illustration of seed-based FC analysis. The representative signal of a predefined seed is extracted and then its synchronies with other voxels are calculated, resulting in maps of co-activated brain regions. This figure is adopted from [96] with courtesy.

The seed-based analysis and ROI-based analysis are based on priori assumptions, which require predefinition of seed and ROIs. ICA, by contrast, is a statistical data-driven method without any priori assumptions and is able to

identify statistically independent components of the resting-state signals [103]. Since ICA is not employed in this thesis, details of this method is not provided here.

1.2.3 Static network analysis based on graph theory

In addition to static FC analysis, studying the brain's structural and functional system as networks would provide a powerful new way to investigate the physiological basis for information processing and mental representations [104, 105]. Through the graph theory, we are able to explore the functional brain networks by regarding the brain regions as nodes and FC among them as edges in a graph (Fig. 1.8) [106]. Based on graph theory and network science, methodological advances enable us to quantify the topological features of brain networks, such as small-worldness [107], modularity [108], hierarchy [109], and centrality [110]. These graph theoretical properties have already been applied in numerous studies of cognitive neuroscience [111], neurology [39], and psychiatry [112].

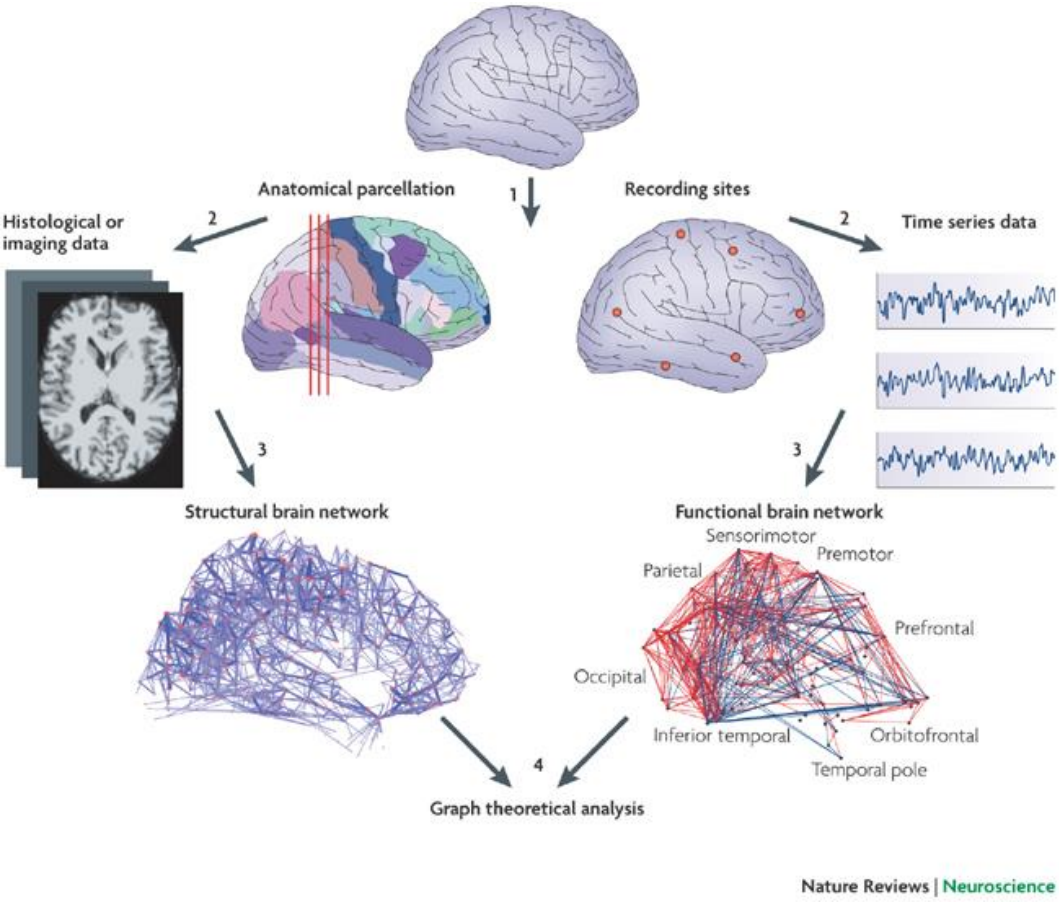

Figure 1.8 Schematic diagram of construction for structural brain network (left) and functional brain network (right). This figure is adopted from[106] with courtesy.

1.2.4 Dynamic FC analysis

Like we discussed above, conventional static FC analysis is most commonly based on a whole recording time course and represents an implicit assumption that the FC is relatively static over this period of time. However, this assumption may not be entirely justified as brain activities and cognitive processes are known to be dynamic and adaptive [113, 114], an observation that has been repeatedly confirmed by work focused on time-varying multivariate connectivity patterns [115] as well as work focused on time-frequency analysis methods [116]. As a result, several dynamic FC studies have appeared and focus on the dynamics in the FC among two or more brain regions [117, 118].

Among the rapidly increased dynamic FC studies, two methods are most commonly employed. The first one is to capture pairwise variations in inter-regional synchrony and the second one is to identify changing patterns of synchrony at a multivariate level. For the first method, the whole signal time courses are divided into several windows and the pairwise synchrony are estimated at each window. After that, the variability of the pairwise synchrony is estimated through calculating the temporal variance of the synchrony across windows and is named FC variability (FCV) [119]. FCV has been adopted by several studies to investigate the daydreaming [119], schizophrenia [120], and cognitive neuroscience [95]. The first method is relatively simple and straightforward, but it mainly focuses on the temporal patterns of dynamic FC.

With respect to the second method, the whole signal time courses are also divided into several windows and the brain networks are estimated at windows [121]. After that, a k-means clustering is performed on the correlation patterns of brain networks over windows to identify FC state matrices (Please see Fig. 1.9 for details) [122]. The second method is able to provide both spatial and temporal information of dynamic FC and has been applied in several fields, including basic cognitive neuroscience [122] and psychological disorder research [123].

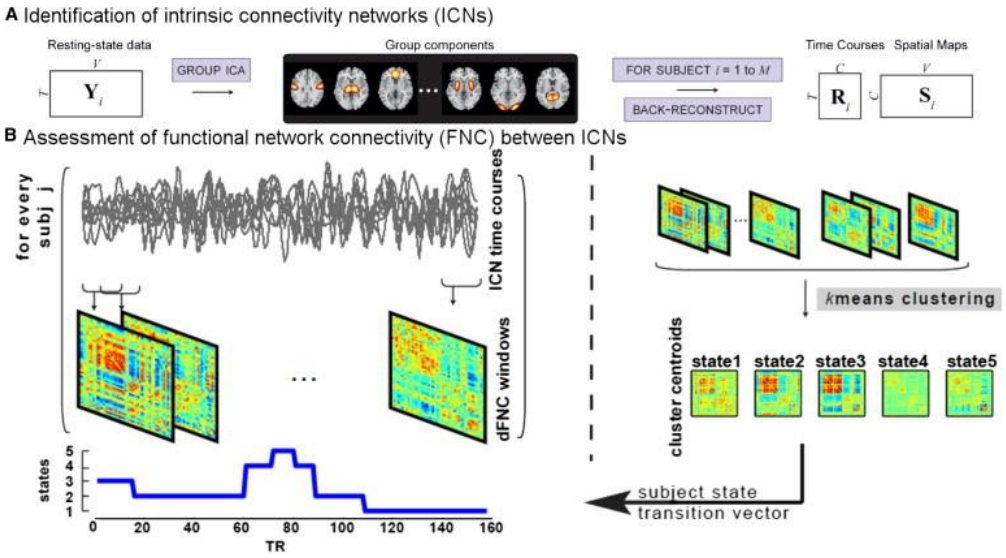

Figure 1.9. Demonstration of the approach to identify time-varying patterns of FC through ICA and k-means clustering method. This figure is adopted from [117] with courtesy.

1.2.5 Contributions

In this thesis, the research focus is the task-state brain networks under motor task. The purpose of this thesis is to investigate the task-state brain networks under motor tasks using both fMRI and fNIRS to reveal the motor task-specific spatiotemporal changes of brain networks compared with resting conditions, and further applied the task-state brain network analysis in the research of stroke recovery. fMRI and fNIRS are employed to record the brain hemodynamic signals, and static FC, dynamic FC and graph theory are used to investigate the task-state brain network. The contributions of this thesis are: 1) reveal the motor task-specific spatiotemporal changes of brain networks compared with resting conditions; 2) demonstrate the reorganization of task-state motor network and its potential clinical prognostic value during stroke recovery; 3) explore the potential of performing static and dynamic FC analysis based on fNIRS data.

1.3 Outline

In this section, an outline of the subsequent chapters is provided. In chapter 2 and chapter 3, the task-state brain networks are investigated during motor preparation and motor execution based on fNIRS using both static FC and dynamic FC analysis. In chapter 4, the focus is the spatiotemporal reorganization of dynamic task-state brain networks during motor execution and the dynamic FC analysis is employed to reveal spatial and temporal patterns

of FC based on fMRI data. In chapter 5, the task-state brain network analysis is applied in the investigation of stroke recovery. The reorganization and potential clinical prognostic value of task-state motor network during stroke recovery are examined. In chapter 6, the findings of this thesis is summarized and the conclusion is given.

Chapter 2: Reorganization of static task-state brain network during motor task based on fNIRS

2.1 Introduction

In the chapter 2 and chapter 3, the task-state brain networks were investigated during motor preparation and motor execution based on fNIRS using both static FC and dynamic FC analysis. In addition to investigating the task-state brain networks during motor tasks, exploring the potential of performing static FC and dynamic FC analysis was another critical purpose.

Unlike the explicit cognitive processes during rest and movement, the cognitive process during transition period between rest and movement, which usually corresponds to the preparation period preceding movement, is implicit [124]. Although there is no actual movement in the transition period, modulation of brain activity has been observed, such as the Readiness Potential recorded by scalp electrodes around 500 milliseconds before a movement [125-128]. However, detailed information of brain activities during the transition period, such as how brain regions interact with each other to establish the motor preparation through FC, is still a pending question [129]. Thorough understanding of it would help with the investigation of the adaptation of brain networks for upcoming movement, and would have implications for improving the precision and latency of anticipation-based brain-computer interfaces [130-132], for neuroergonomic research related to human system integration and automation [133, 134], and various neurorehabilitation approaches such as neurofeedback-based motor function rehabilitation [135, 136].

Several recent fMRI studies have utilized FC analysis to investigate brain dynamics during preparation of movement. Newton and colleagues found that correlations increased within the sensorimotor network during transition from rest to finger tapping [137]. In addition, Treserras and colleagues found that the DMN and sensorimotor network were functionally correlated through an interaction between the posterior cingulate cortex, and precuneus (PCC/Pcu) and the medial superior parietal cortex in the upper precuneus during transition period between resting and motor task state [129]. Also, a positive relationship between DMN and right sensorimotor cortex while a negative relationship of DMN with left sensorimotor cortex during transition period were also reported [137]. Other than the FC-based analysis, a transcranial magnetic stimulation (TMS)-based study found that the excitability of the motor cortex contralateral to the moving hand increased, whereas the excitability of the ipsilateral motor cortex decreased during transition period [138].

Although findings from these studies were encouraging, and fMRI recordings provided extensive detail of the spatial distribution and relationship of activations, the relatively short time length of transition period made the temporal resolution very critical for reliable FC analysis during the transition period. fNIRS, which measures hemodynamic response similar to fMRI but can provide much higher sampling rate, therefore is a good candidate for further follow-up studies for the investigation of the temporal dynamics of the brain network modulation during the transition period [139-141]. In addition, compared with fMRI, fNIRS is cost effective (close to zero run-time cost) and without any operation ambient sound which would help focusing on the task at hand, especially for the transition period [142, 143]. fNIRS has been applied to neuroergonomics, such as the examination of workload and training-related brain dynamics with human performance assessment [144, 145]. For FC analysis, fNIRS has emerged as a new tool that complements the fMRI-based FC analysis and also enable new applications because of its portable and wearable nature. For example of patients with brain-injured or intensive care patients in remote country or outdoors environments, or participant groups that cannot be easily transported to an fMRI facility maybe monitored with portable fNIRS. The reliability of fNIRS in FC analysis has already been demonstrated by several studies. One of the early pilot studies by White and colleagues demonstrated robust correlation maps of fNIRS-based FC in motor and visual cortices [146]. Another study investigated resting-state FC in bilateral sensorimotor and auditory cortices through fNIRS [147]. Mesquita and colleagues further used fNIRS to investigate the FC over the whole head during resting state and found strong correlations between two hemispheres for both sensorimotor and visual cortices [148]. Other than the seed-based FC analysis method [149] used in the above three studies, ICA-based FC analysis was also used in fNIRS and its feasibility was validated [150]. Furthermore, analysis of frequency-specific FC [151] and Granger causality [152] have also been reported on fNIRS. In addition, several studies have investigated the topological configuration of brain networks through fNIRS [153, 154].

In addition to the resting-state FC analysis, fNIRS can also be used to assess task-state FC. Relatively high temporal resolution capacity enables fNIRS to capture more information regarding the task modulation riding on the intrinsic brain networks through the task-state FC.

In this chapter, fNIRS was used to examine the static FC during the transition period between rest and hand movement. Given the relatively high temporal resolution of fNIRS, the fNIRS-based FC during transition period was expected to provide more information regarding adaptation of brain networks for the upcoming task. Understanding the fine detailed relationship of movement intention could be utilized to improve precision and latency of future intention-based brain-computer interface and neuroergonomics research in general.

2.2 Methods

2.2.1 Participants

Nineteen healthy right-handed volunteers (12 Males; Age: 20-30 years, 24.68±3.06 years) participated in this experiment. Subjects did not have any history of mental health, seizures, head injury, or neurological dysfunction (e.g. stroke or seizure). All subjects provided written informed consent and procedures were reviewed and approved by the Institutional Review Board of Drexel University.

2.2.2 Data acquisition

Neuroimaging data was collected by the 24-channel Hitachi ETG-4000 NIRS system (Hitachi Medical Co., Tokyo, Japan) at the Cognitive Neuroengineering and Quantitative Experimental Research Collaborative, Drexel University (www.drexel.edu/conquer/; Philadelphia, PA, USA). The absorptions of the near-infrared light at two wavelengths (695nm and 830mm) were measured with a sampling rate of 10 Hz and the changes of the oxygenated hemoglobin (oxy-Hb) and deoxygenated hemoglobin (deoxy-Hb) concentrations were calculated by the modified Beer-Lambert law [80] at each time point for each channel. Eighteen fiber probes (10 emitter probes and 8 detector probes) were placed on subjects' head using a custom-made cap (Fig. 2.1(A)) and the probes were arranged with Cz (according to the international 10/20 system) located directly in the center of the probes. The probes were connected to the recording device by flexible optical fiber bundles. As a result, 24 optical channels (12 for each hemisphere) were recorded (Fig. 2.1(C)). The positioning of the probe array was determined according to the international 10-20 system and referred to prominent anatomical landmarks such as the bilateral tragus, nasion and inion [140]. Also, based on the measured real coordinates of the probes, we used NIRS-SPM [155] to perform spatial registration and obtained the standard coordinates of probes and channels in MNI (Montreal Neurological Institute) space (Fig. 2.1(B) and (C)). According to the MNI coordinates of channels, four ROIs (i.e. Primary Motor Cortex, Premotor and Supplementary Motor Cortex, Primary Somatosensory Cortex and Dorsolateral Prefrontal Cortex; Abbrev. M1, PMSMC, S1 and DLPFC) were covered by the channels in each brain hemisphere (Fig. 2.1(C)).

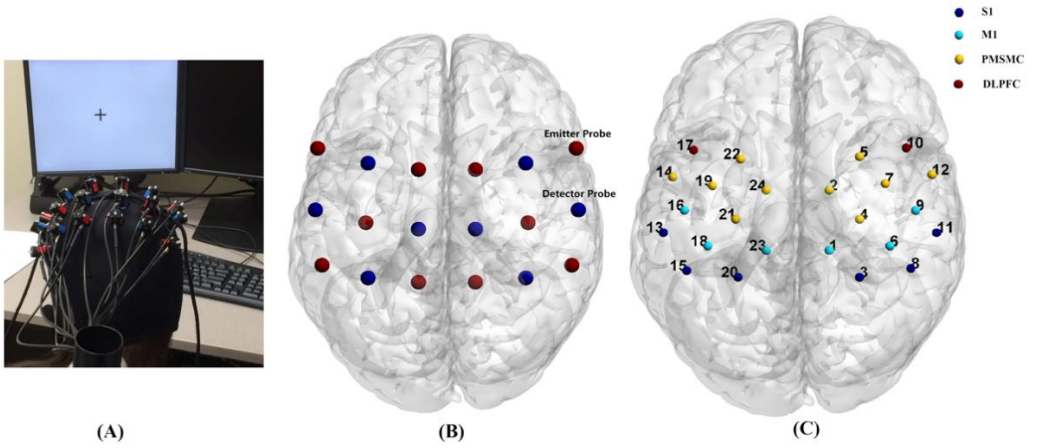

Figure 2.1. (A) Probes configuration and cap placement during the experiment. (B) Positions of the eighteen probes on standard brain template (MNI). (C) Positions of the twenty-four channels on standard brain template and the colors represent the region of interest (ROI) they locate in.

2.2.3 Experiment protocol

Experiment protocol was completed in a single sitting and had three main parts/sessions. The first session consisted of three blocks which were rest, left fist opening and closing (FOC) and right FOC. Each block lasted for 4 minutes. During the rest block, subjects were instructed to relax and refrain from any movement. After the rest block, subjects were cued to perform left FOC and right FOC with randomized order. During the FOC, "0" and "1" were displayed to pace subjects' movements. Subjects were instructed to open their fist when they saw "0" and close when they saw "1". The frequency was set as opening and closing once per second (Fig. 2.2(A)). There were six trials in session 2 and each trial consisted of three blocks which were rest, transition period and left/right FOC. Rest and FOC blocks were identical to the session 1 only with different length (30s in session 2). During transition periods which were between rest and FOC, subjects had already known which hand they were going to use in the coming FOC block through the cue displayed just after rest block, but they were instructed to get ready for the upcoming movement without any movement and waiting for another cue to start the FOC. When the starting cue was displayed, they started FOC as soon as possible. Therefore, the transition periods in session 2 were defined as preparation period preceding the externally-triggered movement [156]. We applied three different lengths of transition periods (5s, 15s and 30s) for both left FOC and right FOC (Fig. 2.2(B)). For session 3, only transition period was different from session 2. In session 3 (Fig. 2.2(C)), there was no cue for FOC start and subjects should decide when to start FOC by themselves which made these transition periods equivalent to preparation period preceding self-initialed movement

[156]. In order to make the analysis feasible, we told subjects neither to make the length of transition period too long (more than 30s) nor too short (less than 5s). There was also six trials in session 3 (three for left and three for right). During the experiment, subjects' immobility was visually checked and no excessive motion was found for any subjects.

2.2.4 Data preprocessing

Raw fNIRS data were band-pass filtered within 0.01 Hz to 0.1 Hz to remove the physiological noise such as respiration and cardiac activities, following previous studies [146, 150, 152, 153]. One of the participants' data were rejected due to low signal quality and artifacts. In addition, motion artifacts were marked by visual inspection (i.e., spikes and deformed burst with large changes of magnitude in less than 1s would be marked as motion artifacts) and confirmed with a variation of coefficient based algorithm using the suggested parameters in these studies [157, 158]. The Sliding-window Motion Artifact Rejection (SMAR) algorithm uses statistical filtering to automatically mark temporally localized artifacts on fNIRS signals and has been shown to be effective for various types of noises such as Burst and Gaussian [158]. We used oxy-Hb signal changes in the current analysis since previous findings showed that oxy-Hb was the most sensitive to locomotion-related activities [159-162].

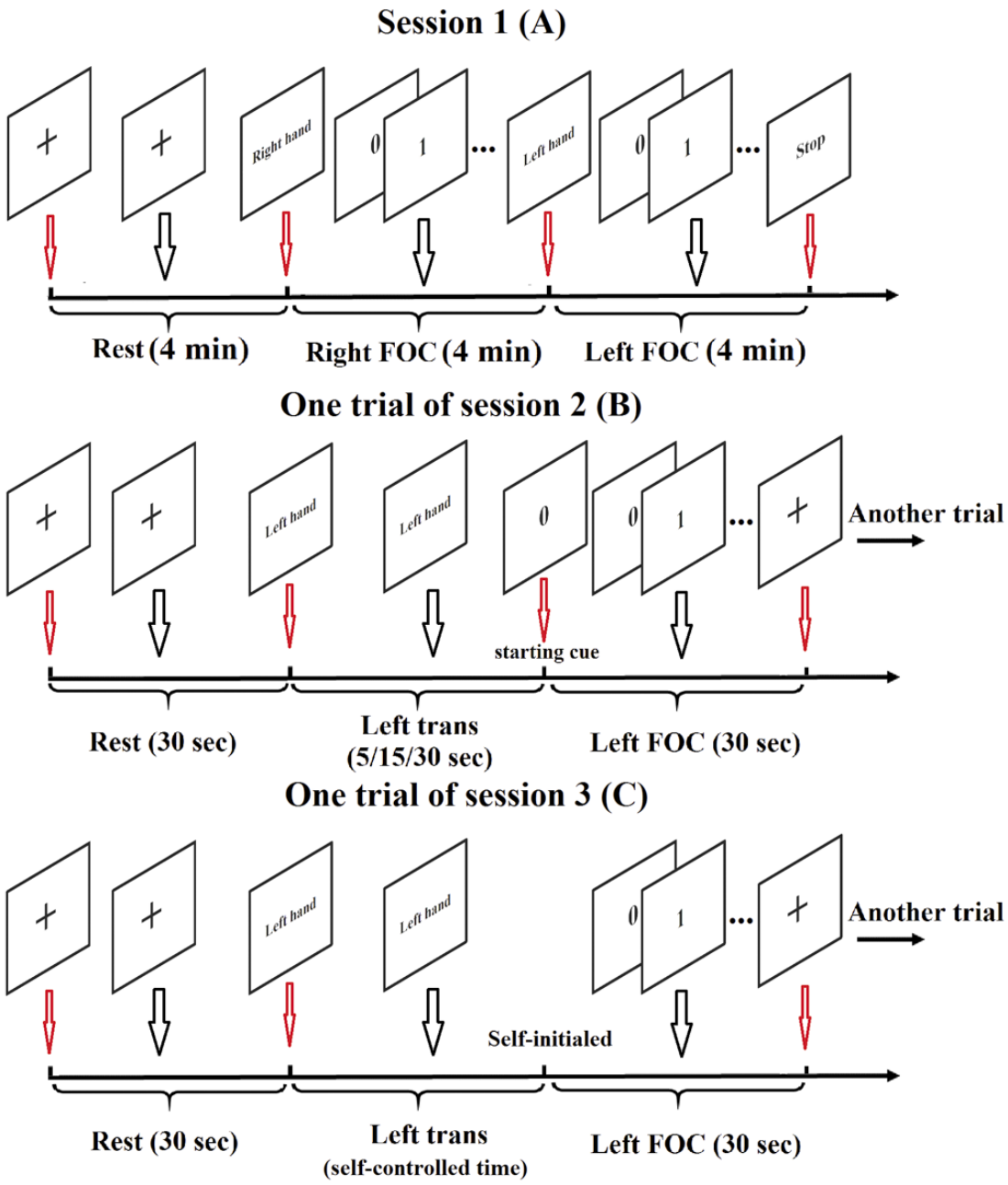

Figure 2.2. Illustration of the experiment protocol. (A) Protocol of session 1 consisted of three blocks which were rest, right FOC and left FOC and each block lasted for 4 minutes; (B) One of the six trials in session 2 consisted of three blocks which were rest, transition period and left/right FOC and the FOC was initialed by a cue; (C) One of the six trials in session 3 consisted of three blocks which were rest, transition period and left/right FOC and the FOC was initialed by subjects themselves. Note that the order of cues of "Left hand" and "Right hand" were randomized for all three sessions.

2.2.5 FC analysis

For FC analysis, five segments of data were used to generate FC which included three blocks (rest, left FOC and right FOC) in session 1 and two 30s-long transition periods preceding the left and right FOC (left trans and right trans) in session 2. For each segment of each subject, oxy-Hb time courses of channels located in the same ROI were averaged to generate a representative oxy-Hb time course for this ROI. Thus, eight representative oxy-Hb time courses (four for each brain hemisphere) were obtained. Based on that, the pair-wise FC was estimated by Pearson's correlation analysis and the correlation coefficient (r) was transformed to z-score by Fisher's transformation [163]. As a result, an 8×8 association matrix was obtained for each segment of each subject. Element a_{ij} in an association matrix represent the FC strength between the ith ROI and the jth ROI (Fig. 2.3). In order to find how transition periods and FOC would modulate the FC compared with resting state, group-level paired t-tests were performed to identify significantly changed FC during transition periods and FOC compared with resting-state. False Discovery Rate (FDR) approach was used to do the multiple comparison correction [164].

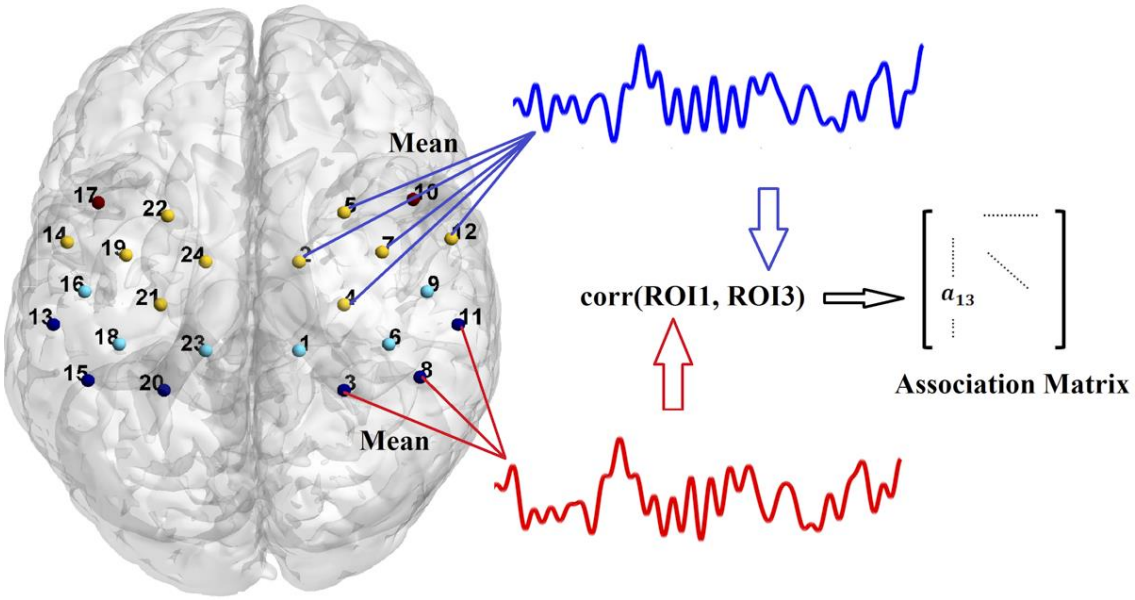

Figure 2.3. Summary of the ROI-based FC analysis. A representative time course of oxy-Hb for each ROI, that is the mean time course of channels in the ROI, was obtained and the pair-wise FC was estimated by Pearson's correlation of time courses for two ROIs.

2.2.6 Activation analysis

For each channel, baseline-adjusted mean level of oxy-Hb was calculated for each block in session 2 and 3. The first 10 time points (1s) of each block were regarded as the baseline and the data of each block were adjusted by subtracting the mean of corresponding baseline. After that, baseline-adjusted mean level of oxy-Hb was obtained by averaging the baseline-adjusted time courses of each block across time. With respect to the transition-related activation, activation during left trans and right trans were estimated for session 2 and 3 respectively. For each session, the six transition blocks were divided into two conditions (left trans and right trans) according to which hand was cued. An averaged baseline-adjusted mean level of oxy-Hb was obtained for left trans and right trans for each subject, and group-level paired t-tests were used to compare left trans and right trans with resting state for each channel and FDR approach was used to do the multiple comparison correction [164]. For FOC-related activation, the FOC blocks in session 2 and 3 were put together to do the same analysis as transition-related activation.

2.3 Results

2.3.1 Modulated FC during transition period

For FC analysis, significantly increased FC were found during left FOC, left trans and right trans compared with resting state (Fig. 2.4), while no significantly changed FC was found during right FOC. Table 2.1 listed increased FC during left FOC, left trans and right trans. There were more modulated FC during transition periods than FOC periods and the average strength of FC during transition periods was greater than that during rest and FOC periods according to the average association matrices (Fig. 2.4(D-G)). With respect to increased FC during transition period compared with resting state (Fig. 2.4(B) and (C)), most FC were inter-hemispheric FC for both left trans and right trans. Especially, FC connecting the right DLPFC with contralateral (right side in left trans and left side in right trans) S1 and M1, and FC connecting contralateral S1 with ipsilateral (left side in left trans and right side in right trans) S1 and M1 were significantly increased for both right trans and left trans, implying the relationship between modulated FC during the transition period and the side of FOC subjects were about to perform.

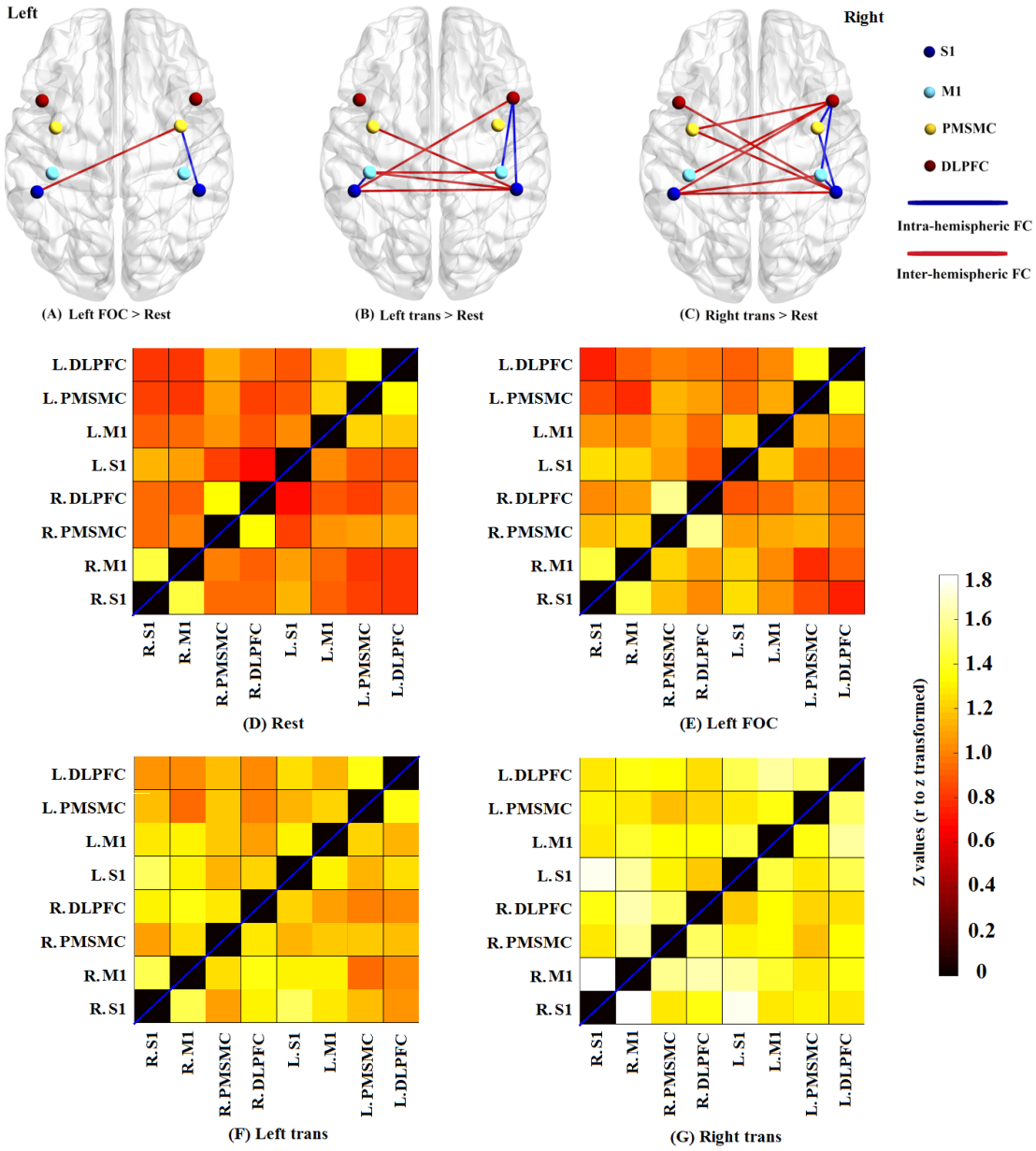

Figure 2.4. Significantly increased ($p<0.05$) FC during left FOC (A), left trans (B) and right trans (C) compared with resting-state by paired t-test. In addition, the average association matrices across subjects were illustrated for rest (D), left FOC (E), left trans (F), and right trans (G). M1 = Primary motor cortex; PMSMC = Premotor and supplementary motor cortex; DLPFC = Dorsolateral prefrontal cortex; S1 = Primary somatosensory cortex.

Table 2.1. Results of paired t-test of FC during left FOC, left trans and right trans compared with resting state.

FC	*t*-value	Unc. *p*
Left FOC > Rest		
R. PMSMC – R. S1	2.134	0.024
R. PMSMC – L. S1	2.122	0.024
Left trans > Rest		
R. S1- R. DLPFC	1.936	0.035
R. S1 – L. S1	2.374	0.015
R. S1 – L. M1	1.757	0.049
R. S1 – L. PMSMC	1.742	0.050
R. M1 – R. DLFPC	2.399	0.015
R. M1 – L. M1	2.207	0.021
R. DLPFC – L. S1	1.995	0.032
L. S1 – L. M1	1.806	0.044
Right trans > Rest		
R. S1 – R. M1	2.979	0.009
R. S1 – R. PMSMC	2.166	0.031
R. S1 – L. S1	3.066	0.008
R. S1 – L. PMSMC	1.923	0.045
R. S1 – L. DLFPC	1.984	0.041
R. M1 – R. DLPFC	1.975	0.045
R. M1 – L. S1	2.522	0.018
R. PMSMC – R. DLPFC	2.347	0.026
R. DLPFC – L. S1	1.932	0.047
R. DLPFC – L. M1	2.388	0.024
R. DLPFC – L. PMSMC	2.031	0.041

Unc. *p* = uncorrected *p* value; M1 = Primary motor cortex; PMSMC = Premotor and supplementary motor cortex; DLPFC = Dorsolateral prefrontal cortex; S1 = Primary somatosensory cortex. R. = right; L. = left.

2.3.2 Task-related activation

In addition to FC analysis, activation analysis is another method which can directly demonstrate how transition periods modulate brain activities. Activated channels during FOC and transition periods were identified by paired t-tests and multiple comparison was corrected by FDR. Activated channels were identified (FDR corrected $p < 0.05$) during FOC periods (Fig. 2.5(A) and 5(B)) as well as transition periods in session 3 (Fig. 2.5(E) and 2.5(F)), which corresponded to the preparation before self-initialized movement. Table 2.2 listed these activated channels and their statistical results. Nine channels were activated during left FOC, which located in bilateral DLPFC, right PMSMC, and right M1, and three channels located in left PMSMC and left M1 were activated during right FOC (Table 2.2). For transition periods in session 3, fifteen channels were activated during left trans, which located in bilateral DLPFC, bilateral M1, bilateral S1 and right PMSMC, and eight channels located in bilateral M1, right S1, right PMSMC and right DLPFC were activated during right trans (Table 2.2). However, no channels were activated during transition periods in session 2, which corresponded to the preparation before externally-triggered FOC, after multiple comparison correction by FDR, even though several activated channels were identified before multiple comparison correction (Fig. 2.5(C) and 2.5(D)).

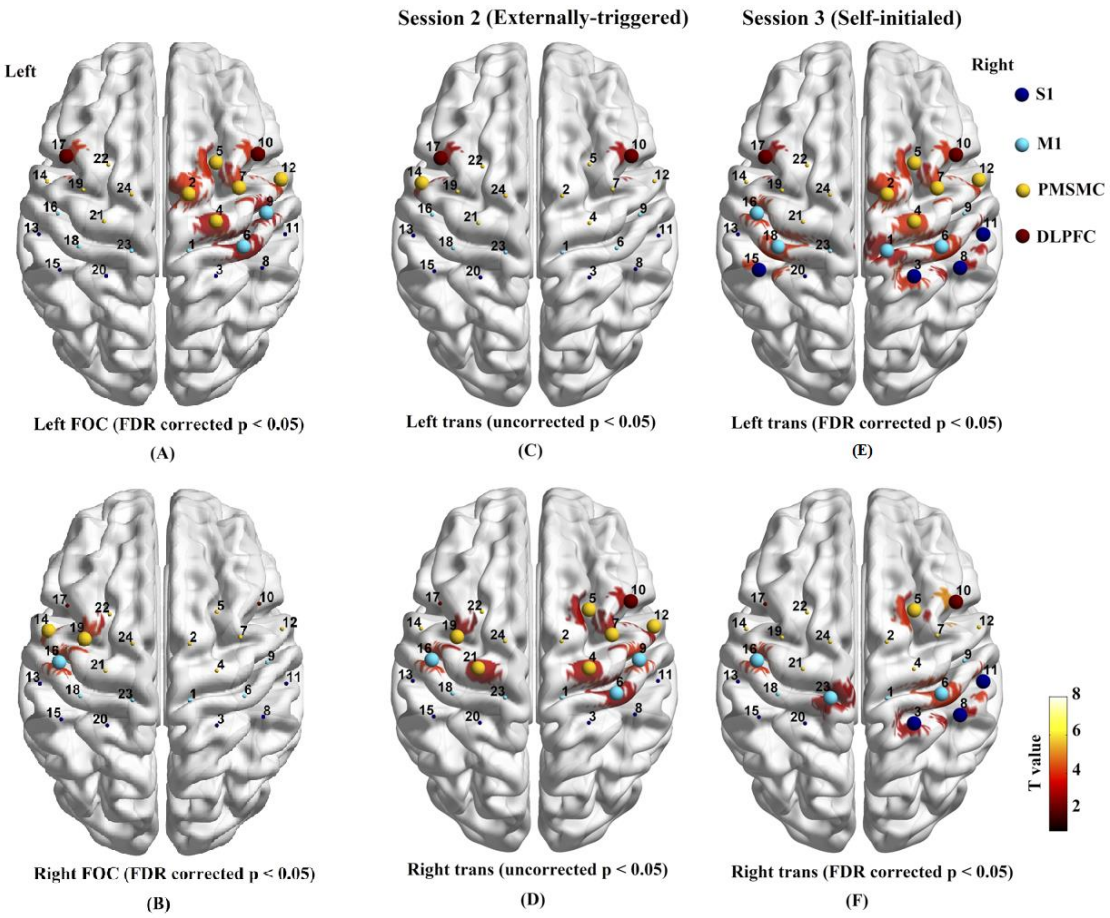

Figure 2.5. Activation of channels during left FOC (A), right (B), left trans and right trans in session 2 (C, D), and session 3 (E, and F). Note that activation of channels during left and right trans in session 2 did not survive the multiple comparison correction by FDR. Spheres represent the channels and color of the spheres indicate which ROI they locate in according to the legend in the figure. Larger spheres indicate that these channels were activated and smaller ones mean no activation in these channels.

Table 2.2. Activated channels and the paired t-test results (after FDR correction) during left and right trans in session 3, as well as left and right FOC.

Activated channels during trans in session 3			Activated channels during FOC		
Channel (ROI)	*t*-value	FDR. *p*	Channel (ROI)	*t*-value	FDR. *p*
Left trans in session 3			Left FOC		
1 (R.M1)	2.390	0.029	2 (R.PMSMC)	3.052	0.025
2 (R.PMSMC)	2.512	0.025	4 (R.PMSMC)	2.475	0.044
3 (R.S1)	3.288	0.013	5 (R.PMSMC)	2.980	0.025
4 (R.PMSMC)	2.722	0.023	6 (R.M1)	2.293	0.047
5 (R.PMSMC)	3.053	0.017	7 (R.PMSMC)	2.998	0.035
6 (R.M1)	3.358	0.013	9 (R.M1)	2.474	0.044
7 (R.PMSMC)	3.050	0.018	10 (R.DLPFC)	3.360	0.025
8 (R.S1)	2.298	0.033	12 (R.PMSMC)	3.046	0.025
10 (R.DLPFC)	3.426	0.013	17 (L.DLPFC)	2.744	0.030
11 (R.S1)	2.165	0.037			
12 (R.PMSMC)	3.410	0.013			
15 (L.S1)	2.567	0.025			
16 (L.M1)	2.893	0.018			
17 (L.DLPFC)	2.229	0.036			
18 (L.M1)	3.016	0.018			
Right trans in session 3			Right FOC		
3 (R.S1)	2.368	0.045	14 (L.DLPFC)	3.111	0.031
5 (R.PMSMC)	2.509	0.045	16 (L.M1)	3.200	0.031
6 (R.M1)	2.908	0.045	19 (L.DLPFC)	3.246	0.031
8 (R.S1)	2.377	0.045			
10 (R.DLPFC)	3.885	0.018			
11 (R.S1)	2.589	0.045			
16 (L.M1)	2.687	0.045			
23 (L.M1)	2.494	0.045			

FDR. *p* = FDR corrected *p* value; R. = right; L. = left.

2.4 Discussion

In this chapter, we examined how the transition period between rest and FOC modulated the motor-related brain activities from the perspectives of static FC and activation. Our results demonstrated that not only would the actual movement in FOC modulate the brain activities, but also the transition period without actual movement modulated the brain activities from the perspectives of both FC and activation.

For FC analysis, our results showed that FC connecting the right DLPFC with contralateral S1 and M1, and FC connecting the contralateral S1 with ipsilateral S1 and M1 were significantly increased for both right trans and left trans (Fig. 2.4). These findings might give us an idea about how brain would achieve the preparation state before actual motor task execution. DLPFC is an intensively researched brain region and many functions have been attributed to it such as executive control of motor system [165] and response inhibition [166]. Specifically, right DLPFC might be involved in the attention to motor timing and decision on when to move based on other studies [167, 168]. In addition, M1 and S1 is known to be the primary brain regions in charge of sensorimotor function. Thus, it was reasonable to believe that these increased FC indicated that right DLPFC was controlling M1 and S1 to maintain the preparation state. Based on the functions of DLPFC found by previous studies, the controlling aspect might consist of two parts. First part was to make the sensorimotor system be ready for the upcoming motor task. Furthermore, since which hand subjects would use in the upcoming task had already been cued, DLPFC might also exert control over contralateral M1 and S1 to withhold the execution of motor task during the preparation, which was supported by previous finding that DLPFC might be important for making the decision on when to move and withholding movement until the right moment [169]. Increased FC connecting contralateral S1 with ipsilateral S1 and M1 further indicated an interaction of bilateral sensorimotor system to process the sensory information and further collaborate with DLPFC to balance the activities in both hemispheres and maintain the preparation state. In summary, these findings proved that brain regions with high-level cognitive functions such as DLPFC collaborated with sensorimotor networks in bilateral hemispheres to maintain the preparation state, under which motor system was ready for the upcoming motor task but also was withheld to execute motor task until the right moment.

With respect to comparison between FOC and rest, only two FC were found significantly increased (unc. $p<0.05$) in left FOC which were FC between right PMSMC and right S1 as well as left S1 (Fig. 2.4(A)). Premotor and supplementary cortex was known to play an important role in control of movement, especially for the sequential movement according to previous studies [170, 171]. During FOC, subjects were instructed to open and close their fist according to the numbers displayed on the screen. Therefore, there might be an interaction between the sensory

component and control component to pace the movement based on external information during this process. The two increased FC between right PMSMC and bilateral S1 might be the “bridge” of information transmission and PMSMC contralateral to moving hand was receiving sensory information from bilateral S1 through them and therefore exerted control over FOC.

For activation analysis, more activation were identified during transition periods in session 3, which corresponded to preparation before self-initialed FOC (Fig. 2.5(E) and 2.5(F)), as no channels survived the multiple comparison correction during transition periods in session 2. Previous studies had similar findings by examining the readiness potentials before movements and they found that the readiness potential preceding self-initialed movements was significantly greater compared with externally-triggered movements [172, 173]. Nevertheless, right DLPFC was activated during left trans and right trans in both session 2 and session 3, which further supported our speculation of the important role that right DLPFC played in the preparation state through the FC analysis. In addition, bilateral S1, M1 and PMSMC which were key brain regions for motor execution and motor control, were also activated even though there was no actual movement, which was in line with previous study [156]. In general, combing these activated channels together, the activation findings also supported our speculation, through FC analysis, that brain regions with high-level cognitive functions such as DLPFC collaborated with sensorimotor networks in bilateral hemisphere to maintain the preparation state.

Activation during FOC was not our major target in this chapter, it was for the validation of our study by comparing with other studies. According to our results, motor-related brain regions contralateral to the moving hand were activated during FOC (Fig. 2.5(A) and 2.5(B)), which was similar with other studies based on either fNIRS or fMRI [174, 175]. Therefore, the results and findings in our study should be reliable.

In addition, our findings regarding transition periods, especially the modulated FC, could potentially be applied in anticipation-based BCI. Previous studies of anticipation-based BCI mainly targeted the anticipation-related potentials obtained through EEG and developed classification methods to detect the anticipation-related potentials to guide the BCI [132, 176, 177]. However, our findings might provide another option for anticipation-based BCI. The increased FC during transition period before actual movement could be used to guide the BCI. Especially, the relationship between modulated FC during transition period and the side of FOC subjects were about to perform, that is, FC connecting the right DLPFC with contralateral (right side in left trans and left side in right trans) S1 and M1, and FC connecting contralateral S1 with ipsilateral (left side in left trans and right side in right trans) S1 and M1 were increased during transition periods, would further help the BCI to understand the anticipation of subjects more specifically.

2.5 Chapter conclusion

In this chapter, we used fNIRS to evaluate how the transition period preceding the task would modulate the task-state brain network compared with the rest period. We found several increased FC during transition period, especially the FC connecting right DLPFC with contralateral S1 and M1 as well as the FC connecting contralateral S1 with ipsilateral S1 and M1. In addition, channels located in sensorimotor networks and right DLPFC were also found activated during transition period by activation analysis. These results demonstrated that sensorimotor network was interacting with high-level cognitive brain network during transition period to maintain the preparation state.

In this thesis, the purpose is to reveal the motor task-specific spatiotemporal changes of brain networks compared with resting conditions, and further applied the task-state brain network analysis in the research of stroke recovery. This chapter revealed the task-specific spatial changes of brain networks under motor preparation and motor execution compared with resting conditions using static FC analysis, which enriched our understanding of how motor network would work under motor preparation and motor execution, especially the interaction between motor network and cognitive network under different conditions. This knowledge could be applied in a lot fields, such as the anticipation-based BCI mentioned above, and the research of stroke based on motor preparation.

Chapter 3: Modulation of dynamic task-state brain network during motor execution based on fNIRS

3.1 Introduction

Recent neuroimaging studies have been focusing on motor-modulated brain activities through either activation analysis [178-182] or static FC analysis [41, 49]. As a rapidly growing method, dynamic FC analysis, which takes the dynamic and adaptive brain activities into account, provides new insights into the dynamic patterns of brain networks. fMRI-based dynamic FC analysis has been a major methodological innovation [117, 118, 183], using sliding-window correlation analysis from seconds up to minutes [116, 122, 123, 184]. Dynamic FC analysis provides not only the temporal dependence of the brain's organization during cognitive processes [116], but also clinically valuable information [123]. In sliding-window-based analysis of fMRI data, the window size is crucial for the robustness and sensitivity of FC estimation [115, 118]. Therefore, neuroimaging modality with higher temporal resolution would be beneficial for dynamic FC analysis [118]. fNIRS has emerged as a new tool that is complementary to fMRI-based FC analysis, especially dynamic FC analysis. fNIRS also facilitates new applications for its portable and wearable nature. The reliability of fNIRS in static FC analysis has already been documented [146-154, 185]. However, to the best of our knowledge, no studies have used fNIRS to perform dynamic FC analysis, though it has relatively higher temporal resolution than fMRI.

In this chapter, our aim was to reveal how task-state brain network would be modulated by motor task execution from the perspective of dynamic FC and also to explore applicability of dynamic FC analysis on fNIRS. fNIRS data were recorded from nineteen volunteers during a FOC task, as well during resting state. Dynamic FC was estimated by both sliding-window correlation and the new phase synchronization approach which was proposed recently as a promising method in dynamic FC analysis [186, 187].

3.2 Methods

3.2.1 Participants

Nineteen healthy right-handed volunteers (12 Males; Age: 20-30 years, 24.68±3.06 years) participated in this experiment. Subjects had no history of mental health, seizures, head injury, or neurological dysfunction (e.g. stroke

or seizure). All subjects provided written informed consent and procedures are reviewed and approved by the Institutional Review Board of Drexel University.

3.2.2 Data acquisition

Neuroimaging data was collected by the 24-channel Hitachi ETG-4000 NIRS system (Hitachi Medical Co., Tokyo, Japan) at the Cognitive Neuroengineering and Quantitative Experimental Research Collaborative, Drexel University (www.drexel.edu/conquer/; Philadelphia, PA, USA), using the same procedure of chapter 2 (Fig. 3.1).

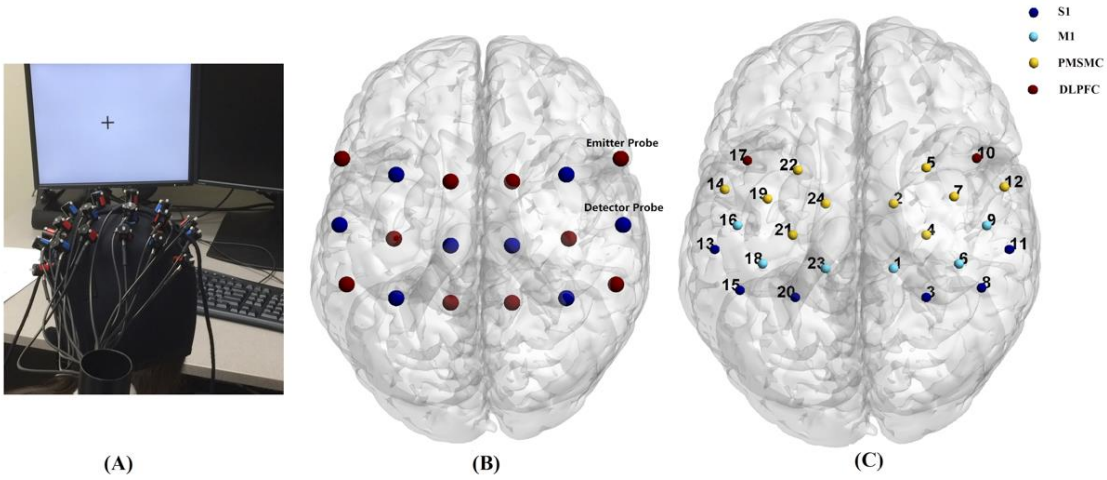

Figure 3.1. (A) Probes configuration and cap placement during the experiment. (B) Positions of the eighteen probes on standard brain template (MNI). (C) Positions of the twenty-four channels on standard brain template and the colors represent the region of interest (ROI) they locate in.

3.2.3 Experiment protocol

Experiment protocol was completed in a single sitting and has two sessions. The first session was resting state and subjects were instructed to relax and refrain from any movements. The second session was right FOC, during which “0” and “1” were displayed to pace subjects’ movements. Subjects were instructed to open their fist when they saw “0” and close when they saw “1”. The frequency was set as opening and closing once per second. Both sessions lasted for 4 minutes. During the experiment, subjects’ immobility was visually checked and no excessive motion was found for any subjects.

3.2.4 Data preprocessing

Raw fNIRS data were band-pass filtered within 0.01 Hz to 0.1 Hz to remove the physiological noise such as respiration and cardiac activities, following previous studies [146, 150, 152, 153]. One of the participants' data were rejected due to low signal quality and artifacts. After that, data were first corrected for motion artifacts using the CBSI method, which used Deoxy-Hb data to estimate movement in Oxy-Hb data through decorrelation [188]. Then, the data was further corrected for residual motion artifacts using the Sliding-window Motion Artifact Rejection (SMAR) algorithm, which used statistical filtering to automatically mark temporally localized artifacts on fNIRS signals and had been shown to be effective for various types of noises [158]. We used Oxy-Hb signal changes in the current analysis since previous findings showed that Oxy-Hb was the most sensitive to locomotion-related activities [159, 160].

3.2.5 Dynamic FC by sliding-window correlation analysis

For both rest session and FOC session, Oxy-Hb time courses of channels located in the same ROI were averaged to generate a representative Oxy-Hb time course for this ROI. Thus, eight representative Oxy-Hb time courses (four for each hemisphere) were obtained. Then, representative Oxy-Hb time courses were analyzed by sliding windows (size: 30 s) with a step of 2 s, resulting in 105 windows in total [95, 122]. Within each window, the pair-wise FC was estimated by Pearson's correlation analysis and an 8×8 association matrix (AM) was obtained for each window (Fig. 3.2).

3.2.6 Dynamic FC by phase synchronization analysis

In addition to the sliding-window-based dynamic FC analysis, phase synchronization analysis was also used to evaluate the dynamic FC through mean phase coherence (MPC). For a real-valued signal $s(t)$, its analytic signal is defined as

$$z(t) = s(t) + jH\{s(t)\} = A(t)e^{j\phi(t)} \tag{3.1}$$

where $A(t)$ and $\phi(t) = \arg[z(t)] = artan\frac{H\{s(t)\}}{s(t)}$ are the instantaneous amplitude and instantaneous phase of signal $s(t)$, respectively, and $H\{\cdot\}$ is the Hilbert transform [186, 187]. Let $s(n)$ denotes $s(n\Delta t)$, i.e., the observation of $s(t)$ at time $n\Delta t$, and $\hat{\phi}(n)$ denotes the estimation of $\phi(t)$ at time $n\Delta t$, where Δt is the sampling interval (0.1 s in this experiment).

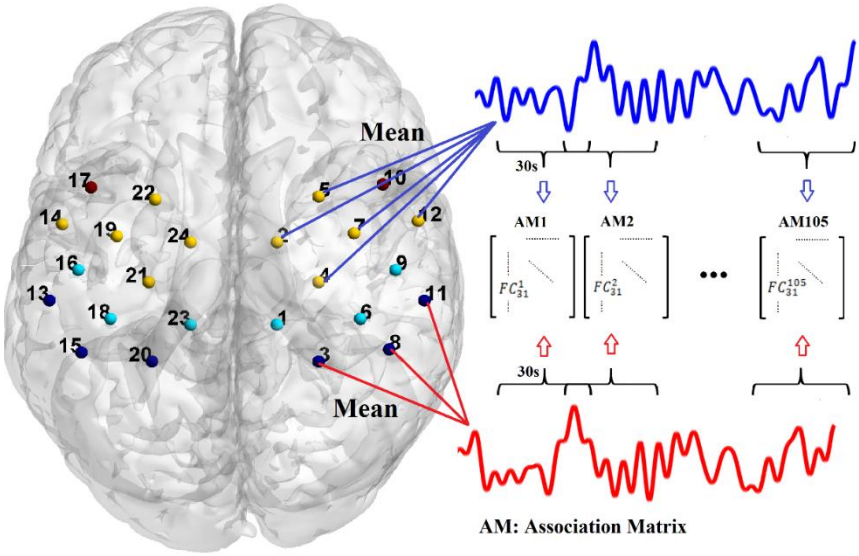

Figure 3.2. Illustration of sliding-window-based dynamic FC analysis. The representative Oxy-Hb time courses were analyzed by sliding windows (size: 30 s) with a step of 2 s, resulting in 105 windows in total.The pair-wise FC was estimated by Pearson's correlation analysis and an 8×8 association matrix (AM) was obtained for each window.

Once the instantaneous phase time courses of two coupled ROIs were obtained, which were denoted by $\hat{\phi}_1(n)$ and $\hat{\phi}_2(n)$. Phase synchrony between two ROIs can then be quantified using MPC [189]. Temporal MPC was used to estimate the phase synchrony among Oxy-Hb time courses of ROIs in study. The instantaneous phase time courses were divided into short sliding windows (size: 3 s; 30 sampling points) with a step of 1.5 s, resulting in 159 windows in total, so that the sampling points in each window were enough to estimate reliable phase synchrony [190], which can be regarded as FC among ROIs. The MPC-based phase synchrony was estimated as follow:

$$\lambda = \frac{1}{N}\left|\sum_{n=0}^{N-1} e^{j(\hat{\phi}_1(n)-\hat{\phi}_2(n))}\right| \tag{3.2}$$

where N denotes the number of sampling points in a window. As a result, for each of the 159 windows, an 8×8 association matrix is obtained (Fig. 3.3).

3.2.7 Variability analysis of FC and ROI

In order to examine the dynamic patterns of ROIs as well as FC between ROIs, the FCV and nodal strength variability (NV) were estimated over time for both rest and FOC. The FCV based on two methods was calculated as follow:

$$FCV_{ij} = \frac{1}{M} \times \sqrt{\sum_{k=1}^{M} (FC_{ij}^{k} - \overline{FC}_{ij})^2} \tag{3.3}$$

where M represents the number of sliding windows; FC_{ij}^{k} denotes the FC between ROI i and ROI j at window k; $\overline{FC}_{ij}$ denotes the mean of FC_{ij}^{k} across sliding windows. For nodal strength of ROIs, the NV was calculated as follow:

$$NV_i = \frac{1}{M} \times \sqrt{\sum_{k=1}^{M} (N_i^k - \bar{N}_i)^2} \tag{3.4}$$

where $N_i^k = \sum_{j=1, j\neq i}^{R} FC_{ij}^{k}$, representing the nodal strength of ROI i at window k and R denotes the number of ROIs; $\bar{N}_i$ denotes the mean of N_i^k across sliding windows.

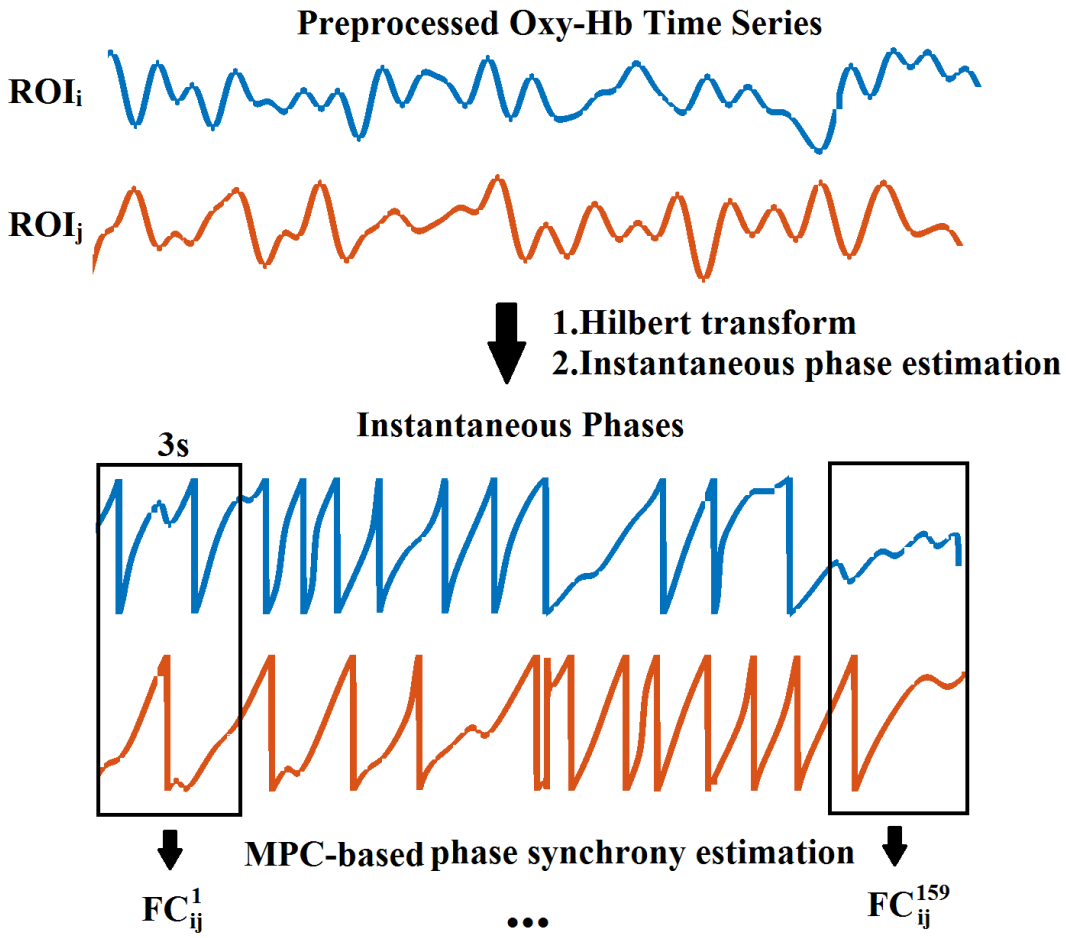

Figure 3.3. Illustration of dynamic FC analysis based on phase synchronization. Through Hilbert transform, the instantaneous phases are extracted from preprocessed time series and then are divided into small sliding windows with size of 3 s and step of 1.5 s, resulting in 159 windows. For each window, the phase synchrony between each pair of ROIs is estimated through MPC and an 8×8 association matrix is obtained.

3.3 Results

3.3.1 Increased dynamic FCV during FOC

In order to investigate how the FOC would modulate the dynamic FC among motor-related ROIs, the FCV was compared between rest and FOC by paired t-test. Multiple comparison correction was performed using False

Discovery Rate (FDR) approach [164]. For dynamic FC based on sliding-window correlation analysis, statistical results (Table 3.1) showed that the FCV of L. M1-L. PMSMC (FDR-corrected p = 0.034) and L. M1 – R. S1 (FDR-corrected p = 0.045) were significantly increased during FOC comparing with rest (Fig. 3.4). With respect to dynamic FC based on phase synchronization analysis, similar results (Table 3.1) were obtained that the FCV of L. M1 – L. PMSMC (FDR-corrected p = 0.031) was also significantly increased during FOC (Fig. 3.5).

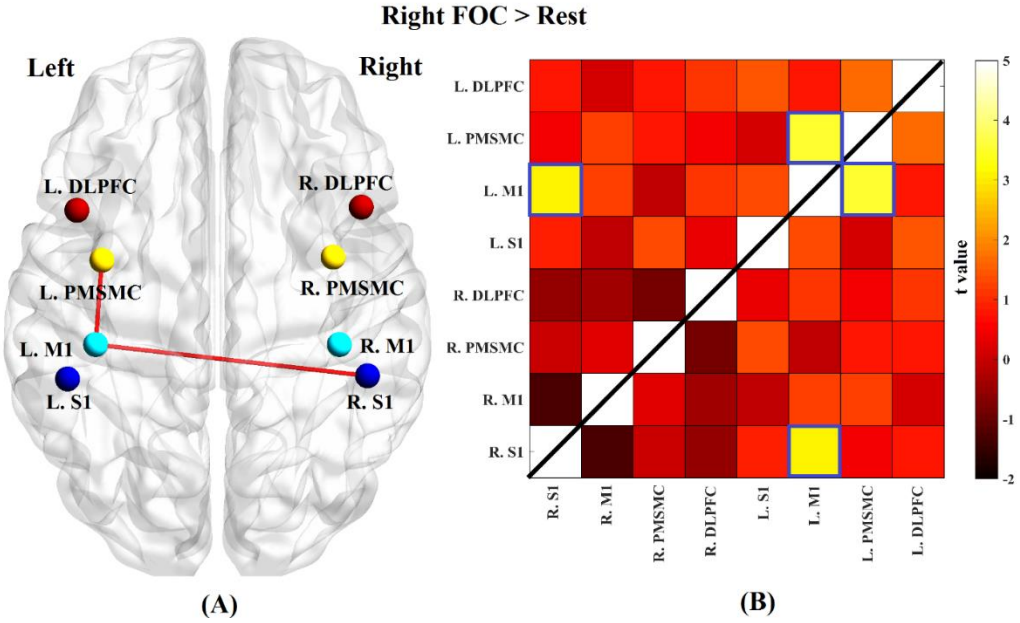

Figure 3.4. (A) Significantly increased FCV based on sliding-window correlation analysis (L. M1 – L. PMSMC: FDR-corrected p = 0.034; L. M1 – L.S1: FDR-corrected p = 0.045) during FOC compared with rest. (B) Map of t-value of paired t-test, and the blue outlined squares represent the FC with increased FCV during FOC compared with rest.

Table 3.1. Statistical Results of Paired t-test of FCV between FOC and rest

FC	*t*-value	Unc. *p*	FDR *p*
Dynamic FC by sliding-window correlation analysis			
L. PMSMC – L. M1	3.562	0.001	0.033
L. M1 – R.S1	3.108	0.003	0.045
Dynamic FC by phase synchronization analysis			
L. PMSMC – L. M1	3.602	0.001	0.031

Unc. *p* = uncorrected *p* value; FDR *p* = FDR corrected *p* value.

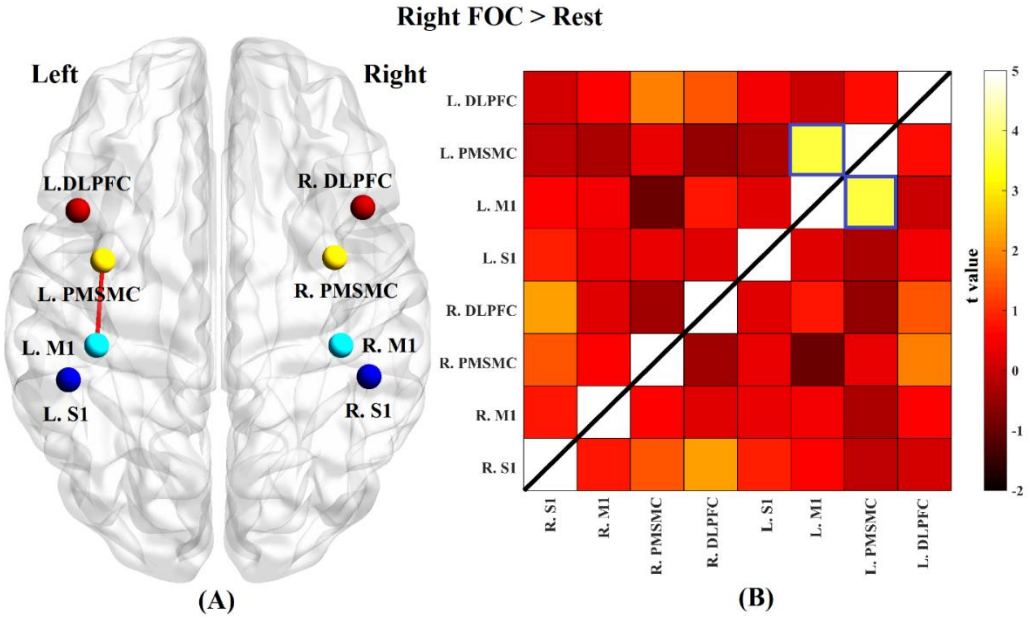

Figure 3.5. (A) Significantly increased FCV based on phase synchronization analysis (L. M1 – L. PMSMC: FDR-corrected p = 0.031) during FOC compared with rest. (B) Map of t-value of paired t-test, and the blue outlined squares represent the FC with increased FCV during FOC compared with rest.

3.3.2 Increased NV during FOC

For dynamic FC based on two methods, the nodal strength as well as NV were estimated. NV based on two methods were also compared between rest and FOC, respectively. According to the statistical results of paired t-test, the NV based on phase synchronization analysis was not changed significantly between rest and FOC. However, with respect to the nodal strength based on sliding-window correlation analysis, the NV increased significantly during FOC comparing with rest in L. PMSMC (FDR-corrected p = 0.045) and L. M1 (FDR-corrected p = 0.046) (Fig. 3.6). Note that these two ROIs were also involved in the dynamic FC with significantly increased FCV during FOC for both methods (Table 3.1).

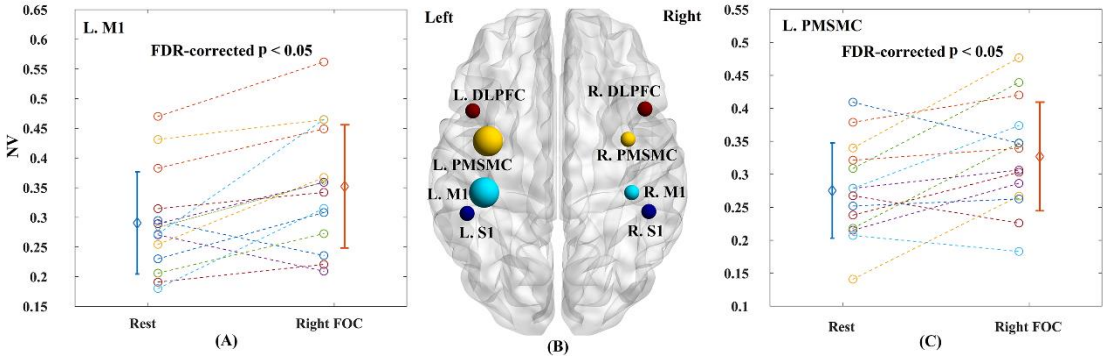

Figure 3.6. Increased NV based on sliding-window correlation analysis in L. M1 (FDR-corrected p = 0.046) (A) and L. PMSMC (FDR-corrected p = 0.045) (C) during FOC compared with rest. Subjects are coded by different colors and the error bars indicate the standard errors of the mean.

3.4 Discussion

In this chapter, two methods, which were sliding-window correlation analysis and phase synchronization analysis, were adopted to estimate the dynamic FC during rest and FOC based on fNIRS. Similar results were found based on two methods. Specifically, the FCV of L.PMSMC - L.M1 was increased during FOC comparing with rest, which was found based on two methods.

M1 and PMSMC were reported to be the key brain regions in the motor system [191, 192]. However, they are in charge of different aspects of motor function based on their properties. The strong presence of large corticospinal

neurons is a unique property of M1. Among the corticospinal neuros which arise from M1, 31% are considered large and these neurons represent 79% of all large corticospinal neurons, which are important for the fractionation of independent finger movement as they directly influence the lateral motor-nuclei in the spinal cord [193, 194]. Based on the findings of unilateral ablations of M1 in the rhesus monkey, the importance of M1 for generating movement of the distal forelimb muscles was proven as monkeys still had difficulties in grasping small objects and making isolated movement of the wrist six months post lesioning [195, 196]. With respect to PMSMC, studies found that it was critical for implementing associations between arbitrary cues and motor responses. An experiment on monkey discovered that dorsal premotor (PMd) neurons discharged after the presentation of an arbitrary cue which instructed the monkey to make a particular motor movement [197]. In a TMS study, subjects' abilities to use color cues to select appropriate motor responses were disrupted after low-frequency repetitive TMS, which reduced the neuronal excitability, was applied over PMd [198]. In addition, PMSMC also plays significant role in the control of hand movements required for the manipulation of objects. Several neuroimaging studies identified changes of brain activity in PMSMC when subjects altered grip forces during precision grip [199], and changed finger configurations while manipulating objects by tactile exploration [199].

Though M1 and PMSMC are in charge of different motor function based on their features, the interaction between them contributes significantly to the motor system. According to previous studies, the interaction between M1 and PMSMC reflected the hierarchical organization of the motor system in humans [200, 201]. In a TMS study, neural modulation occurred in a small number of brain regions, including non-primary motor areas and subcortical motor structure, after M1 stimulation. However, after PMSMC stimulation, neural modulation occurred in multiple brain regions, including motor regions in frontal cortex and associational regions in the parietal and prefrontal cortices [201]. Visual, auditory, and/or other information that affected movements was usually processed by associational and higher order sensory cortices and then was communicated to the PMSMC [202]. Thus, PMSMC was collecting motor-related information from other cortices and used it to assist M1 in motor execution through its interaction with M1.

In this chapter, through dynamic FC, new insights into the interaction between M1 and PMSMC during motor execution were provided. The FCV of L.PMSMC - L.M1 was increased during FOC comparing with rest. The FOC task was a visual-cued hand movement, which required subjects to open their fist when "0" was displayed and to close their fist when "1" was displayed. Thus, based on the above information regarding the features of M1 and PMSMC, it was reasonable to speculate that the PMSMC was collecting processed visual information from other cortices, and used it to assist the M1 to control the hand movement, especially implementing associations between

arbitrary cues and motor responses. Thus, the increased FCV between M1 and PMSMC reflected they were interacting with each other dynamically during FOC, as the increased FCV represented active dynamic interaction [28], and it also demonstrated that our findings fitted previous studies about motor system. In addition, the NV in M1 and PMSMC were also increased during FOC, further indicating their active dynamic interaction.

Another purpose of this chapter was to explore the potential of application of fNIRS in dynamic FC analysis. Though dynamic FC analysis is a hot topic recently, most studies were based on fMRI [117, 118]. To the best of our knowledge, no studies have tried to perform dynamic FC analysis through fNIRS. The reliability of fNIRS in static FC analysis has already been demonstrated by several studies [146-148]. Actually, the features of fNIRS, including portability, wearability, especially relatively higher temporal resolution than fMRI, make it a promising modality for dynamic FC analysis. For instance, the size of sliding window in correlation analysis is 30 s, with 300 fNIRS samples under the sampling rate of 10 Hz. In contrast, for regular fMRI scanner with TR of 2 s, there would be only 15 samples in a window of 30 s, which would hardly result in reliable FC estimation [115, 203]. With its relatively high temporal resolution, fNIRS is also able to detect potentially interesting transients [115, 118]. To the best of our knowledge, this is the first study on dynamic FC analysis of fNIRS, which offer new insights into the dynamic interaction between M1 and PMSMC during motor execution.

In this chapter, in addition to sliding-window correlation analysis, phase synchronization analysis was also used to estimate dynamic FC. Phase synchronization analysis employed the concept of analytic associates based on the Hilbert information [187] to extract the phase information and estimate temporal/spatial phase synchrony of time series. This method was recently adopted in the dynamic FC analysis based on fMRI. In that fMRI study, because of high spatial resolution, spatial phase synchrony was estimated, resulting in an instantaneous measure of local FC [204]. In our study, given relatively high temporal resolution and low spatial resolution, temporal phase synchrony was estimated. Though the temporal phase synchrony cannot result in an instantaneous measure of FC, the window was still shorter than that used in sliding-window correlation analysis, indicating that phase synchronization analysis can detect the dynamic changes of FC during in a shorter time scale than sliding-window correlation analysis. In addition, the results based on phase synchronization analysis were similar with that based on sliding-window correlation analysis. Thus, phase synchronization is a promising method in the fNIRS-based dynamic FC analysis.

3.5 Chapter conclusion

In this chapter, the task-state brain networks were investigated during motor execution based on fNIRS using dynamic FC analysis. fNIRS data were recorded from nineteen volunteers when they were resting and performing

FOC task. Dynamic FC was estimated by sliding-window correlation analysis and phase synchronization analysis of fNIRS. In addition, dynamic FC was compared between rest and FOC to investigate the modulation of motor task on dynamics of motor-related FC and network. The FCV of L.PMSMC - L.M1 as well as their NV were increased during FOC comparing with rest, which was consistent by either sliding-window correlation analysis or phase synchronization analysis. Our results demonstrated that contralateral M1 and PMSMC were interacting with each other dynamically during FOC, and the relatively high temporal resolution of fNIRS provides robust FC estimation and transient detection simultaneously.

Chapter 4: Spatiotemporal pattern of task-state brain networks during motor tasks based on fMRI

4.1 Introduction

In this chapter, the spatiotemporal pattern of task-state brain networks during motor task was investigated based on fMRI. Like the fNIRS, the task-state brain networks can be investigated using static FC analysis and dynamic FC analysis. However, so far, several fMRI studies have examined the task-state brain networks during a variety of tasks, including motor tasks, using static FC analysis [41, 49, 50, 205-208]. Therefore, in this chapter, the focus was examining task-state brain networks during motor task using dynamic FC analysis, and an introduction of fMRI studies using static FC analysis to investigate the task-state brain networks during motor tasks was provided first.

Jiang and colleagues conducted an fMRI study to investigate modulation of FC during motor task compared with resting state [41]. They recorded the fMRI data of eight healthy right-handed volunteers during resting state and finger tapping task. Based on a newly developed approach, which took into account n-to-1 FC using 1-to-1 FC measures, instead of conventional pairwise FC, their findings showed that a large organized brain network related to motor function existed in the resting brain, More importantly, they further revealed that the brain network could be modulated during the motor task state. Figure 4.1 illustrated the main finding of this study, they estimated the normalized FC degree of nodes $\bar{\Gamma}$ to describe the amount of information of a node receiving from the particular network. In order to examine the modulation of brain network during motor task state, paired Student's t-test was adopted to compare the $\bar{\Gamma}$ of each brain region between two states. Significant difference in $\bar{\Gamma}$ for some pairs of brain regions were identified (Fig. 4.1).

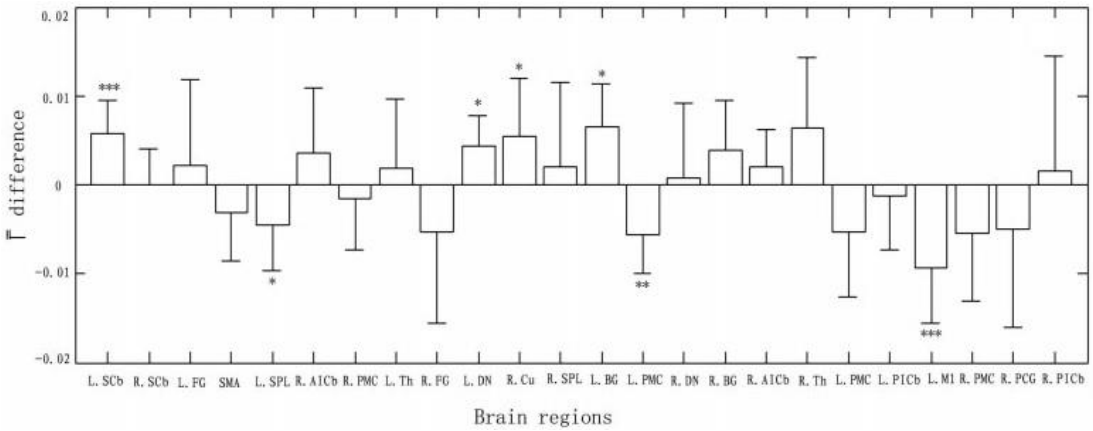

Figure 4.1. Difference in $\bar{\Gamma}$ between resting state and motor task. *p < 0.05; **p < 0.01; ***p < 0.001 (paired t-test). R: Right; L: Left; FG: fusiform gyrus; SCb: superior cerebellum; M1: primary motor cortex; Th: thalamus; SPL: superior parietal lobule; SMA: supplementary motor area; PMC: premotor cortex; DN: dentate nucleus; AICb: anterior inferior cerebellum; PCG: postcentral gyrus; BG: basal ganglia; PICb: posterior inferior cerebellum; Cu: cuneus. This figure was adopted from [41] with courtesy.

Another fMRI targeted to investigate the task-related modulation on interregional correlations within the motor system [50]. fMRI data of eleven healthy right-handed subjects were recorded during resting state and three steady-state finger tapping tasks with different tapping rates being 1, 2 and 4 Hz. Based on the four steady-state functional scans (rest, 1, 2, 4 Hz tapping), partial correlation maps were generated to illustrate the partial correlation between the average M1 time course and the time course of every voxel, excluding the effects of the global time course. Then, the FC between motor-related brain regions and M1 was examined under four states to evaluate the modulation of FC within motor system by the varying task demands. According to the results, the FC of several brain regions with M1 was modulated by tapping rate, indicating that the task demand was a significant factor in determining the FC of some brain regions to PM, and the FC measured during tapping increased compared with resting state in general.

In addition to above two studies, several fMRI studies adopted static FC analysis to investigate the task-state brain network during motor preparation [129], and fist-edge-palm task [209]. Since the task-state brain networks have already been investigated by several fMRI studies using static FC analysis, this thesis focused on investigating the spatiotemporal patterns of task-state brain networks during motor task based on fMRI using dynamic FC analysis.

Dynamic brain activities have been extensively studied using EEG methods and commonly observed functional microstates have been considered to form the basic building blocks of information processing [210-215]. fMRI-based investigations using dynamic FC have been the focus of recent methodological innovations and studies are also accumulating [117, 118, 183]. Dynamic FC has been explored in fMRI using sliding window correlation analysis to examine time scales ranging from seconds to minutes [116, 122, 123, 184]. These studies demonstrated that dynamic FC analysis not only delivered a more complete description of the temporal dependence of the brain's organization during cognitive processes, but that this perspective provided clinically valuable information. For example, schizophrenia patients exhibited shorter states of strong and large-scale FC than healthy controls during rest, which could not be observed when using static FC analysis [123]. Another study of dynamic FC in Alzheimer's disease patients showed longer state persistence in the strong anterior DMN sub-network, but shorter states in the strong posterior DMN sub-network when compared with healthy elderly subjects during rest [184]. A recent resting-state dynamic FC study reported that multiple FC states could co-exist, which was interpreted as an indication of the unconstrained mental activities of resting state [122], an observation further supported by positive correlation between frequency of "mind-wandering" and FCV of core regions of interest (ROIs) in DMN [119].

The above studies showed that the dynamic FC could depict the underlying ongoing cognitive process during rest. Furthermore, the spatiotemporal dynamics of brain networks during task may provide more insights into the adaptation of the brain in response to modulated cognitive processes [117, 118]. However, investigation on the task-related modulation of dynamic FC is still in an early stage. To the best of our knowledge, only one study has used dynamic FC to investigate the task-related modulation of FCV [95] so far, and found significant task-related decreases of FCV at the regional, network and system levels. In addition, the task-induced decrease in FCV was significantly correlated with task performance. It was proposed that the task-related reduction in FCV was likely related to the stabilization of the FC pattern to a certain task-specific functional organization. Nevertheless, FCV is still a relatively simple measure, which can only quantify the overall temporal pattern of dynamic FC but ignore the spatial pattern of the networks. New methods are needed to depict the detailed spatiotemporal dynamics of brain networks during both rest and task. Thus, we propose to use k-means clustering to investigate spatiotemporal patterns of dynamic brain networks during both rest and task. Based on previous findings by static and dynamic FC analysis, we hypothesize the presence of overall spatial similarity while distinct temporal patterns between the rest and task.

In order to test this hypothesis, we analyzed the spatiotemporal patterns of the task-state brain networks during motor task and compared with resting state. The hand closing and closing (HCO) task was utilized in our study for its easiness to perform and its ability to effectively activate the motor system [216-218]. The HCO task has also been

widely used in upper limb rehabilitation after stroke [219-221]. Thus, investigating the alteration of the task-state brain networks during HCO may also help understand the mechanisms underlying stroke rehabilitation. In addition to the motor-related networks (represented by MN hereafter) activated by HCO, DMN has also been demonstrated to be a key network in motor task performance and other cognitive processes [222-224]. Studying the dynamic interactions between MN and DMN during HCO could help to reveal the brain's cognitive adaptation to task demands. Therefore, both DMN and MN were selected as networks of interest. Principal dynamic FC states were identified by *k*-means clustering of sliding windows [115, 122]. We then compared the spatiotemporal patterns of principal FC states as well as the FCV under both rest and HCO conditions.

4.2 Methods

4.2.1 Participants

Twenty-eight healthy right-handed subjects volunteered for this experiment and two subjects were excluded because of excessive head motions (maximal head motion above 2mm or 2°). As a result, data of the twenty-six subjects (male/female: 13/13; Age: 54.9 ± 6.3 years) were used for further analysis. All subjects provided written informed consents. Procedures were reviewed and approved by the Ethics Committee of Shanghai Second People's Hospital, Shanghai, China.

4.2.2 Task design

The fMRI experiment for each subject consisted of two FC sessions (REST and HCO) and one block-design activation session. During REST session, subjects were instructed to remain motionless, relaxed and awake. During HCO session, subjects were asked to perform HCO with the instructed hand at a rate of one time per second paced by the cues on the display. For both of these sessions (REST and HCO), 4 minutes and 20 seconds data were used for FC analysis. The third session was a block-design task consisting of six REST blocks alternated with five HCO task blocks, preceded by an 8-sec inter-task period. Each block lasted for 20s. This block-design session was used to generate candidate ROIs of the MN for FC analysis. All subjects were divided into the left hand group (LHG, n=16) or the right hand group (RHG, n=10). Subjects were instructed to use only the given hand during HCO task performance.

4.2.3 Image acquisition

All images were acquired with a 3.0 T Signa Excite Gemse MRI system (GE Healthcare, Milwaukee, WI, USA) at Rui Jin Hospital, School of Medicine, Shanghai Jiao Tong University, Shanghai, China. The head of the subject

was snugly fixed by a foam pad to reduce head movements and scanner noises. 3D structural MRI was acquired from each subject using a T1-weighted MPRAGE sequence (TR = 5.6 ms; TE = 1.7 ms; filp angle = 12°; matrix size = 256×256; voxel size = 1×1×1 mm^3), yielding 196 contiguous sagittal slices (1 mm thick) covering the whole brain. BOLD data were acquired with an EPI sequence (TR = 2000 ms; TE = 30 ms; flip angle = 90°; matrix size = 64×64; voxel size = 3.75×3.75×4 mm^3) for each subject.

4.2.4 FC data preprocessing

For both REST and HCO periods, identical preprocessing procedures were performed using SPM8 (Wellcome Trust Centre for Neuroimaging, University College London, London, UK) and MATLAB scripts from the DPARSFA toolbox [225]. The data of the first 10s (5 volumes) were discarded to avoid magnetization equilibrium effects and to allow the subjects to get ready for the experiments. The remaining fMRI data were spatially realigned to the mean image and then were slice-timing corrected using the middle slice as the reference frame, de-trended and band-pass filtered (0.01 Hz – 0.08 Hz). In addition, the fMRI data were co-registered with each subject's anatomical data using mutual information as the cost function. fMRI data were interpolated using 4^{th} degree B-spline method [225] for its lower spatial resolution than anatomical images. The anatomical images were then segmented [226]. Spherical ROIs with 10 mm diameter were centered at predefined coordinates and warped to the subject's native brain-space based on the deformation field obtained from segmentation step. The representative BOLD time course for each ROI was defined as the average over all voxels within the ROI in the native brain space. Nuisance covariates, including Friston 24 parameters of head motion [227], white matter and cerebrospinal fluid signals were then regressed out from the representative BOLD time courses.

4.2.5 Motor network ROI identification

In order to define the motor-related brain regions, activation based on block-design session was analyzed. Separate preprocessing was performed for block-design session data with SPM8 and DPARSFA toolbox, including spatial realignment to the mean volume of a series of images, slice-timing correction, co-registration, spatial normalization to the MNI template, spatial smoothing (4 mm isotropic kernel) and high-pass filtering (eliminating slow signal drifts with a period longer than 128 s). For the first-level analysis of each subject, general linear model (GLM) in SPM8 was used to generate the individual activation map. Boxcar vectors for task blocks were convolved with the hemodynamic response function (HRF) and the head movement parameters were included as covariates to remove head motion artifacts. One-sample *t*-test based on single-subject contrasts obtained in the first-level analysis were performed for LHG and RHG, respectively, resulting in group-level activation mappings ($p<0.001$). By

combining group-level activation maps of LHG and RHG, we obtained the MNI coordinates of 44 activated motor-related brain regions.

4.2.6 Analysis of dynamic FC

ROIs included regions in MN and DMN. For MN, the coordinates of the 44 activated local maxima obtained during the block-design session were regarded as the coordinates of ROIs. The coordinates of the 46 ROIs in DMN were defined according to [228]. Thus, there were a total of 90 ROIs in the network-of-interest (denoted as DMN-MN hereafter) in total. The representative BOLD time courses of all ROIs were obtained by the methods in Data Preprocessing section.

For each subject, representative BOLD time courses of REST and HCO were analyzed by sliding windows (size: 30 TRs or 60 s each) with a step of 1 TR (2 s), resulting in 96 windows in total [95, 122]. The choice of sliding window size was justified by previous studies, which reported that cognitive states may be correctly identified from covariance matrices estimated on as little as 30-60 s of data [118, 229]. Within each sliding window, Fisher-transformed correlations were calculated between representative BOLD time courses of every pair of ROIs and a 90×90 association matrix was estimated.

4.2.7 Clustering

In order to identify reoccurring FC states, the *k*-means clustering algorithm [230] was implemented to classify the sliding windows into a set of separate clusters by their association matrices. L1 distance function (Manhattan distance or L1-norm), defined as

$$d_1(\boldsymbol{p}, \boldsymbol{q}) = \sum_{i=1}^{n} |(p_i - q_i)| \quad (4.1),$$

was used to estimate the within- and between- clusters distances [231], where $d_1(\boldsymbol{p}, \boldsymbol{q})$ represents the L1 distance between two vectors $\boldsymbol{p}, \boldsymbol{q}$ in an *n*-dimensional real vector space, p_i and q_i represent the *i*th elements of $\boldsymbol{p}$ and $\boldsymbol{q}$ respectively.

As described by Allen and colleagues [122], two-step clustering was used. In the first step, the sliding windows with local maxima in spatial variance of association matrices were selected as exemplars for each subject. Then, *k*-means clustering was performed on those exemplars selected from subjects. The clustering was repeated 100 times independently with a random initial centroid position every time and the best result was selected so as to increase the chance of escaping the local minima. The optimal number of clusters was determined based on the elbow criterion of cluster validity index, i.e., the ratio of within-cluster distances to between-cluster distances using *k* from 2 to 10

[122]. For LHG, one set of exemplars was selected from sliding windows of 16 subjects for REST and HCO respectively. For the clustering of exemplars in LHG, the optimal numbers of clusters were estimated as 6 (i.e., k=6) in each session (REST and HCO). With respect to RHG, identical procedures were performed and *k*=4 was estimated as optimal in each session (REST and HCO). In the second step, the centroids of resulting clusters for each session and each group were used to initialize the clustering used in the analysis of the full sliding time-windows.

4.2.8 FCV over time

FCV was estimated to further examine the temporal patterns of dynamic FC during both REST and HCO in each network: DMN, MN, DMN-MN and the inter-network connecting DMN and MN (denoted as iDMN-MN hereafter). FCV of a network was estimated by calculating the standard deviation of the averaged FC strength in a network across all sliding time-windows [95, 119], that is,

$$\mathrm{FCV} = \sqrt{\frac{1}{M} \times \sum_{i=1}^{M} (\bar{x}_i - \bar{X})^2} \tag{4.2}$$

where $\bar{x}_i$ represents the mean strength of FC among networks in the ith window, $\bar{X}$ represents the mean of $\bar{x}_i$ across all sliding windows, and M is the number of the windows.

4.2.9 Statistical analysis

In order to evaluate how the task modulated the temporal patterns of FC states, the frequency of state shifting (number of shifting times between FC states within 125 TR-long recording time) was compared between REST and HCO for both LHG and RHG. Since the frequency of state shifting was count data, they did not follow a normal distribution and ANOVA was not considered statistically appropriate.

According to previous studies, generalized linear model (GLM) with Poisson distributed error can be used to perform statistical analysis for count data [232, 233]. Nonetheless, the Poisson distribution requires the mean equals to the variance, whereas the variance of our data was significantly larger than the mean, which is called "overdispersion". Thus, the best option for our data is to specify that the data follow the negative binomial distribution according to previous studies [234, 235]. A generalized linear model with negative binomial distributed error was used to examine the effect of session (REST vs. HCO) as well as group (LHG vs. RHG) on the state shifting frequency [234, 235]. The negative binomial regression model is as follows:

$$\tilde{\mu}_{ij} = \exp(\alpha + \beta_1 s_j + \beta_2 g_i) \tag{4.3}$$

where $\tilde{\mu}_{ij}$ is the expected state shifting frequency for subject i (i = 1 to N; N = 26) during session j (REST and HCO), s_j represents the categorical variable of the session (i.e., s_j = 1 for REST; s_j = 0 for HCO), g_i represents the

categorical variable of the group (i.e., g_i = 1 for subjects in LHG, g_i = 0 for subjects in RHG), β_1 and β_2 are the coefficients to be estimated and α is the intercept. If the estimated β_1 is significantly greater (less) than zero, the statistical result would indicate that the state shifting frequency during REST is greater (less) than that during HCO. If the estimated β_2 is significantly greater (less) than zero, the statistical result would indicate that the state shifting frequency of LHG is greater (less) than that of RHG. Incidence rate ratios (IRR, i.e., exp(β)) were calculated [235], which indicates the relative difference of state shifting frequencies between two categories (e.g., REST vs. HCO; LHG vs. RHG). Taking β_1 as an example, with all other factors being equal, the greater IRR(β_1) is, the greater state shifting frequency in REST is, comparing with that in HCO. In addition, the Chi-square goodness of fit test was conducted to how much the data could fit a negative binomial model [236].

4.3 Results

4.3.1 FC states by k-means clustering

As estimated by the elbow criterion of cluster validity, the optimal number of clustering FC states was six in LHG and four in RHG for both REST and HCO states. In both groups, only two principal FC states were identified in all subjects during REST. The remaining FC states during REST (4 FC states in LHG and 2 FC states in RHG) were absent in multiple subjects. While for HCO condition, only one principal FC state was identified in each handed group. Centroids of the principal FC states for REST and HCO in both groups were illustrated in Fig. 4.2. Similarities of principal FC states between LHG and RHG were estimated through correlational analysis, indicating significant similarities between the principal FC states in two groups (i.e., the 1st principal FC state of LHG REST and RHG REST: R = 0.619, p < 0.001; the 2nd principal FC state of LHG REST and RHG REST: R = 0.449, p < 0.001; the 1st principal FC state of LHG HCO and RHG HCO: R = 0.672, p < 0.001). In addition, in both groups, significant similarity was observed between the principal FC state in HCO and the 1st principal FC state in REST (i.e., LHG: R = 0.716, p < 0.001; RHG: R = 0.626, p < 0.001).

4.3.2 Dwell time ratios of principal FC states in REST

To understand the temporal patterns of dynamic FC in REST, we examined the “dwell time” of the two principal FC states in REST. Dwell time ratio, i.e., the number of windows in one principal FC state over the total number of windows, was defined to quantify the “dwell time” of the corresponding state. Mixed-design ANOVA with one between-subjects variable (i.e., GROUP: LHG vs. RHG) and one within-subjects variable (i.e., STATE: the 1st principal FC state vs. the 2nd principal FC state) were performed. The main effect of STATE was significant (F(1,19) = 4.773, p = 0.042), but the main effect of GROUP was not significant (Fig. 4.3). The statistical results demonstrated

that the "dwell time" of the 1st principal FC state was significantly longer than that of the 2nd principal FC state in REST for either LHG or RHG.

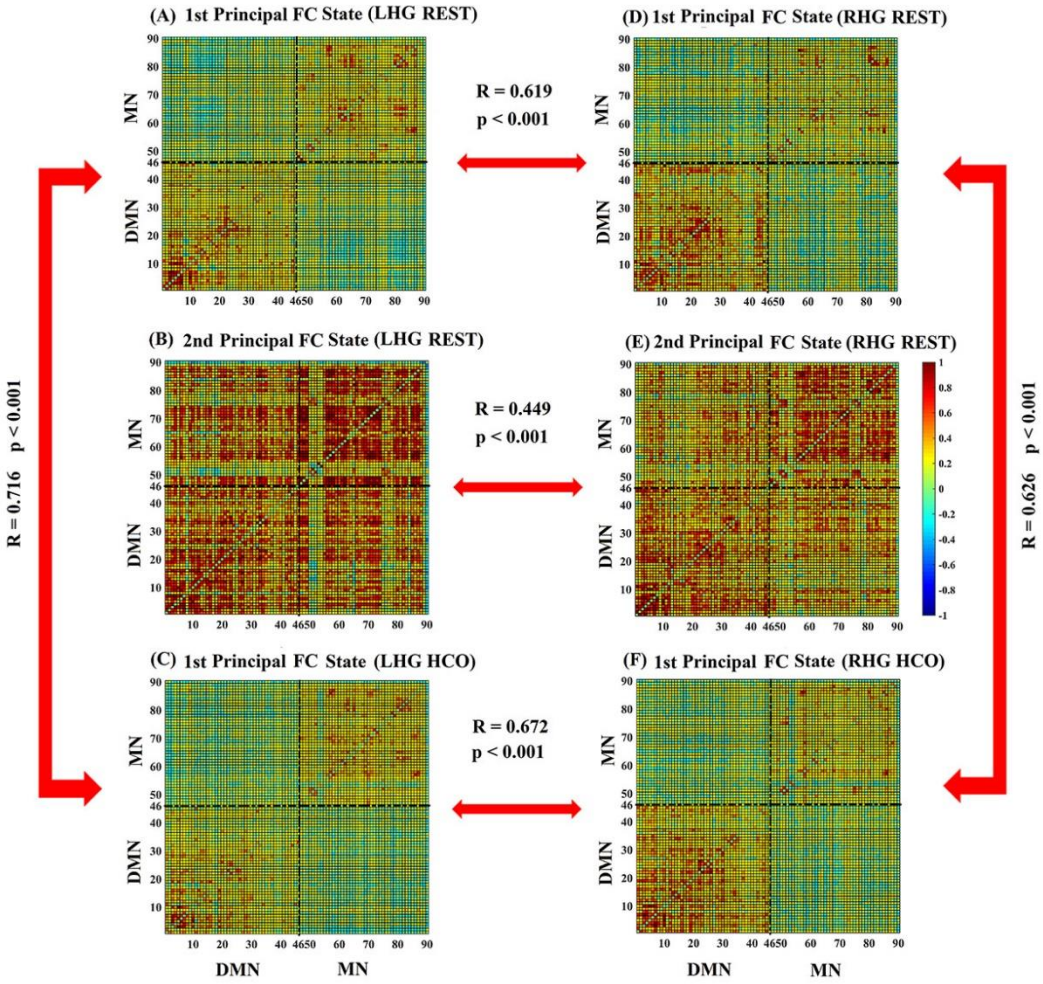

Figure 4.2. (A-B) Centroids of two principal FC states of REST in LHG; (C) Centroid of the only principal FC state of HCO in LHG; (D-E) Centroids of two FC principal FC states of REST in RHG; (F) Centroid of the only principal FC state of HCO in RHG. DMN: ROI 1 to ROI 46; MN: ROI 47 to ROI 90.

4.3.3 Difference between two principal FC states in REST

In addition to "dwell time", FC pattern between the two principal FC states were also investigated for both LHG and RHG. Paired *t*-test showed significantly different FC between two principal FC states in REST ($p < 0.01$).

For LHG (Fig. 4.4(A)), among the 132 significantly different connections, 13 (percentage in all connections in DMN: 13/1035 = 1.26%) corresponded with the DMN, and 46 (46/946 = 4.86%) were found in the MN and 73 (73/2024 = 3.61%) were present in the iDMN-MN. For RHG (Fig. 4.4(E)), 147 significantly different connections were identified, with 11 (1.06%) located in the DMN, 41 (4.33%) in the MN, and 95 (4.69%) were associated with iDMN-MN. For both LHG and RHG, all significantly different connections increased in strength during the 2nd principal FC state in contrast to the 1st principal FC state of REST. The majority of significantly different connections were located in the iDMN-MN for both LHG and RHG. As the matrix of principal FC state was symmetric, only the lower part of diagonal was shown in Figs. 4.4(A) and 4.4(C). Figure 4.4 also presents the ROIs and significant connections between other regions. We observed that there were less significantly different connections in the DMN compared with MN and iDMN-MN networks in both LHG and RHG groups.

In addition to the specific differences in FC, the overall similarities of the DMN, MN, and iDMN-MN networks with the principal FC states were also investigated by correlational analysis (correlation coefficient was r-to-z transformed by Fisher transformation) for each subject. Mixed-design ANOVA with one between-subjects variable (i.e., GROUP: LHG vs. RHG) and one within-subject variable (i.e., NETWORK: DMN, MN, and iDMN-MN) was performed. Post-hoc comparisons of transformed correlation coefficients in each network (i.e. DMN, MN and iDMN-MN) were adjusted using Bonferroni correction. It was noted that the transformed correlation coefficients of iDMN-MN between the principal FC states were significantly smaller than those of either DMN or MN (Fig. 4.5).

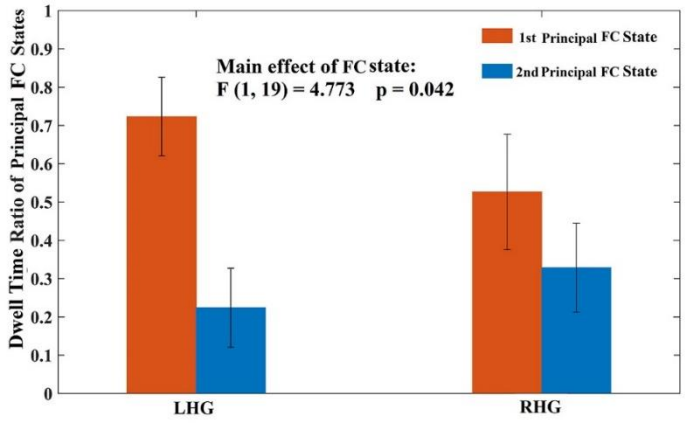

Figure 4.3. Illustration of dwell time ratio of principal FC states in LHG and RHG in REST. Error bars indicate the standard error of the mean (SEM) across subjects.

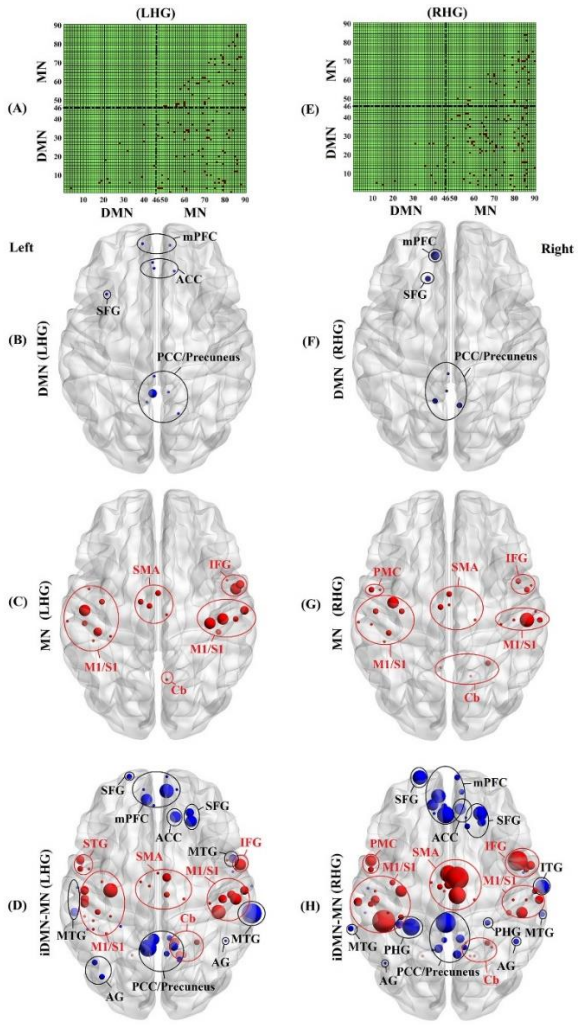

Figure 4.4. Illustration of significantly different FC between the principal FC states of REST in LHG (A) and RHG (E); ROIs in DMN (blue nodes) connected by significantly different DMN FC in LHG (B) and RHG (F); ROIs in MN (red nodes) connected by significantly different MN FC in LHG (C) and RHG (G); and ROIs in DMN (blue nodes) and MN (red nodes) connected by significantly different iDMN-MN FC in LHG (D) and RHG (H). The size of the nodes indicates the ROI degree of FC (i.e., the number of significantly different FC connected to ROI). PCC = posterior cingulate cortex; mPFC = medial prefrontal cortex; SFG = superior frontal gyrus; MTG = middle temporal gyrus; M1 = primary motor cortex; S1 = primary somatosensory cortex; SMA = supplementary motor cortex; STG = superior temporal gyrus; ACC = anterior cingulate cortex; IFG = inferior frontal gyrus; PMC = premotor cortex; AG = angular gyrus; Cb = cerebellum; PHG = parahippocampal gyrus.

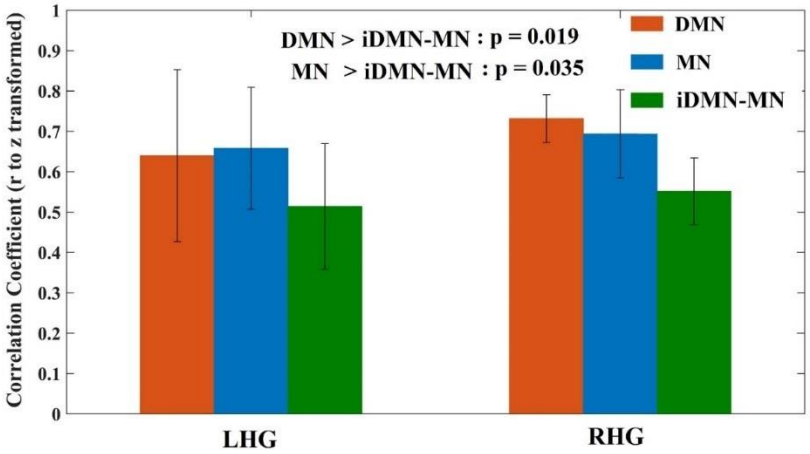

Figure 4.5. Similarities (indicated by correlation coefficient, which was r to z transformed) of DMN, MN, and iDMN-MN between two principal FC states in REST for LHG and RHG respectively. Error bars indicate the standard error of the mean (SEM) across subjects.

4.3.4 Differences in state shifting frequency between REST and HCO

In order to compare the dynamic patterns of the networks in REST and HCO, we investigated the state shifting frequency (i.e., number of shifting times across different FC states including non-principal states) in both groups. Table 4.1 lists the results of negative binomial regression model estimation. The estimated coefficient for session type variable (1 for REST and 0 for HCO) was positive and significantly different than zero ($p = 0.030$). Even though the coefficient of group variable (1 for LHG and 0 for RHG) was also positive, it did not significantly differ from 0. The IRR for the session variable was 3.212, indicating that with all other factors being equal, an average increase of 212.2% in the state shifting frequency was observed during REST compared with HCO. The statistical results suggest that state shifting frequency was significantly increased during REST compared with HCO in either group. In addition, Chi-square goodness-of-fit test suggested that the negative binomial model could be appropriately used to fit the data since the null hypothesis that the data were consistent with the negative binomial model could not be rejected ($p = 0.191$).

4.3.5 Different FCV between REST and HCO

For each subject, the FCVs of DMN, MN, DMN-MN, iDMN-MN were calculated for both REST and HCO. Mixed-design ANOVA with one between-subjects variable (i.e., GROUP: LHG vs. RHG) and one within-subject variable (i.e., SESSION: REST vs. HCO) were performed for each network examine the effect of session on the FCV. Significant main effect of session type was found on FCV of the DMN-MN ($F(1, 24) = 5.466$, $p = 0.028$), MN FC

(F(1, 24) = 9.131, p = 0.006) and iDMN-MN FC (F(1, 24) = 6.404, p = 0.018) (Fig. 4.6). These results suggest that the FCV of the DMN-MN network, MN, and iDMN-MN significantly decreased during HCO compared with REST for both LHG and RHG groups.

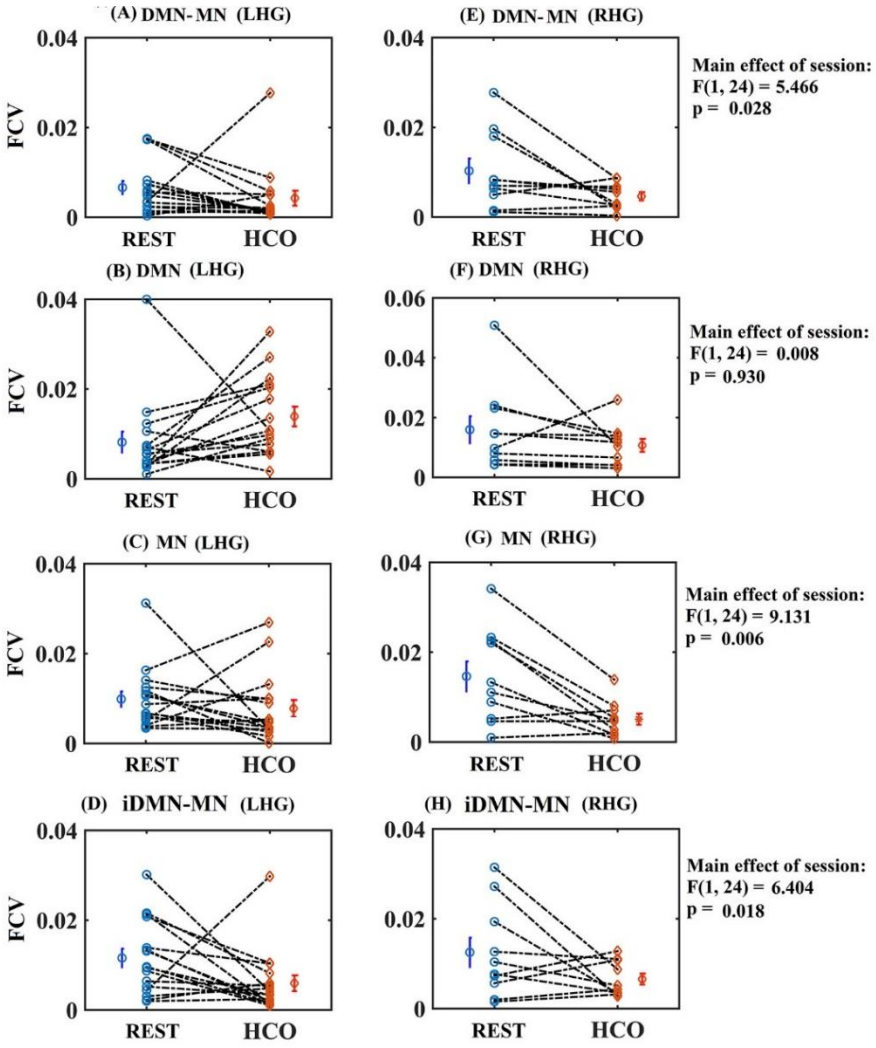

Figure 4.6. Demonstration of FCV in the DMN-MN during REST and HCO in the LHG (A) and RHG (E); FCV in the DMN in LHG (B) and RHG (F); FCV in the MN in LHG (C) and RHG (G); and FCV in the iDMN-MN in LHG (D) and RHG (H). Blue circles and each red diamonds represent FCV during REST and HCO respectively for individual subjects. Error bars with corresponding markers represent the mean and its standard error of mean (SEM) across subjects.

Table 4.1. Estimated coefficients of negative binomial regression model for incidence rate ratios in state shifting frequency.

	Estimate (IRR)	Std. Error	*z* value	*p* value
(Intercept)	-1.486	0.582	-2.554	0.011*
Coefficient (Group)	0.673 (1.960)	0.558	1.206	0.228
Coefficient (Session)	1.167 (3.212)	0.537	2.171	0.030*

4.4 Discussion

In this chapter, the dynamic FC of brain networks including DMN and MN, as well as their variability (FCV), were examined using sliding windows and *k*-means clustering. Principal FC states were identified and their spatiotemporal patterns were compared between REST and HCO. During REST, two principal FC states were identified in both the LHG (Figs. 4.2(A) and 4.2(B)) and RHG (Figs. 4.2(D) and 4.2(E)), with significant similarities between the two groups. For HCO, a single principal FC state was identified in LHG (Fig. 4.2(C)) and RHG (Fig. 4.2(F)), which also featured a significant similarity between the two groups. These results indicated a correspondence of principal FC states between both groups across both REST and HCO experimental conditions. When comparing principal FC states in REST and HCO, significant similarity was also found between the single principal FC state in HCO and the 1st principal FC state in REST regardless of the hand used (Fig. 4.2). This finding verified our hypothesis on the overall spatial similarity of dynamic FC between rest and task states. Previous studies on static FC have observed overall FC similarity between rest and task [34, 237, 238]. Specifically, Cole and colleagues used static FC to investigate the similarities of large-scale networks, which covered hundreds of brain regions encompassing every major brain system, examining differences between dozens of task sessions and the resting state. Their results proposed that task-state functional networks were shaped primarily by an intrinsic network architecture that was also present during rest, and secondarily by evoked task-related network changes [239]. In another study on the relationship between structural connectivity (SC) and FC, Hermundstad and colleagues found that structural properties (i.e., length, number and spatial location of white matter fibers) were indicative of the strength of FC in both rest and task states [240]. These results based on static FC both proposed that the brain networks during both rest and task might be primarily shaped by a common intrinsic network architecture. Our dynamic FC study found similar principal FC states between REST and HCO, which were the 1st principal FC state in REST and the only

principal FC state during HCO. We observed that these two related principal FC states were dominant during REST and HCO as measured by dwell time ratios (Fig. 4.2). Thus, we speculated that the common intrinsic network architecture, which primarily shapes both resting-state and task-state network in static FC study, presented itself in similar dominating principal FC states observed in REST and HCO. Despite these similarities with static analysis, dynamic FC can provide more information than static FC. The 2nd principal FC state in REST might reflect a specific mental activity in REST not present during HCO, and its absence in HCO might represent a focus on motor task execution. A previous study demonstrated that mental activity during rest was unconstrained and individuals could freely engage in several types of mental activity [241]. This unconstrained mental activity might be represented in part by the 2nd principal FC state of REST.

Though the 2nd principal FC state in REST might indicate unconstrained mental activity during REST, what kind of brain activity it represents and its role in the "default mode", especially for motor system, are still not well understood. From the perspective of individual connection changes in FC, differences between two principal FC states in REST were most numerous in the iDMN-MN and MN. In addition, all significantly different FC increased in strength during the 2nd principal FC state compared with the 1st principal FC state (Fig. 4.3). Furthermore, from the perspective of overall network pattern, the differences between these two principal FC states were mainly observed in the iDMN-MN (Fig. 4.3). Strengthened interactions between DMN and MN during the 2nd principal FC state of REST, was consistent with previous findings that core ROIs in DMN, such as PCC, most frequently engaged with non-DMN ROIs through inter-network FC [119, 242]. A recent study using network control theory investigated how the brain shifts between cognitive states based on network organization of white matter microstructure. The authors found that the "default mode" during resting state was a pluripotent "ground status" which was able easily to migrate to multiple task-based statuses with less cognitive effort by using connections between DMN and other networks [243]. Taken together with these findings, our results implied that during the REST, DMN could be interacting with MN through iDMN-MN FC, manifested by the 2nd principal FC state, to establish a "default mode" of the MN and prepare for the subsequent motor tasks. During HCO itself, maintaining the "default mode" in motor system may have been of no need, resulting in an absence of a 2nd principal FC state.

In addition, according to the model described in Table 4.1, the maintenance of "default mode" for motor system in REST might be a dynamic process, that is, the DMN-MN network could be observed to frequently shift between the two principal FC states. Concordantly, FCV of the DMN-MN network significantly decreased during HCO compared with REST (Fig. 4.5(A)), a finding which was also in line with recent findings during an attention task [95]. With respect to the individual networks, FCV of MN and iDMN-MN also decreased during HCO (Figs. 4.5(C)

and 5(D)), while no significant change of FCV was observed in DMN (Fig. 4.5(B)). Considering the findings of principal FC states, the increase of FCV in iDMN-MN and MN was probably due to the frequent shift between the principal FC states in REST as the differences between two principal FC states were mainly located in iDMN-MN and MN. During HCO, such a dynamic maintenance of "default mode" in motor system would disappear and result in a stable and lower FCV in iDMN-MN and MN [244]. These findings verified our hypothesis that differences in temporal patterns of dynamic FC between REST and HCO still existed and could reflect distinct mental states present in REST and HCO.

Unlike the MN and iDMN-MN, the FCV of DMN did not change significantly in HCO compared with REST, implying a special role for the DMN in REST and HCO. During the REST, the DMN might not only interact with MN, but also with other networks such as the auditory network, attention network, etc. When involved in a motor task, the MN and iDMN-MN were relatively stable due to an absence of influence of DMN on the motor system, but the DMN might still be interacting with other networks to establish a "default-mode" for other brain functions. Previous studies reported the FCV during resting state was partially caused by the predominance of mind-wandering or day-dreaming during this "uncontrolled" state [95, 119]. Another study suggested that mind-wandering might be part of a larger class of mental phenomena that enable executive processes without diminishing the potential contribution of DMN to other cognitive functions [245]. These descriptions correspond to our speculation that DMN was interacting with multiple function-related networks during REST and its interaction with non-motor networks was not diminished during HCO.

4.5 Chapter conclusion

This chapter investigated the spatiotemporal patterns of task-state brain networks during motor task using fMRI, and focused on the dynamic FC analysis method. We examined FC states and FCV in REST and HCO using sliding windows and *k*-means clustering. Two principal FC states in REST and one principal FC state in HCO were identified. The 1st principal FC state in REST was similar to that in HCO, which likely represented intrinsic network architecture and validated the broadly similar spatial patterns between REST and HCO. However, the presence of a 2nd principal FC state with increased iDMN-MN in REST with shorter "dwell time" could imply the transient functional relationship between DMN and MN to establish the "default mode" for motor system. In addition, the more frequent shifting between two principal FC states in REST indicated that the brain networks dynamically maintained the "default mode" for the motor system. In contrast, during HCO, the presence of a single principal FC state and reduced FCV implied a more temporally stable FC, validating the distinct temporal patterns between REST and HCO. Our

findings suggested that the principal states could show a link between the rest and task states, and verified our hypothesis on overall spatial similarity but distinct temporal patterns of dynamic brain networks between rest and task states. These results showed the effectiveness of dynamic FC analysis when applied to brain activities during rest and task states, and offer new insights into understanding the adaptation of brain networks in response to task performance.

As we proposed in the chapter 1, the purpose of this thesis is to reveal the motor task-specific spatiotemporal changes of brain networks compared with resting conditions, and further applied the task-state brain network analysis in the research of stroke recovery. The chapter 2 revealed the task-specific spatial changes of brain networks compared with resting condition. Because the static FC analysis was used, the findings were mainly from the perspective of spatial patterns of brain networks. In chapter 3 and 4, dynamic FC analysis was adopted so as to provide not only the spatial patterns but also the temporal patterns of the task-state brain networks. Based on fNIRS and fMRI, the spatiotemporal patterns of task-specific changes of brain networks were revealed and the findings illustrated that the temporal patterns of brain networks were also very informative. In general, combining chapter 2 to chapter 4 together, the purpose of revealing the motor task-specific spatiotemporal changes of brain networks compared with resting conditions was comprehensively investigated using static FC and dynamic FC analysis based on both fNIRS and fMRI modalities, and the findings pieced together the understanding of how brain networks work spatiotemporally under motor task compared with resting condition.

Chapter 5: Relationship between task-state motor network and motor function restoration post stroke

5.1 Introduction

In chapter 2 to 4, the task-state brain networks were investigated during motor preparation and motor execution based on fNIRS and fMRI using both static and dynamic FC analysis. In this chapter, the task-state brain network was investigated during stroke and its relationship with stroke recovery was also examined.

Longitudinal neuroimaging studies have found recovery-related hyper-activation in contralesional motor areas [16] and secondary motor areas [17] during the recovery. Dynamic change of brain activity was found in acute stroke based on electroencephalograph (EEG) and event-related de-synchronization (ERD) [246]. In addition, brain reorganization also manifested in the change of FC between different brain regions [247]. For example, brain reorganization induced by stroke would not only significantly suppress the bidirectional ipsilesional effective connectivity between supplementary motor area (SMA) and M1 [248], but also lead to the alteration of inter-hemispheric FC between the bilateral motor areas [38]. Wang and colleagues further found that the motor execution network shifted towards a non-optimal topological configuration with less functional segregation by examining topological change of the motor execution network based on resting-state fMRI during the recovery after stroke [39].

Besides dynamic brain reorganization during the stroke recovery, other studies focused on the prognostic value of brain activity and FC at the early recovery stage. The activity of sensorimotor areas around 5 weeks after stroke was reported to have close relationship with motor function recovery [249]. Furthermore, Loubinoux and colleagues reported relationships between positive outcomes and early activity of ipsilesional M1 (iM1), primary sensorimotor area and insula [250]. Resting-state FC of iM1 with several motor areas at early recovery stage has also been found positively associated with long-term motor function restoration [251].

Previous studies mainly focused on the reorganization of task-related brain activation and resting-state networks after stroke. The reorganization of task-state brain network and its relationship with motor function recovery were rarely reported. Furthermore, resting-state FC and task-state FC were reported to represent different aspects of functional integration [252-254]. Therefore, it is reasonable to infer that the status of resting-state and task-state functional brain networks during stroke recovery, as well as network parameters (FC and topological parameters), might be different, which was verified by a EEG study [255]. In addition, task-state network might provide new information about underlying mechanism of neural response under specific task state and was a promising application

of network models [256]. Furthermore, most recovery after stroke occurred in the first three months post stroke [257], thus, significant motor function recovery would accompany significant changes of brain in this period. With above consideration, we conducted a longitudinal study on the dynamic reorganization of task-state motor execution network during finger-tapping task from several days to three months post stroke. Meanwhile, we investigated the relationships between the initial status of task-state brain networks and the motor function restoration from stroke onset to sub-acute phase (medical stable and no longer than three months post stroke) [258].

In this chapter, BOLD data of twelve stroke patients were acquired while performing blocked finger-tapping task within 10 days (P1), around 2 weeks (P2), 1 month (P3), and 3 months (P4) after stroke respectively. For the blocked finger-tapping task, only the segments of task conditions were concatenated for further analysis. The rest conditions were discarded considering that a recent study found that resting-state was not a stationary process which might be affected by task state and cannot represent real pure resting-state [259]. Therefore, for each scan, only task-state motor execution networks containing 21 motor related brain regions were constructed by within-task FC estimation [237, 260, 261] and the dynamic reorganization was evaluated from the perspectives of pair-wise FC and network topology. Furthermore, the Spearman's correlation coefficients between networks parameters at P1 and motor function restoration during sub-acute phase (indicated by absolute difference of Fugl-Meyer Index (FMI) between P1 and P4) were computed to identify the prognostic network parameters. In general, examining the changes of task-state motor execution networks in stroke recovery would broaden our understanding of rehabilitation and brain reorganization post stroke.

5.2 Methods

5.2.1 Subjects

Twelve stroke patients (male/female: 9/3; mean age: 61.5 years; range of age: 47 to 77 years) were recruited from the Ruijin Hospital affiliated to the School of Medicine, Shanghai Jiao Tong University. Inclusion criteria of patients were: (i) age from 45 to 80 years; (ii) right handedness; (iii) first-onset ischemic stroke with motor deficits; (iv) no history of neuropsychiatric diseases, epilepsy, cerebral vascular abnormalities and trauma; (v) FMI ranging from 50 to 95. For each patient, fMRI BOLD signals were acquired at four post-stroke time points respectively (i.e., P1, P2, P3 and P4 as mentioned in **5.1 Introduction**). Starting from P2, some subjects quit in the follow-up fMRI scans, i.e., ten of twelve patients participated at P2; seven patients participated at P3 and five patients participated at P4, which were listed in Table 5.1. The demographic data and FMIs of patients were also summarized in Table 5.1. The T1-weighted images of one representative patient at four fMRI scans were illustrated in Fig. 5.1(B). Sixteen age-matched

healthy subjects were recruited as a control group. The fMRI data of control group were acquired for only one time with the same scanner in Ruijin Hospital. Note that the network topology of healthy subjects has been reported to be stable across different time [39]. Thus, we presumed that the data of control group were stable across four time points. Inclusion criteria of control group were: (i) age from 45 to 80 years; (ii) right handedness; (iii) no history of neuropsychiatric disease, epilepsy, cerebral vascular abnormalities and trauma. The Ethics Committee of Ruijin Hospital approved the experiment protocols which were in accordance with the Helsinki Declaration of 1975, and each participant gave an informed consent before experiment.

5.2.2 Task design

The fMRI experiment for each subject consisted of two consecutive sessions with a 15 min interval. Patients performed the finger-tapping task with their unaffected hands in the first session and then with their affected hands in the second session, while the control subjects used the left hand in the first session followed by the right hand task in the second session. Each session consisted of resting state (30 s) alternated with task state (30 s) for three repetitions, preceded by 12 s of preparing period (Fig. 5.1(A)). At resting state, subjects were instructed to remain motionless, relaxing and awake; while under finger-tapping task state, subjects tapped the thumb with other fingers one time per second under the voice cues delivered by a physician via a speaker. For patients, fMRI data were acquired at four time points (P1, P2, P3, and P4) after stroke, while the healthy controls only had one fMRI scan.

5.2.3 Data acquisition

All images were acquired by a 1.5 Tesla MRI scanner (Excite HD, General Electric Medical System, Milwaukee, WI, USA) and an 8-channel NVHEAD coil in Ruijin Hospital. The head of the participant was snugly fixed by foam pad to reduce head movements and scanner noises. Whole brain fMRI BOLD data were acquired from the top of the brain to the lower part of the medulla oblongata, using an echo-planar imaging sequence: 32 axial slices, thickness/gap=5/0 mm, matrix=64×64, repetition time=3000 ms, echo time=60 ms, flip angle=90º, and field of view=240 mm×180 mm.

5.2.4 Preprocessing of fMRI data

Before preprocessing of fMRI data, we flipped the data of five right-hemispheric stroke patients from right to left, so that lesions for all patients locate in the left hemisphere, which makes the group analysis convenient. Note this strategy has been used and validated in previous studies [251, 262]. After that, for each subject, the data of the first 12 s preparing period (4 volumes) in each session were abandoned to avoid the magnetization equilibrium effects and also allow the subjects to get ready for the experiments. The remaining fMRI data (60 volumes) were

preprocessed with SPM8 (Wellcome Trust Centre for Neuroimaging, University College London, London, UK) including spatial realignment to the mean volume of a series of images, co-registration, spatial normalization to the MNI template, and spatial smoothing (6 mm isotropic kernel). Finally, the fMRI data was high pass-filtered to get rid of artifacts in extremely low frequencies (<0.01Hz) and regressed out the spurious variance unlikely to reflect neuronal activity (head motion, white matter signal and cerebrospinal fluid signal).

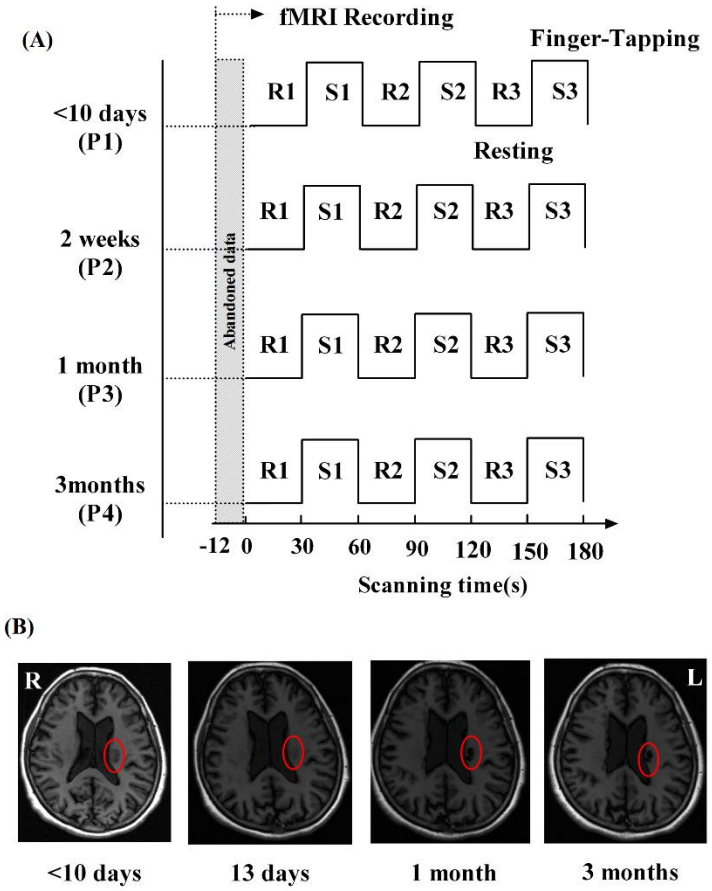

Figure 5.1. (A) The diagram of one session in fMRI experiment. The fMRI experiment consisted of two consecutive sessions with a 15 min interval. Each session was a block design consisting of three resting states (30 s each, R1, R2, R3) alternated with three finger-tapping task states (30 s each, S1, S2, S3). For each patient, the FMI was assessed and fMRI data were acquired at 4 different time points (P1, P2, P3 and P4) after stroke. (B) T1-weighted images of one patient at P1 (<10 days), P2 (2 weeks), P3 (1 month) and P4 (3 months) after stroke. The location of lesion (basal ganglia) is indicated by red ellipse. L=left; R=right.

5.2.5 Regions of interest

In order to investigate the reorganization of motor related system, we constructed a motor execution network consisting of 21 regions of interest (ROIs, see Fig. 5.5) related to the movement of affected hand [39].

5.2.6 Activation analysis of fMRI data

In order to validate the important roles of 21 ROIs in motor execution, we also did activation analysis based on blocked finger-tapping task data at P1. For every subject at affected hand session, the box-car vectors for task state were convolved with a hemodynamic response function. In addition, the head movement parameters were included as covariate to remove the variance induced by head motions, and the default temporal frequency cut off (128 sec high pass) in SPM8 was used. After that, the general linear model was used to perform one-sample t-test based on single-subject contrasts and obtained the group activation maps ($P<0.01$, extent threshold= 10 voxels).

5.2.7 Construction of functional brain networks

Task-state brain networks were constructed by the within-task FC estimation [237, 260, 261] with the following procedures. In each session (moving affected hand and moving unaffected hand), the whole representative time course (60 volumes) for each ROI was obtained by averaging across all voxels within a 10 mm diameter sphere centered at a predefined coordinate. Based on neurovascular coupling, a neuronal activation typically induces an increase in oxygenated hemoglobin and a lower-amplitude decrease in deoxygenated hemoglobin which can be detected by fMRI. However, the hemodynamic response is delayed compared with neural activation. So we shifted each task block by 6s (2 volume) [260] and then the whole representative time course was then split into segments of two different conditions (i.e., rest condition and task condition) After that, the three segments of task conditions in each session were concatenated to represent the whole within-task activities (84 s, 28 volumes, Fig. 5.2) in this session. Pearson's correlation coefficients in within-task concatenated segments for all ROIs in pairs were calculated to obtain the corresponding symmetric association matrix (denoted by *A*). Each entry a_{ij} in the association matrix *A* represented the FC strength, which was the absolute correlation coefficient between the *i*th and the *j*th ROIs. After the estimation of FC, each association matrix was converted into an adjacency matrix *W* by thresholding *A*. The entries (w_{ij}) in *W* were set to be a_{ij} only if they were greater than the threshold (τ), and otherwise set to be zeros (i.e., $w_{ij} = a_{ij}$, if $a_{ij} \geq \tau$, and $w_{ij} = 0$, if $a_{ij} < \tau$). Here, τ was selected according to a preset sparsity defined as the ratio of the existing edge number over the maximum possible number of edges in a network. After repeating the procedures for all association matrices of a subject, at each scanning time point, two task-state motor execution networks (for affected and unaffected hand session respectively) were built.

We set three constraints for the selection of sparsity: (i) in order to estimate the small-world index by graph theory, the average degree of the functional brain networks should not be smaller than $2 \times \ln(N)$ (N is the number of ROIs. For $N = 21$ the sparsity should be greater than 0.3); (ii) in order to study the dynamic change of the whole functional brain networks, at least 99% of the ROIs in the functional brain networks should be connected (in this chapter, the sparsity should be larger than 0.4); (iii) in order to reduce the false discovery rate, the sparsity should be as small as possible [263]. Under these constraints, we chose 0.41 as the sparsity of motor execution networks. In addition, we also calculated the results with sparsities ranging from 0.30 to 0.45 for comparison.

5.2.8 Graph theoretical analysis of functional brain networks

There are various parameters which can be used to evaluate features of networks in graph theory. Among them, clustering coefficient and characteristic path length are widely used to evaluate the functional segregation and integration of brain networks. Previous study about resting-state network reorganization after stroke has already found significantly decreased clustering coefficient during stroke recovery [39]. So we adopted these two parameters and their ratio called small-worldness index to evaluate the small-worldness of networks.

Table 5.1. Patient information and the Fugl-Meyer indexes at four fMRI scan time points after stroke.

No.	**Age**	**G.**	**Lesion locations**	<10d (FMI)	2wk (FMI)	1mon (FMI)	3mon (FMI)
1	70	M	R. lateral ventricle	93 (√)	92 (√)	99 (√)	99 (√)
2	56	M	L. Basal ganglia	53 (√)	55 (√)	61 (√)	66 (√)
3	68	M	L. Parietal lobe	51 (√)	50	53(√)	57(√)
4	77	F	L. Parietal lobe	54 (√)	54 (√)	54	59
5	47	M	R. lateral ventricle	85 (√)	87 (√)	96	97
6	67	F	R. Basal ganglia	73 (√)	77 (√)	79	96
7	60	F	L. lateral ventricle	72 (√)	78 (√)	77 (√)	86 (√)
8	56	M	L. Corona radiate	71 (√)	75 (√)	75	75
9	69	M	L. Basal ganglia	59 (√)	55	62	63
10	58	M	R. Basal ganglia	94 (√)	94 (√)	99 (√)	99 (√)
11	60	M	R. Basal ganglia	63 (√)	62 (√)	71 (√)	81 (√)
12	50	M	L. Basal ganglia	95 (√)	95 (√)	99 (√)	99

G = Gender; M=Male; F=Female; R = Right; L = Left; yr=year; d=day; wk=week; mon=month; FMI=Fugl-Meyer Index; (√) indicates that the fMRI data of the subject were collected as well in the corresponding time point.

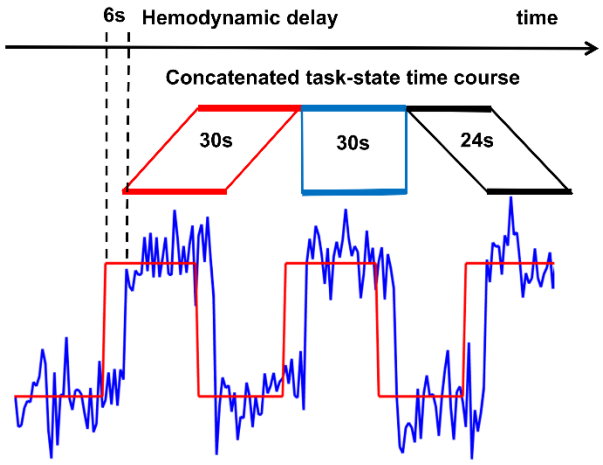

Figure 5.2. A schematic diagram for extracting within-task representative time courses. A temporal shift of 6 s (2 volumes) was adopted accounting for the hemodynamic delay. This method was adopted and verified by previous studies [237, 260]

For nodal parameters, we chose nodal betweenness as an index of centrality in functional networks, considering that nodal degree is dependent on the size of network and thus may be biased[256].

The clustering coefficient and the characteristic path length are two basic parameters characterizing the local and the global topological properties of a network respectively [101, 264]. For a weighted graph (representing a functional brain network), the clustering coefficient of a node (representing an ROI) j is defined as

$$C_{ij}^{w} = \frac{1}{s_j(k_j-1)} \sum_{(i,k)} \frac{w_{ij}+w_{ik}}{2} a_{ij} a_{ik} a_{jk}, \tag{5.1}$$

where s_j represents the nodal strength, which is defined as the sum of the weights (representing the strength of FC) w_{ij} of the edges (representing the FC) connected to node j, k_j is the node degree, which is defined as the number of the edges connected to node j [265]. The clustering coefficient C^w of the whole network is accordingly defined as the average of the nodal clustering coefficients of all nodes. C^w indicates how densely the nodes in a network are locally connected to each other.

The characteristic path length of a weighted network is defined as

$$L^w = \frac{N(N-1)}{\sum_{i=1}^{N} \sum_{j \neq i}^{N} 1/l_{ij}^{w}} \tag{5.2}$$

where l_{ij}^{w} represents the weighted shortest path length between node i and node j , and N is the number of nodes in the network [266]. L^{w} generally quantifies the length of the shortest path that links two nodes in a network.

In this chapter, we also calculated the nodal betweenness, which is defined as

$$B_i = \sum_{s \neq i \neq t} \frac{P_{st}(i)}{P_{st}} \tag{5.3}$$

for node *i*, where $P_{st}(i)$ represents the number of shortest paths from node *s* to node *t* via node *i*, and P_{st} is the total number of shortest paths connecting node *s* and node *t* [267].

In order to account for the variability across different scanning sessions and subjects, we calculated the normalized clustering coefficient ($C^{n} = C^{w}/C_{rand}^{w}$), characteristic path length ($L^{n} = L^{w}/L_{rand}^{w}$) and nodal betweenness ($B^{n} = B^{w}/B_{rand}^{w}$) by comparing the values of parameters with the corresponding average values across 50 random graphs with preserved degree distribution [268]. In addition, we computed the small-world index ($S = C^{n}/L^{n}$) to evaluate the small-worldness of the functional brain networks.

5.2.9 Statistical analysis

To study the longitudinal trend of task-state motor execution networks during stroke recovery, a mixed-effects regression model was adopted to estimate the correlation between network measurements (i.e., FC strength, topological parameters) and the days of recovery or FMIs [269]. This model takes advantages of the data from every time points of patients, including the available time points of those patients who missed some follow-ups. The model is as follows,

$$Y_{ij} = \mu + b_i + X_{ij}\beta + \varepsilon_{ij}, \tag{5.4}$$

where μ is the common intercept for all subjects, b_i is the random intercept for the *i*th patient, β is the scalar (i.e., the trend) of fix effect. Y_{ij} denotes a parameter of the brain network for the *j*th fMRI scan of the *i*th patient and X_{ij} represents the number of days from stroke onset to the *j*th fMRI scan of the *i*th patient when estimating the longitudinal trend over time. However, when estimating the relationship with motor function restoration, Y_{ij}represents the FMI at the *j*th fMRI scan of the *i*th patient and X_{ij} denotes a parameter of the brain network for the *j*th scan of the *i*th patient. ε_{ij} represents the residual error of the model, and *K* is the number of patients.

In addition, Spearman's correlation coefficients between network measurements (topological parameters, FC and nodal betweenness) at P1 and the difference of FMI between P1 and P4 (denoted by $D_{FMI} = FMI(P4) - FMI(P1)$)

were computed to investigate the link between network measurements at the early stage post stroke and the motor function recovery during sub-acute phase.

5.3 Results

5.3.1 Dynamic change of task-state motor execution networks

C^n, L^n and S quantify the local information processing efficiency, the overall information transferring efficiency and small-worldness of networks respectively. Two-sample *t*-tests were performed between patients (C^n: 1.18±0.15; L^n: 0.99±0.01; S: 1.19±0.16) and controls (C^n: 1.17±0.12; L^n: 0.99±0.03; S: 1.17±0.13) for these three parameters at P1, but no significant results were found. In addition, we examined the changes of these topological parameters over recovery time (days after stroke) and their correlations with FMI by mixed-effects regression model (Eq. 5.4). Here, we only presented the results in affected hand session to figure out the reorganization of disrupted motor execution networks under task state. Note that changes of the topological parameters in unaffected hand sessions were calculated but no significant results were found. Hereafter, without specific note, the task-state networks denote the task-state networks in affected hand sessions. We found that C^n had a significantly negative ($p = 0.04$) correlation with the FMI (Fig. 5.3(A)). In addition, L^n significantly decreased ($p = 0.04$) over recovery time (Fig. 5.3(C)) and had a significantly negative ($p = 0.03$) correlation with FMI (Fig. 5.3(B)). However, S did not show any significant correlations with recovery time and FMI. Results of topological parameters in motor execution networks are presented at a sparsity of 0.41. Nevertheless, we have also calculated results at sparsities from 0.3 to 0.45 and found that the statistical results at sparsities around 0.41 were similar (Fig. 5.3(D)).

5.3.2 Potential prognostic value of topological parameters at early recovery stage

In order to investigate the potential prognostic value of the topological parameters in task-state motor execution networks at early recovery stage, the Spearman's correlation coefficients between topological parameters at P1 and D_{FMI} were computed to indicate the statistical dependence between these two variables. Significant positive correlations with D_{FMI} were found for C^n and S (Figs. 5.4(A) and 5.4(B)). Similar results were found at sparsities from 0.4 to 0.45 (Fig. 5.4(C)).

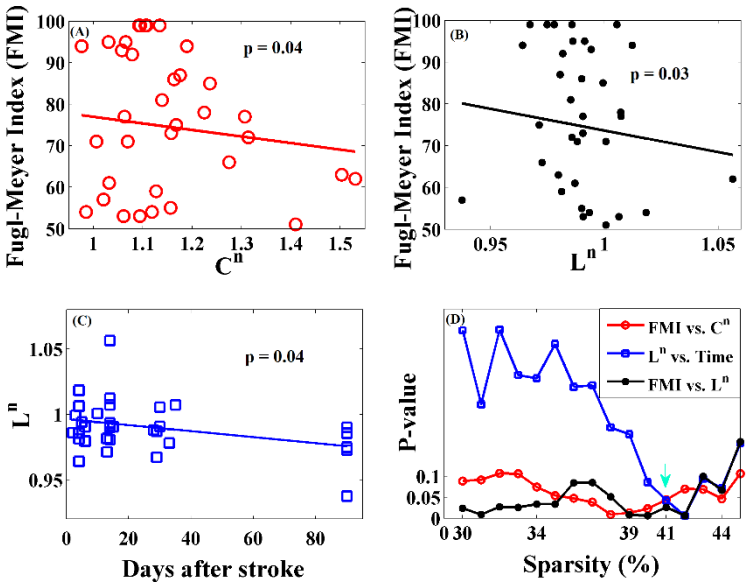

Figure 5.3. Change of task-state motor execution network over time and FMI. Panel (A) illustrates the significant negative (p=0.04) correlation between C^n and FMI; panel (B) shows the significant negative (p=0.03) correlation between L^n and FMI; panel (C) demonstrates the significant negative (p=0.04) correlation between L^n and days after stroke. Panels (A) to (C) are the results at sparsity of 0.41. Each line in panel (D) with the same marker and color as one in panels (A) to (C) represents the p values of corresponding results at sparsity from 0.3 to 0.45. The green arrow in panel (D) indicates the p values at sparsity of 0.41. Note that the regression lines in panels (A), (B) and (C) were not estimated by standard least squares linear regression analysis. Instead, we used mixed-effects regression model which regarded all subjects' data as a panel dataset, and each subject had an individual random intercept and shared a common trend as well as a fixed intercept. The lines in panels (A), (B) and (C) represented the common trends (i.e., the scalar β in Eq. (5.4)) and fixed intercepts (i.e., the common intercept μ in Eq. (5.4)) for all patients. Therefore, the regression lines for different patients were parallel and spaced by the intercepts (i.e., random intercept b_i in Eq. (5.4)).

5.3.3 Group-level activated regions of affected hand session

Based on group-level activation analysis, we found several activated brain regions during affected hand session. Among the activated brain regions, we found 14 brain regions which overlapped with most predefined 21 ROIs

except for BG. Some of these brain regions were activated in bilateral hemisphere (i.e., Dorsal premotor cortex; Ventral premotor cortex; Thalamus; Cerebellum and Supplementary motor area) and some were only activated in ipsilesional hemisphere (i.e., Primary motor cortex; Superior parietal lobe and Postcentral gyrus). Table 5.2 listed all group-level activated brain regions which overlapped with predefined 21 ROIs during affected hand session at P1. Note that there were several activated peaks in some brain regions (i.e., contralesional Thalamus and bilateral Cerebellum) and the SCb, AICb and DN of the predefined 21 ROIs are all located in the cerebellum.

Table 5.2. Group-level activated brain regions which overlapped with predefined 21 ROIs during affected hand session at P1

Region (Side)	*z* value	*p* value	Coordinates (MNI)		
			x(mm)	y(mm)	z(mm)
Primary motor cortex (IL)	4.20	0.0000	-39	-30	72
Dorsal premotor cortex(IL)	3.71	0.0001	-15	-24	81
Ventral premotor cortex (IL)	3.68	0.0001	-60	9	24
Supplementary motor area (IL)	3.11	0.0009	-9	-6	81
Thalamus (IL)	3.30	0.0005	-12	-18	-9
Superior parietal lobe (IL)	2.87	0.0021	-21	-51	57
Postcentral gyrus (IL)	2.79	0.0026	-33	-39	33
Cerebellum (IL)	2.73	0.0032	-33	-54	-27
	2.64	0.0041	-27	-66	-21
Cerebellum (CL)	3.56	0.0002	30	-51	-27
	3.36	0.0004	6	-81	-15
Anterior cerebellar lobe (CL)	3.20	0.0007	9	-54	-21
Dorsal premotor cortex (CL)	3.30	0.0005	36	12	66
Supplementary motor area (CL)	3.20	0.0008	9	-3	60
Thalamus (CL)	2.99	0.0014	21	-21	15
	2.93	0.0016	6	-6	12
	2.57	0.0050	3	-15	15
Ventral premotor cortex (CL)	2.59	0.0048	54	6	9

IL=ipsilesional; CL=contralesional;

5.3.4 Dynamic change of FC

For FC, two sample *t*-test was performed between control group and patient group at P1. Eleven FC were significantly different ($p<0.05$) between control group and patient group. Among them, only one FC between cSMA and cDN (prefix *c* representing contralesional) decreased, while other connections increased in stroke patients (Fig. 5.5(B)). In addition, mixed effects regression model was used to estimate the relationship of FC with recovery time and FMI. We found several FC strongly ($p<0.05$) correlated with recovery time (in red), FMI (in blue) and with both recovery time and FMI (in green, Fig. 5.5(A)). In particular, two FC (i.e., iM1-iSCb and iPMv-iAICb) were found to have significant positive correlations with both recovery time and FMI, while the iPMd-iTh FC had negative correlation with both recovery time and FMI. The quantitative data of these three FC are demonstrated in Table 5.2. Combining Fig. 5.5(A) and Fig. 5.5(B), there were four FC (i.e., cPMd-iTh, cPMd-cPMv, iPMd-iTh and cPMv-cBG) which both significantly correlated with either recovery time or FMI and significantly increased at P1 comparing with control group (indicated by purple lines in Fig. 5.5(B)). Especially, iPMd-iTh FC which negatively correlated with both recovery time and FMI was also found increased at P1 comparing with control group (highlighted in Table 5.3).

5.3.5 Potential prognostic value of FC at early recovery stage

In order to examine the potential prognostic value of FC in motor execution networks at early recovery stage, we calculated the spearman's correlation coefficients between FC strength at P1 and D_{FMI}. Six FC (i.e., iPMv-cPMd, iSMA-cPMv, iSMA-cPCG, cPMv-cPCG, iPMv-cBG and cSCb-cDN) at P1 were found to be positively correlated ($p<0.05$) with D_{FMI}, and another FC (i.e., iTh-cM1) showed negative correlation ($p<0.05$) with D_{FMI} (Fig. 5.6). Their quantitative data are listed in Table 5.4. In addition, the FC between cPCG and cPMv at P1 both significantly changed compared with control group and correlated with motor function recovery (indicated by yellow line in Fig. 5.6 and highlighted in Table 5.4).

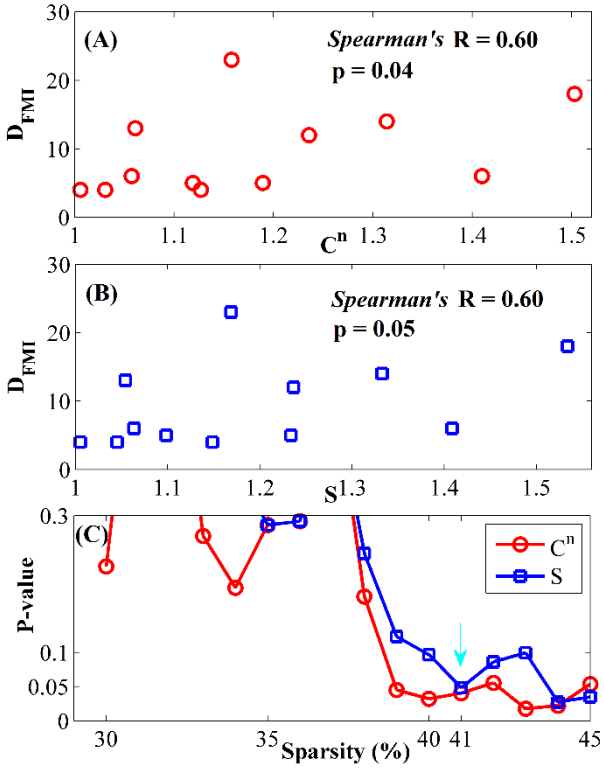

Figure 5.4. Potential prognostic value of topological parameters in task-state motor execution networks. Significant positive correlations between D_{FMI} and topological parameters C^n (A) and S (B) in task-state motor execution networks respectively. Panel (C) illustrates the p values of Spearman's correlation coefficients at sparsity from 0.3 to 0.45 in task-state motor execution networks. The green arrow in panel (C) indicates the p values of results at sparsity 0.41.

Table 5.3. Quantitative data of three FC significantly correlated with both recovery time and FMI.

Region	Region	Change over time		Change over FMI	
		t value	*p* value	*t* value	*p* value
iSCb	iM1	2.56	0.0154	2.12	0.0412
iAlCb	iPMv	2.92	0.0063	2.09	0.0448
iPMd	iTh	-2.44	0.0202	-2.49	0.0180

FC which changed significantly compared with control group at P1 is highlighted.

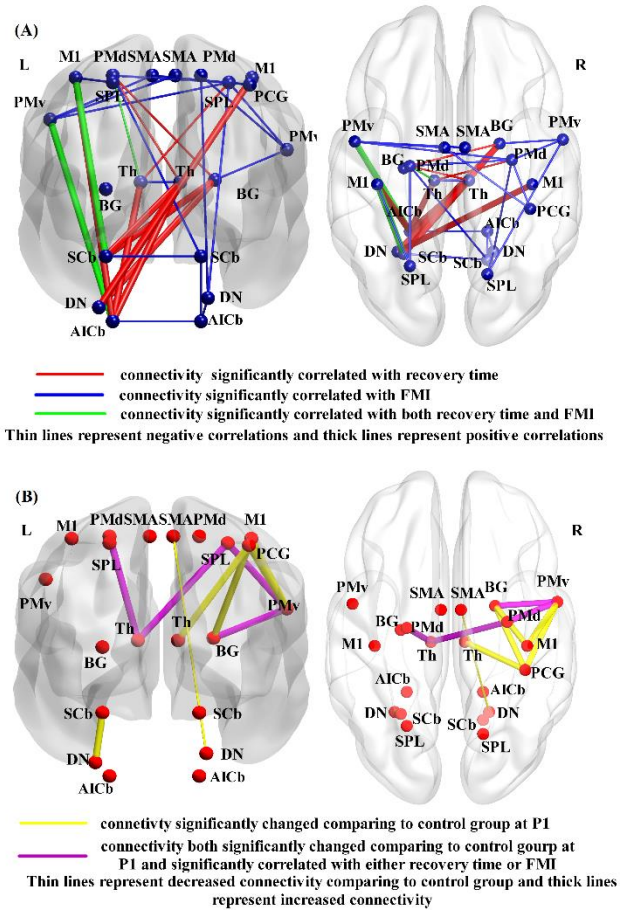

Figure 5.5. Panel (A) demonstrates the FC significantly ($p<0.05$) correlated with recovery time (in red), FMI (in blue) and with both recovery time and FMI (in green) in motor execution networks. Thin lines represent negative correlations and thick lines represent positive correlations. Panel (B) demonstrates the FC which significantly changed comparing with control group at P1. Among them, purple lines denote the overlapped FC in panel (A) and (B). Thin lines represent decreased FC comparing with control group and thick lines represent increased FC in panel (B). L=left; R=right; M1=primary motor cortex; Th=Thalamus; SPL=Superior parietal lobule; SMA=Supplementary motor area; PMd=Dorsolateral premotor area; PMv=Ventrolateral premotor cortex; SCb=Superior cerebellum; DN=Dentate nucleus; AICb=Anterior inferior cerebellum; PCG=Postcentral gyrus; BG=Basal ganglia.

5.3.6 Dynamic change and potential prognostic value of nodal betweenness

Nodal betweenness indicates the importance of nodes in networks. In this chapter, we also investigated the dynamic change of nodal betweenness during recovery in task-state motor execution networks. As a result, we found significant negative correlations ($p<0.05$) between nodal betweenness of cDN and D_{FMI} although no significant correlation was found with recovery time.

Table 5.4. Quantitative data of all six FC significantly correlated with the recovery during the sub-acute phase (FC which changed significantly compared with control group at P1 is highlighted.)

Region	Region	Spearman's R	*p* value
iTh	cM1	-0.63	0.0284
iPMv	cPMd	0.78	0.0027
iSMA	cPMv	0.61	0.0360
iSMA	cPCG	0.65	0.0211
cPMv	cPCG	0.63	0.0284
iPMv	cBG	0.73	0.0073
cSCB	cDN	0.72	0.0086

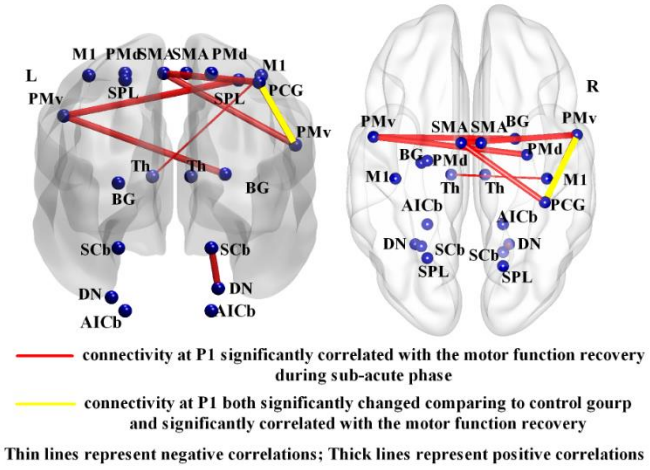

Figure 5.6. Illustration of FC at P1 significantly correlated with D_{FMI} in motor execution networks. Thin lines represent negative correlations and thick lines represent positive correlations. Note that the yellow

line represents the FC which both significantly changed compared with control group and correlated with motor function recovery at P1. L=left; R=right. Figures 5.5 and 5.6 were visualized with the BrainNet Viewer (http://www.nitrc.org/projects/bnv/).

5.4 Discussion

Graph theory has been widely used to investigate the change in brain networks organization induced by diseases. For example, Alzheimer's disease patients were reported to show abnormal small-world organization in their brain compared with controls [270]. Patients with lesions due to brain tumor and spinal cord injury were reported to show disruption in brain networks topology [271, 272]. With respect to stroke, several studies have also found evidence of the reorganization of brain networks. Wang and colleagues, for the first time, found that the motor execution network shifted towards a non-optimal topological configuration with less functional segregation by examining topological change of the motor execution network based on resting-state fMRI during the recovery after stroke [39]. In addition, Ovadia-Caro and colleagues found that the brain networks containing lesions presented more changes during recovery compared with networks without lesions [273].

Wang and colleagues also investigated the dynamic reorganization of motor execution network during stroke recovery [39]. In contrast to the motor execution network at resting-state in Wang's work, in this chapter we focused on the reorganization of motor execution network under task state, which might provide new information about underlying mechanisms of neural response under specific task state [256]. According to our results, the characteristic path length L^n of motor execution network significantly decreased over recovery time and was negatively correlated with motor function restoration, which was different from the increased L^n (although insignificantly) reported in Wang's study[39]. This inconsistent results may be due to the different states of subjects, that is, Wang et al. studied the motor execution network in resting-state, while our results are of the motor execution network in task state. The clustering coefficient C^n of motor execution network did not show significant change over recovery time but had a significant negative correlation with motor function restoration. Note that the significant relationship between L^n and recovery time was only found in a small range of sparsity around 0.41, but notably, results at sparsities from 0.4 to 0.45 were close to a significant level. In addition, the significant correlations between L^n (or C^n) and FMI do exist in a large range of sparsity.

The significant decrease of L^n in task-state motor execution networks during recovery time demonstrated the enhanced efficiency in global information transferring. As L^n was calculated based on weighted networks, we attributed this phenomenon to the strengthening FC which would shorten the weighted characteristic path length and further result in a decreasing L^n. Our inference was validated by Fig. 5.5 that majority (10 among 14) of the FC with significant change over recovery time in task-state motor execution networks (red and green lines in Fig. 5.5(A)) were increased. Moreover, both C^n and L^n in task-state motor execution networks had significant negative correlations with FMI. Since decreasing C^n and L^n indicated a randomizing trend of the network topology, our results suggested that the motor function restoration was associated with randomizing task-state motor execution networks. Wang and colleagues found similar results in resting-state motor execution networks [39]. In contrast, task-state motor execution networks in unaffected hand sessions showed few reorganizations and no significant changes or correlations with FMI over recovery time. This is in line with the findings that stroke patients and healthy controls shared similar task-based fMRI activation pattern when moving their unaffected hand [248]. Moreover, compared with control group, the motor execution network had significant changes in some FC at P1 (Figs. 5.5(B) and 5.6), but showed no significant change in the topological configuration, which is similar with the results reported in Wang's study [39]. We therefore speculated that the FC and topological configuration were influenced at different stages of the stroke recovery.

Besides the dynamic brain reorganization after stroke, the potential prognostic value of neuroimaging data at early recovery stage post stroke was another focus of current stroke studies. Our results showed that C^n and S of task-state motor execution networks within ten days after stroke had significant positive correlations with the motor function restoration during sub-acute phase (indicated by D_{FMI}). According to graph theory, higher C^n and S at early recovery stage indicate more optimal configuration of networks after stroke and therefore result in better motor function restoration during sub-acute phase. Previous studies had reported the prognostic value of brain activity and FC in stroke recovery [249-251]. However, to the best of our knowledge, our study, for the first time, observed the brain network topology as prognostic of functional recovery.

Besides the topological parameters, the FC in task-state motor execution network also underwent changes which significantly correlated with FMI during stroke recovery (Fig. 5.5). We found FC between ipsilesional cerebellum (iAICb, iSCb and iDN) and other key motor areas (bilateral M1, bilateral Th and cBG) significantly increased during the recovery (Fig. 5.5(A)). Recent studies validated that the cerebellar networks consisting of cerebellum, subcortical areas and cerebral cortex contributed to the motor and non-motor functions [274-276]. Our results also substantiated that the activated cerebellar network played a critical role in stroke recovery. In addition, three ipsilesional

connections (iM1-iSCb, iPMv-iAICb and iPMd-iTh) were found to be significantly correlated with both FMI and recovery time (see the green lines in Fig. 5.5(A)), implying that the change of FC in task-state motor execution networks mainly occurred in ipsilesional hemisphere. This result was in line with previous findings of increased ipsilesional intra-hemispheric synchronization after stroke [277, 278]. Furthermore, enhanced FC of iPMv-iAICb and iM1-iSCb confirmed the critical role of cerebellar networks in stroke recovery. When taking into account control group, eleven FC were found significantly altered at P1 comparing with control group (Fig. 5.5(B)). Among them, four increased FC (i.e., cPMd-iTh, cPMd-cPMv, iPMd-iTh and cPMv-cBG) overlapped with FC with dynamic changes over recovery. Especially, all these four FC had negative correlation with FMI and one of them (iPMd-iTh) even had negative correlation with both FMI and recovery time. These results suggested that the strength of these FC increased at the acute stage due to lesion induced by stroke, but gradually decreased and approach the normal level as control group as the motor function recovered during recovery.

The 21 ROIs in motor execution network were defined based on previous studies. To validate the important roles of the 21 predefined ROIs, we also did activation analysis for affected hand session at P1, and found that most ROIs of the 21 predefined ROIs were activated except for Basal ganglia (BG), which may be attributed to the lesion locations of patients that six of twelve patients had lesions in BG (Table 5.1). Although there was no activation in BG, we still found FC between cBG and iPMv significantly correlated with the recovery during sub-acute phase (Table 5.4), which implied the important role of BG in motor function recovery after stroke. In order to substantiate that adding inactivated BG into the motor execution network will not affect the results of topological parameters, we also did the same analysis for the motor execution network without bilateral BG, and found significant negative (p=0.02) correlation between C^n and FMI, significant negative (p=0.001) correlation between L^n and FMI, significant negative (p=0.04) correlation between L^n and days after stroke, and significant positive correlations of D_{FMI} with C^n (p=0.01, Spearman's R=0.63) and S (p=0.03, Spearman's R=0.54), which is in line with the results of the motor execution network including bilateral BG.

With respect to the potential prognostic value of FC, the increase of FC between bilateral key motor areas at the early stage of stroke was positively correlated with the motor function restoration during sub-acute phase (Fig. 5.6). Our findings were supported by a previous task-based fMRI study, which reported that increases of activity in bilateral motor cortices was significantly correlated with motor functional recovery [279].

For nodal betweenness, the significance of cDN in predicting the motor function recovery during sub-acute phase was found in task-state motor execution networks. Considering the increased activity in contralesional cerebellum during the recovery of motor function after stroke reported in previous studies [39, 280], our results not only

confirmed the important role of contralesional cerebellum in the recovery but also substantiated its potential prognostic value in stroke.

5.5 Chapter conclusion

In summary, this chapter reported the topological reorganization of task-state motor execution networks during sub-acute phase post stroke. Especially, we found the topological configuration of task-state motor execution networks at the early recovery stage were capable of predicting the motor function restoration during sub-acute phase. In addition, we found increasing FC between ipsilesional cerebellum and motor cortices in task-state motor execution networks and the significance of cDN in predicting the motor function recovery during sub-acute phase. In general, this chapter demonstrated the reorganization and potential prognostic value of task-state brain network after stroke, which provided new insights into understanding the brain reorganization and rehabilitation after stroke.

In this thesis, other than the understanding of task-specific spatiotemporal changes of brain networks under motor task compared with resting condition, further application of task-state brain network in the research of stroke is another key component of the purpose of this thesis. In this chapter, the task-state brain network was applied in the research of post-stroke motor function restoration, which validated the effectiveness of task-state brain network in the stroke research and provided an alternatively way to investigate the stroke-induced reorganization of brain activities other than activation analysis and resting-state FC analysis.

Chapter 6: Summary and conclusion

Examining the modulation of task-state brain network during motor task plays a critical role of understanding how cerebral motor system works and could be further applied in the research of stroke. Recent advances in neuroimaging have resulted in numerous studies focusing on motor-related modulation of brain activity and most widely used strategy of these studies was identifying activated brain regions during motor task through event-related/block-design experiment paradigms. Despite progress obtained, motor-related activation analysis mainly focused on modulation of brain activities for individual brain regions. However, brain has been demonstrated to consist of discrete, large-scale networks. Investigating the task-related spatiotemporal modulation of brain networks is still in an early stage. Thus, this thesis used two neuroimaging modalities (fMRI and fNIRS) to investigate how brain networks, especially the motor network and high-level cognitive network, would reorganize spatiotemporally from resting-state to motor tasks through both static and dynamic FC analysis, and further applied the task-state brain network analysis in the research of motor disability due to stroke. Our findings revealed the underlying spatiotemporal adaptation of brain networks in response to motor task and demonstrated the potential clinical prognostic value of task-state motor network during stroke recovery.

6.1 Modulation of static task-state brain networks during motor preparation based on fNIRS

Through static FC analysis of fNIRS during rest and motor preparation, increased FC were identified during motor preparation, especially the FC connecting right DLPFC with contralateral S1 and M1 as well as the FC connecting contralateral S1 with ipsilateral S1 and M1. Channels located in sensorimotor networks and right DLPFC were also found activated during motor preparation. Our findings demonstrated that the sensorimotor network was interacting with high-level cognitive brain network to maintain the motor preparation state.

6.2 Modulation of dynamic task-state brain network during motor execution based on fNIRS

Through dynamic FC analysis of fNIRS during rest and motor execution, increased variability of FC connecting contralateral PMSMC and M1 was identified, and the nodal strength variability of these two ROIs were also increased

during motor execution. Our findings demonstrated that contralateral M1 and PMSMC were interacting with each other actively and dynamically to facilitate the fist opening and closing.

6.3 Spatiotemporal modulation of dynamic task-state brain network during motor execution based on fMRI

Based on fMRI data, two principal FC states during rest and one principal FC state during motor execution were identified using dynamic FC analysis and *k*-means clustering. The 1st principal FC state during rest was similar to that during motor execution, which likely represented intrinsic network architecture. However, the presence of a 2nd principal FC state during rest with shorter "dwell time" could imply the interaction between DMN and MN through inter-network FC. In addition, the more frequent shifting between two principal FC states during rest indicated that the brain networks dynamically maintained the "default mode" for motor system. In contrast, because of focusing on motor execution, there was reduced FCV and only a single principal FC state during motor execution. Our findings suggested overall spatial similarity of primary principal FC states, but distinct temporal patterns of principal FC states between rest and motor execution.

6.4 Topological reorganization and its potential clinical prognostic value of task-state brain network

Task-state motor network was applied in the research of motor disability due to stroke and topological reorganization of task-state motor network was identified during sub-acute phase post stroke. In addition, for the first time, our study found the topological configuration of task-state motor network at the early recovery stage were capable of predicting the motor function restoration during sub-acute phase. In general, this thesis demonstrated the reorganization and potential prognostic value of task-state brain network after stroke, which provided new insights into understanding the brain reorganization and stroke rehabilitation.

6.5 fNIRS is a promising neuroimaging modality for static and dynamic FC analysis

Previous static and dynamic FC studies were mainly based on fMRI. However, fNIRS has emerged as a new tool that is complementary to fMRI-based FC analysis, especially for dynamic FC analysis because of its relatively higher temporal resolution and lower cost than fMRI. In this thesis, we explored the potential of fNIRS in both static and dynamic FC analysis. Our results demonstrated that fNIRS was a promising and reliable neuroimaging modality for

static and dynamic FC analysis, and the relatively high temporal resolution of fNIRS provided robust FC estimation and transient detection simultaneously.

Chapter 7: Future work

In this thesis, we investigated the task-specific spatiotemporal changes of brain networks under motor task through both static and dynamic FC analysis using fNIRS and fMRI, which deepened the understanding of how cerebral motor system work under different mental conditions. In addition, we explored the application of task-state brain networks in the research of stroke and demonstrated the relationship between task-state brain network features and motor function restoration post stroke. However, the applications of task-state brain network in stroke research and other fields are far broader and a lot of work are needed to be explored in the future.

7.1 More applications of task-state brain networks in stroke research

In this thesis, task-state brain network was used in the stroke research and the topological configuration of the task-state brain network was demonstrated to relate to the motor function restoration post stroke. However, more applications of task-state brain networks in stroke research could be explored in the future.

In chapter 2, we found that several FC, including FC between sensorimotor network and cognitive network, increased during motor preparation without any actual hand movements, and more increased FC were identified during motor preparation than motor execution. In addition, most increased FC during motor preparation were inter-hemispheric. Previous studies found that post-stroke loss and recovery of sensorimotor function was associated with acute deterioration and subsequent retrieval of inter-hemispheric FC within sensorimotor system [281, 282]. Thus, the task-state brain network during motor preparation could be applied in both indicating motor function restoration and helping the treatment of stroke-induced motor dysfunction. First, since the motor preparation would lead to the increasing of inter-hemispheric FC within sensorimotor network and the inter-hemispheric FC were correlated with motor function recovery, it would be reasonable to speculate that the task-state brain network during motor preparation would be very effective to indicate the motor function restoration post stroke, which could potentially contribute to the neuroimaging-based evaluation of stroke recovery. In addition, like motor imagery, motor preparation could also be used in the motor function restoration since it is able to increase the inter-hemispheric FC within sensorimotor network. For stroke patients with severe deficit, motor functional restoration through actual motor movements might not be feasible. Thus, motor preparation paradigms without any actual movements could be used in the motor rehabilitation exercise as it could activate sensorimotor network, especially the inter-hemispheric

FC. Furthermore, since motor preparation task is easier to perform than motor imagery task, we think it would be a very promising exercise in motor rehabilitation for severely impaired stroke patients.

With respect to the methods used in stroke research, task-state brain networks applied in the stroke research were estimated through static FC analysis in this thesis. However, the brain activities and cognitive processes were proven to be dynamic and adaptive. Dynamic FC analysis is able to provide more information, especially the temporal information, than static FC analysis. Through dynamic FC analysis, schizophrenia patients exhibited shorter states of strong and large-scale FC than healthy controls during rest, which could not be observed when using static FC analysis [123]. Another study of dynamic FC in Alzheimer's disease patients showed longer state persistence in the strong anterior DMN sub-network, but shorter states in the strong posterior DMN sub-network when compared with healthy elderly subjects during rest [184]. Therefore, if the task-state brain networks based on dynamic FC analysis could be applied in stroke recovery, not only the stroke-induced spatial reorganization but also the stroke-induced temporal reorganization of task-state brain networks would be revealed, which might further deepen our understanding of spatiotemporal reorganization of functional brain networks post stroke.

7.2 Brain stimulation on FC and brain networks

The studies performed in this thesis were mainly observation studies, which targeted to identify changes of task-state brain networks and relationships between task-state brain networks and stroke recovery. However, the ultimate goal of neuroimaging studies is the application of these findings obtained the observation studies. With respect to the application in the treatment of stroke, brain stimulation-based stroke treatment is an appropriate application for the findings of task-state brain networks in this thesis.

In fact, previous studies have developed a strategy to use functional neuroimaging to guide the brain stimulation-based stroke treatment. For example, based on previous findings that patients with good recovery usually had higher activities in motor cortex of lesioned hemisphere but lower activities in motor cortex of intact hemisphere, two strategies were developed to treat the stroke using brain stimulation methods, which were either upregulating the excitability in the lesioned hemisphere or downregulating the excitability in the intact hemisphere (Fig. 7.1) [283].

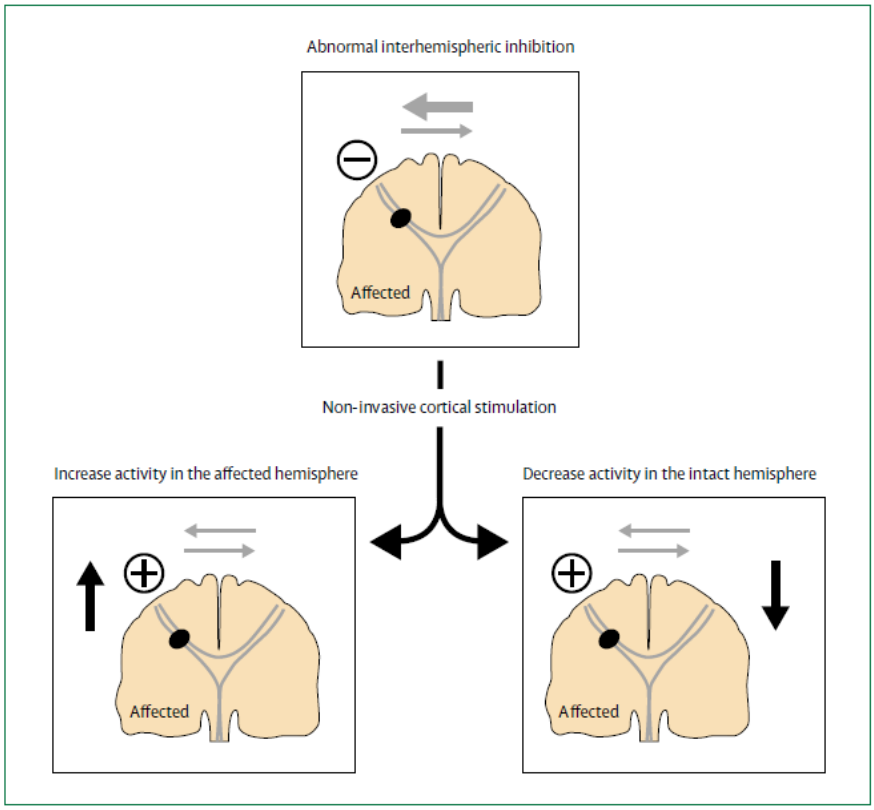

Figure 7.1 Targets for intervention strategies based on possible pathophysiological mechanisms**.** Movements of the paretic hand are associated with unbalanced interhemispheric inhibition targeting the motor cortex of the lesioned hemisphere in patients with subcortical stroke. Two interventional approaches might normalize this pattern leading to improvements in motor function: upregulation of excitability of the motor cortex of the lesioned hemisphere and downregulation of excitability of the motor cortex in the intact hemisphere. This figure was adopted from [283] with courtesy.

The previous studies were mainly based on the activation analysis and focused on individual brain regions. However, the brain was demonstrated to consist of FC and networks. If we could modulate the FC and brain networks through brain stimulation methods, it would be more effective to help the treatment of stroke. Paired associative stimulation has been demonstrated to be able to alter the FC [284], which provided a technique to modulate the FC through brain stimulation methods. In addition, a recent study identified the controllability of brain networks, which offered a mechanistic explanation for how the brain moves between cognitive states drawn from the network organization of white matter microstructure [285]. Through the controllability of brain networks, it would be possible

to modulate the brain networks through several key elements in the brain networks. Thus, if we could combine the controllability of brain networks and paired associative stimulation technique together, it would be possible for us to modulate the key features of the brain networks identified in this thesis so as to help the treatment of stroke more effectively in the future.

7.3 Application of task-state brain networks in other areas

In this thesis, stroke rehabilitation research was proposed as a clinical application of task-state brain networks. However, other movement disorders and neurological diseases also stand to benefit from the task-state brain network analysis. One potential conditions is early detection of auto-immune disease such as Amyotrophic Lateral Sclerosis (ALS) onsets that currently eludes clinical markers. Exploring the role of task-state brain networks in indicating the onset of ALS would be a very attractive and meaningful topic in the future.

In addition, the task-state brain network analysis could also be applied in the kinesiology and brain-computer interface (BCI). For example, our findings regarding motor preparation could potentially be applied in anticipation-based BCI. Previous studies of anticipation-based BCI mainly targeted the anticipation-related potentials obtained through EEG and developed classification methods to detect the anticipation-related potentials to guide the BCI [132, 176, 177]. However, our findings might provide another option for anticipation-based BCI. The increased FC during motor preparation before actual movement could be used to guide the BCI. Especially, the relationship between modulated FC during motor preparation and the side of FOC subjects were about to perform, that is, FC connecting the right DLPFC with contralateral (right side in left trans and left side in right trans) S1 and M1, and FC connecting contralateral S1 with ipsilateral (left side in left trans and right side in right trans) S1 and M1 were increased during motor preparation, would further help the BCI to understand the anticipation of subjects more specifically.

7.4 The research of motor-related structural brain networks

With respect to the imaging modalities, this thesis used two functional imaging modalities (fNIRS and fMRI) and mainly focused on the functional aspect of the brain networks. However, investigating the brain networks from the structural perspective is also very important and might provide the underlying mechanism of how cerebral motor system work under both normal and pathological conditions.

Diffusion tensor imaging (DTI) has already been applied in the stroke research and neuronal tract damage, especially the damage of corticospinal tract, has been identified by DTI by previous studies [286, 287]. However, the integration of structural and functional brain networks would be the main direction of the future, which would not

only provide more comprehensive information regarding the brain organization but also offer new tools to investigate the brain networks under both normal and pathological conditions (Fig. 7.2) [288]. Thus, if we could collect data using both functional and structural modalities under both normal and pathological conditions, it would be possible for us to investigate the integrative spatiotemporal patterns of motor-related brain networks under different conditions as well as exploring the methodological advances in integrating functional and structural brain networks together in the future.

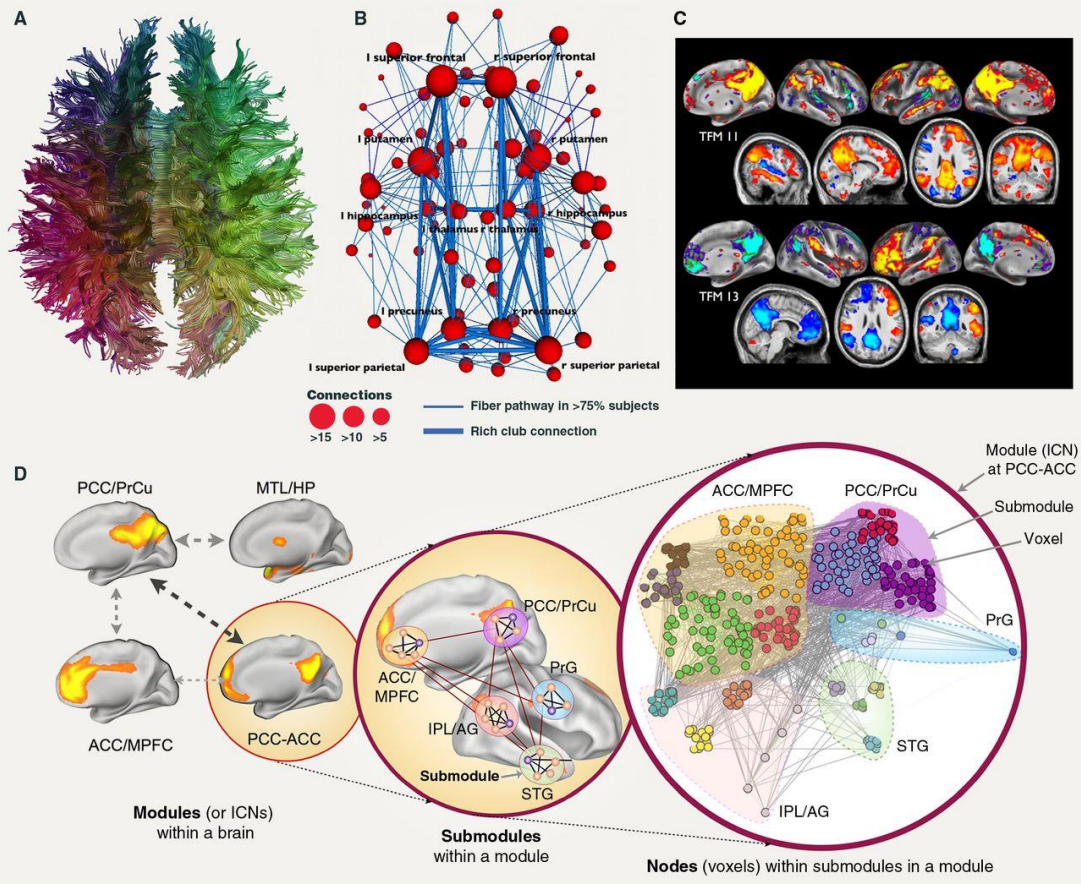

Figure 7.2 Convergence: structural and functional brain network organization. (A) Whole-brain fiber bundles reconstructed from diffusion tensor MRI are colored according to their connection similarity. (B) The human brain's structural network constructed from DTI. (C) Repertoires of spatial modules have emerged from the analysis of spontaneous BOLD fluctuations in the brain at rest. (D) Hierarchical (modular) resting-state functional network. The figure was adopted from [288] with courtesy.

List of References

1. Fritsch, G. and E. Hitzig, Uber die elektrische Erregbarkeit des Grossihirns, Arch. f. Anat., Physiol., u. Wissen. Med, 1870: p. 300.
2. Leyton, A.S.F. and C.S. Sherrington, Observations on the Excitable Cortex of the Chimpanzee, Orang-Utan, and Gorilla. Quarterly Journal of Experimental Physiology, 1917. 11(2): p. 135-222.
3. Penfield, W. and E. Boldrey, Somatic motor and sensory representation in the cerebral cortex of man as studied by electrical stimulation. Brain: A journal of neurology, 1937.
4. Penfield, W. and T. Rasmussen, The cerebral cortex of man. 1952: MacMillan Company.
5. Kawashima, R., et al., Regional cerebral blood flow changes in human brain related to ipsilateral and contralateral complex hand movements – a PET study. European Journal of Neuroscience, 1998. 10(7): p. 2254-2260.
6. Cramer, S.C., et al., Activation of Distinct Motor Cortex Regions During Ipsilateral and Contralateral Finger Movements. Journal of Neurophysiology, 1999. 81(1): p. 383.
7. Gelnar, P.A., et al., Fingertip representation in the human somatosensory cortex: an fMRI study. Neuroimage, 1998. 7(4): p. 261-283.
8. Rao, S.M., et al., Somatotopic mapping of the human primary motor cortex with functional magnetic resonance imaging. Neurology, 1995. 45(5): p. 919-924.
9. Kwong, K.K., et al., Dynamic magnetic resonance imaging of human brain activity during primary sensory stimulation. Proceedings of the National Academy of Sciences, 1992. 89(12): p. 5675-5679.
10. Benaron, D.A., et al., Noninvasive functional imaging of human brain using light. Journal of Cerebral Blood Flow & Metabolism, 2000. 20(3): p. 469-477.
11. Gratton, G., et al., Rapid changes of optical parameters in the human brain during a tapping task. Journal of Cognitive Neuroscience, 1995. 7(4): p. 446-456.
12. Maki, A., et al., Spatial and temporal analysis of human motor activity using noninvasive NIR topography. Medical physics, 1995. 22(12): p. 1997-2005.
13. Hirth, C., et al., Non-invasive functional mapping of the human motor cortex using near-infrared spectroscopy. Neuroreport, 1996. 7(12): p. 1977-1981.
14. Roland, P. and R. Seitz, Positron emission tomography studies of the somatosensory system in man, in Exploring brain functional anatomy with positron tomography. 1991, Wiley Chichester. p. 113-124.
15. Obrig, H., et al., Cerebral oxygenation changes in response to motor stimulation. Journal of applied physiology, 1996. 81(3): p. 1174-1183.
16. Ward, N.S., et al., Neural correlates of motor recovery after stroke: a longitudinal fMRI study. Brain, 2003. 126(Pt 11): p. 2476-96.
17. Fridman, E.A., et al., Reorganization of the human ipsilesional premotor cortex after stroke. Brain, 2004. 127(Pt 4): p. 747-58.
18. Enzinger, C., et al., Functional MRI Correlates of Lower Limb Function in Stroke Victims With Gait Impairment. Stroke, 2008. 39(5): p. 1507-1513.

19. Antelis, J.M., et al., Decoding Upper Limb Movement Attempt From EEG Measurements of the Contralesional Motor Cortex in Chronic Stroke Patients. IEEE Trans Biomed Eng, 2016. 64(1): p. 99-111.

20. Li, X., et al., Examination of Hand Muscle Activation and Motor Unit Indices Derived from Surface EMG in Chronic Stroke. IEEE Trans Biomed Eng, 2014. 61(12): p. 2891-2898.

21. Rehme, A.K., et al., The role of the contralesional motor cortex for motor recovery in the early days after stroke assessed with longitudinal FMRI. Cereb cortex, 2010: p. bhq140.

22. Feydy, A., et al., Longitudinal study of motor recovery after stroke: recruitment and focusing of brain activation. Stroke, 2002. 33(6): p. 1610-7.

23. Tombari, D., et al., A longitudinal fMRI study: in recovering and then in clinically stable sub-cortical stroke patients. NeuroImage, 2004. 23(3): p. 827-839.

24. Rehme, A.K., et al., The role of the contralesional motor cortex for motor recovery in the early days after stroke assessed with longitudinal FMRI. Cerebral cortex, 2011. 21(4): p. 756-768.

25. Biswal, B., et al., Functional connectivity in the motor cortex of resting human brain using echo‐planar mri. Magn. Reson. Med., 1995. 34(4): p. 537-541.

26. Biswal, B.B., J.V. Kylen, and J.S. Hyde, Simultaneous assessment of flow and BOLD signals in resting‐state functional connectivity maps. NMR Biomed, 1997. 10(4‐5): p. 165-170.

27. Lowe, M.J., et al., Correlations in low-frequency BOLD fluctuations reflect cortico-cortical connections. Neuroimage, 2000. 12(5): p. 582-587.

28. Deng, L., et al., Characterizing dynamic local functional connectivity in the human brain. Scientific Reports, 2016. 6: p. 26976.

29. Sun, J., Z. Li, and S. Tong, Inferring Functional Neural Connectivity with Phase Synchronization Analysis: A Review of Methodology. Computational and Mathematical Methods in Medicine, 2012. 2012: p. 13.

30. Lowe, M., B. Mock, and J. Sorenson, Functional connectivity in single and multislice echoplanar imaging using resting-state fluctuations. Neuroimage, 1998. 7(2): p. 119-132.

31. Cordes, D., et al., Frequencies contributing to functional connectivity in the cerebral cortex in "resting-state" data. AJNR Am. J. Neuroradiol., 2001. 22(7): p. 1326-1333.

32. van de Ven, V.G., et al., Functional connectivity as revealed by spatial independent component analysis of fMRI measurements during rest. Hum. Brain Mapp., 2004. 22(3): p. 165-178.

33. Biswal, B., et al., Functional connectivity in the motor cortex of resting human brain using echo‐planar mri. Magnetic resonance in medicine, 1995. 34(4): p. 537-541.

34. Greicius, M.D., et al., Functional connectivity in the resting brain: a network analysis of the default mode hypothesis. Proceedings of the National Academy of Sciences, 2003. 100(1): p. 253-258.

35. Rosazza, C. and L. Minati, Resting-state brain networks: literature review and clinical applications. Neurological Sciences, 2011. 32(5): p. 773-785.

36. Van Dijk, K.R., et al., Intrinsic functional connectivity as a tool for human connectomics: theory, properties, and optimization. Journal of neurophysiology, 2010. 103(1): p. 297-321.

37. Vanhaudenhuyse, A., et al., Default network connectivity reflects the level of consciousness in non-communicative brain-damaged patients. Brain, 2010. 133(1): p. 161-171.

38. van Meer, M.P., et al., Recovery of sensorimotor function after experimental stroke correlates with restoration of resting-state interhemispheric functional connectivity. J Neurosci, 2010. 30(11): p. 3964-72.

39. Wang, L., et al., Dynamic functional reorganization of the motor execution network after stroke. Brain, 2010. 133(Pt 4): p. 1224-38.

40. Grefkes, C. and G.R. Fink, Reorganization of cerebral networks after stroke: new insights from neuroimaging with connectivity approaches. Brain, 2011: p. awr033.

41. Jiang, T., et al., Modulation of functional connectivity during the resting state and the motor task. Hum. Brain Mapp., 2004. 22(1): p. 63-71.

42. Jin, S.H., P. Lin, and M. Hallett, Reorganization of brain functional small‐world networks during finger movements. Hum. Brain Mapp., 2012. 33(4): p. 861-872.

43. Tan, B., et al., The Difference of Brain Functional Connectivity between Eyes-Closed and Eyes-Open Using Graph Theoretical Analysis. Computational and Mathematical Methods in Medicine, 2013. 2013: p. 15.

44. Mutlu, A.Y., E. Bernat, and S. Aviyente, A Signal-Processing-Based Approach to Time-Varying Graph Analysis for Dynamic Brain Network Identification. Computational and Mathematical Methods in Medicine, 2012. 2012: p. 10.

45. Newton, A.T., et al., Modulation of steady state functional connectivity in the default mode and working memory networks by cognitive load. Hum. Brain Mapp., 2011. 32(10): p. 1649-1659.

46. Arfanakis, K., et al., Combining independent component analysis and correlation analysis to probe interregional connectivity in fMRI task activation datasets. Magn. Reson. Imaging, 2000. 18(8): p. 921-930.

47. Hampson, M., et al., Changes in functional connectivity of human MT/V5 with visual motion input. Neuroreport, 2004. 15(8): p. 1315-1319.

48. Nir, Y., et al., Widespread functional connectivity and fMRI fluctuations in human visual cortex in the absence of visual stimulation. Neuroimage, 2006. 30(4): p. 1313-1324.

49. Bardouille, T. and S. Boe, State-related changes in MEG functional connectivity reveal the task-positive sensorimotor network. PloS one, 2012. 7(10): p. e48682.

50. Newton, A.T., V.L. Morgan, and J.C. Gore, Task demand modulation of steady‐state functional connectivity to primary motor cortex. Hum. Brain Mapp., 2007. 28(7): p. 663-672.

51. Huettel, S.A., A.W. Song, and G. McCarthy, Functional magnetic resonance imaging. Vol. 1. 2004: Sinauer Associates Sunderland.

52. Ogawa, S., et al., Brain magnetic resonance imaging with contrast dependent on blood oxygenation. Proceedings of the National Academy of Sciences, 1990. 87(24): p. 9868-9872.

53. Turner, R., et al., Echo‐planar time course MRI of cat brain oxygenation changes. Magnetic Resonance in Medicine, 1991. 22(1): p. 159-166.

54. Matthews, P. and P. Jezzard, Functional magnetic resonance imaging. Journal of Neurology, Neurosurgery & Psychiatry, 2004. 75(1): p. 6-12.

55. Matthews, P.M., G.D. Honey, and E.T. Bullmore, Applications of fMRI in translational medicine and clinical practice. Nature Reviews Neuroscience, 2006. 7(9): p. 732-744.

56. Lotze, M., et al., Activation of cortical and cerebellar motor areas during executed and imagined hand movements: an fMRI study. Journal of cognitive neuroscience, 1999. 11(5): p. 491-501.

57. Buccino, G., et al., Action observation activates premotor and parietal areas in a somatotopic manner: an fMRI study. European journal of neuroscience, 2001. 13(2): p. 400-404.

58. Pfurtscheller, G. and C. Neuper, Motor imagery activates primary sensorimotor area in humans. Neuroscience letters, 1997. 239(2): p. 65-68.

59. Calvert, G.A., et al., Activation of auditory cortex during silent lipreading. science, 1997. 276(5312): p. 593-596.

60. Bergerbest, D., D.G. Ghahremani, and J.D. Gabrieli, Neural correlates of auditory repetition priming: reduced fMRI activation in the auditory cortex. Journal of Cognitive Neuroscience, 2004. 16(6): p. 966-977.

61. Pekkola, J., et al., Primary auditory cortex activation by visual speech: an fMRI study at 3 T. Neuroreport, 2005. 16(2): p. 125-128.

62. Culham, J.C., et al., Cortical fMRI activation produced by attentive tracking of moving targets. Journal of neurophysiology, 1998. 80(5): p. 2657-2670.

63. Postle, B., et al., An fMRI investigation of cortical contributions to spatial and nonspatial visual working memory. Neuroimage, 2000. 11(5): p. 409-423.

64. Martinez, A., et al., Involvement of striate and extrastriate visual cortical areas in spatial attention. Nature neuroscience, 1999. 2(4): p. 364-369.

65. Wittmann, B.C., et al., Reward-related FMRI activation of dopaminergic midbrain is associated with enhanced hippocampus-dependent long-term memory formation. Neuron, 2005. 45(3): p. 459-467.

66. D'Esposito, M., B.R. Postle, and B. Rypma, Prefrontal cortical contributions to working memory: evidence from event-related fMRI studies. Experimental brain research, 2000. 133(1): p. 3-11.

67. Graydon, F.X., et al., Learning-related fMRI activation associated with a rotational visuo-motor transformation. Cognitive brain research, 2005. 22(3): p. 373-383.

68. Toni, I., et al., The time course of changes during motor sequence learning: a whole-brain fMRI study. Neuroimage, 1998. 8(1): p. 50-61.

69. Lee, M., et al., The motor cortex shows adaptive functional changes to brain injury from multiple sclerosis. Annals of neurology, 2000. 47(5): p. 606-613.

70. Adcock, J., et al., Quantitative fMRI assessment of the differences in lateralization of language-related brain activation in patients with temporal lobe epilepsy. Neuroimage, 2003. 18(2): p. 423-438.

71. Fu, C.H., et al., Attenuation of the neural response to sad faces in major depressionby antidepressant treatment: a prospective, event-related functional magnetic resonance imagingstudy. Archives of general psychiatry, 2004. 61(9): p. 877-889.

72. Wexler, B.E., et al., Functional magnetic resonance imaging of cocaine craving. American Journal of Psychiatry, 2001. 158(1): p. 86-95.

73. Koeppe, C., et al., The influence of the 5 - HT3 receptor antagonist tropisetron on pain in fibromyalgia: a functional magnetic resonance imaging pilot study. Scandinavian Journal of Rheumatology, 2004. 33(sup119): p. 24-27.

74. Gur, R.E., et al., An fMRI study of facial emotion processing in patients with schizophrenia. American Journal of Psychiatry, 2002. 159(12): p. 1992-1999.

75. Manoach, D.S., et al., Schizophrenic subjects show aberrant fMRI activation of dorsolateral prefrontal cortex and basal ganglia during working memory performance. Biological psychiatry, 2000. 48(2): p. 99-109.

76. Sabatini, U., et al., Cortical motor reorganization in akinetic patients with Parkinson's disease. Brain, 2000. 123(2): p. 394-403.

77. Rombouts, S.A., et al., Altered resting state networks in mild cognitive impairment and mild Alzheimer's disease: an fMRI study. Human brain mapping, 2005. 26(4): p. 231-239.

78. Chance, B., et al., A novel method for fast imaging of brain function, non-invasively, with light. Optics express, 1998. 2(10): p. 411-423.

79. Bunce, S.C., et al., Functional near-infrared spectroscopy. IEEE engineering in medicine and biology magazine, 2006. 25(4): p. 54-62.

80. Delpy, D.T., et al., Estimation of optical pathlength through tissue from direct time of flight measurement. Physics in medicine and biology, 1988. 33(12): p. 1433.

81. Chance, B., et al., Cognition-activated low-frequency modulation of light absorption in human brain. Proceedings of the National Academy of Sciences, 1993. 90(8): p. 3770-3774.

82. Hoshi, Y. and M. Tamura, Dynamic multichannel near-infrared optical imaging of human brain activity. Journal of Applied Physiology, 1993. 75(4): p. 1842-1846.

83. Kato, T., et al., Human visual cortical function during photic stimulation monitoring by means of near-infrared spectroscopy. Journal of Cerebral Blood Flow & Metabolism, 1993. 13(3): p. 516-520.

84. Coyle, S.M., T.E. Ward, and C.M. Markham, Brain–computer interface using a simplified functional near-infrared spectroscopy system. Journal of neural engineering, 2007. 4(3): p. 219.

85. Derosière, G., et al., NIRS-measured prefrontal cortex activity in neuroergonomics: strengths and weaknesses. Frontiers in human neuroscience, 2013. 7: p. 583.

86. Azar, A. Monitoring blood oxygenation changes due to acute pain stimuli using functional near-infrared spectroscopy (fNIRS). in Conference proceedings:... Annual International Conference of the IEEE Engineering in Medicine and Biology Society. IEEE Engineering in Medicine and Biology Society. Annual Conference. 2008.

87. Soshi, T., et al., Sleep deprivation influences diurnal variation of human time perception with prefrontal activity change: a functional near-infrared spectroscopy study. PLoS One, 2010. 5(1): p. e8395.

88. Murata, A., et al., Culturally non-preferred cognitive tasks require compensatory attention: a functional near infrared spectroscopy (fNIRS) investigation. Culture and Brain, 2015. 3(1): p. 53-67.

89. Plichta, M.M., et al., Auditory cortex activation is modulated by emotion: a functional near-infrared spectroscopy (fNIRS) study. Neuroimage, 2011. 55(3): p. 1200-1207.

90. Quaresima, V., S. Bisconti, and M. Ferrari, A brief review on the use of functional near-infrared spectroscopy (fNIRS) for language imaging studies in human newborns and adults. Brain and Language, 2012. 121(2): p. 79-89.

91. Sato, H., et al., A NIRS–fMRI investigation of prefrontal cortex activity during a working memory task. Neuroimage, 2013. 83: p. 158-173.

92. Fallgatter, A., et al., Loss of functional hemispheric asymmetry in Alzheimer's dementia assessed with near-infrared spectroscopy. Cognitive Brain Research, 1997. 6(1): p. 67-72.

93. Kato, H., et al., Near-Infrared Spectroscopic Topography as a Tool to Monitor Motor Reorganization After Hemiparetic Stroke A Comparison With Functional MRI. Stroke, 2002. 33(8): p. 2032-2036.

94. Kubota, Y., et al., Prefrontal activation during verbal fluency tests in schizophrenia—a near-infrared spectroscopy (NIRS) study. Schizophrenia Research, 2005. 77(1): p. 65-73.

95. Elton, A. and W. Gao, Task‐related modulation of functional connectivity variability and its behavioral correlations. Human brain mapping, 2015.

96. Hernandez, L.M., et al., Neural signatures of autism spectrum disorders: insights into brain network dynamics. Neuropsychopharmacology, 2015. 40(1): p. 171-189.

97. Meinzer, M., et al., Electrical brain stimulation improves cognitive performance by modulating functional connectivity and task-specific activation. The Journal of Neuroscience, 2012. 32(5): p. 1859-1866.

98. Vincent, J.L., et al., Evidence for a frontoparietal control system revealed by intrinsic functional connectivity. Journal of neurophysiology, 2008. 100(6): p. 3328-3342.

99. Di Martino, A., et al., Aberrant striatal functional connectivity in children with autism. Biological psychiatry, 2011. 69(9): p. 847-856.

100. Zeng, L.-L., et al., Identifying major depression using whole-brain functional connectivity: a multivariate pattern analysis. Brain, 2012. 135(5): p. 1498-1507.

101. Bullmore, E. and O. Sporns, Complex brain networks: graph theoretical analysis of structural and functional systems. Nat. Rev. Neurosci., 2009. 10(3): p. 186-98.

102. Bullmore, E. and O. Sporns, The economy of brain network organization. Nature Reviews Neuroscience, 2012. 13(5): p. 336-349.

103. McKeown, M.J., et al., Analysis of fMRI data by blind separation into independent spatial components, 1997, DTIC Document.

104. Bressler, S.L., Large-scale cortical networks and cognition. Brain Research Reviews, 1995. 20(3): p. 288-304.

105. McIntosh, A.R., Towards a network theory of cognition. Neural Networks, 2000. 13(8): p. 861-870.

106. Bullmore, E. and O. Sporns, Complex brain networks: graph theoretical analysis of structural and functional systems. Nature Reviews Neuroscience, 2009. 10(3): p. 186-198.

107. Sporns, O., et al., Organization, development and function of complex brain networks. Trends in cognitive sciences, 2004. 8(9): p. 418-425.

108. Girvan, M. and M.E. Newman, Community structure in social and biological networks. Proceedings of the national academy of sciences, 2002. 99(12): p. 7821-7826.

109. Ravasz, E. and A.-L. Barabási, Hierarchical organization in complex networks. Physical Review E, 2003. 67(2): p. 026112.

110. Barthelemy, M., Betweenness centrality in large complex networks. The European Physical Journal B-Condensed Matter and Complex Systems, 2004. 38(2): p. 163-168.

111. Dosenbach, N.U., et al., Distinct brain networks for adaptive and stable task control in humans. Proceedings of the National Academy of Sciences, 2007. 104(26): p. 11073-11078.

112. van den Heuvel, M.P., et al., Aberrant frontal and temporal complex network structure in schizophrenia: a graph theoretical analysis. The Journal of Neuroscience, 2010. 30(47): p. 15915-15926.

113. Arieli, A., et al., Dynamics of ongoing activity: explanation of the large variability in evoked cortical responses. Science, 1996. 273(5283): p. 1868-1871.

114. Onton, J., et al., Imaging human EEG dynamics using independent component analysis. Neuroscience & Biobehavioral Reviews, 2006. 30(6): p. 808-822.

115. Sakoğlu, Ü., et al., A method for evaluating dynamic functional network connectivity and task-modulation: application to schizophrenia. Magnetic Resonance Materials in Physics, Biology and Medicine, 2010. 23(5-6): p. 351-366.

116. Chang, C. and G.H. Glover, Time–frequency dynamics of resting-state brain connectivity measured with fMRI. Neuroimage, 2010. 50(1): p. 81-98.

117. Calhoun, V.D., et al., The chronnectome: time-varying connectivity networks as the next frontier in fMRI data discovery. Neuron, 2014. 84(2): p. 262-274.

118. Hutchison, R.M., et al., Dynamic functional connectivity: promise, issues, and interpretations. Neuroimage, 2013. 80: p. 360-378.

119. Kucyi, A. and K.D. Davis, Dynamic functional connectivity of the default mode network tracks daydreaming. Neuroimage, 2014. 100: p. 471-480.

120. Zalesky, A., et al., The relationship between regional and inter‐regional functional connectivity deficits in schizophrenia. Human brain mapping, 2012. 33(11): p. 2535-2549.

121. Calhoun, V.D. and T. Adali, Multisubject independent component analysis of fMRI: a decade of intrinsic networks, default mode, and neurodiagnostic discovery. IEEE reviews in biomedical engineering, 2012. 5: p. 60-73.

122. Allen, E.A., et al., Tracking whole-brain connectivity dynamics in the resting state. Cerebral cortex, 2012: p. bhs352.

123. Damaraju, E., et al., Dynamic functional connectivity analysis reveals transient states of dysconnectivity in schizophrenia. Neuroimage: Clinical, 2014. 5: p. 298-308.

124. Trevena, J.A. and J. Miller, Cortical Movement Preparation before and after a Conscious Decision to Move. Consciousness and Cognition, 2002. 11(2): p. 162-190.

125. Libet, B., et al., Time of conscious intention to act in relation to onset of cerebral activity (readiness-potential). Brain, 1983. 106(3): p. 623-642.

126. Libet, B., Unconscious cerebral initiative and the role of conscious will in voluntary action, in Neurophysiology of consciousness. 1993, Birkhäuser Boston. p. 269-306.

127. Brunia, C., Movement and stimulus preceding negativity. Biological psychology, 1988. 26(1): p. 165-178.

128. Deecke, L., P. Scheid, and H.H. Kornhuber, Distribution of readiness potential, pre-motion positivity, and motor potential of the human cerebral cortex preceding voluntary finger movements. Experimental Brain Research, 1969. 7(2): p. 158-168.

129. Treserras, S., et al., Transition from rest to movement: brain correlates revealed by functional connectivity. Neuroimage, 2009. 48(1): p. 207-216.

130. Deng, J., J. Yao, and J.P. Dewald, Classification of the intention to generate a shoulder versus elbow torque by means of a time–frequency synthesized spatial patterns BCI algorithm. Journal of neural engineering, 2005. 2(4): p. 131.

131. Williams, J.J., et al., Differentiating closed-loop cortical intention from rest: building an asynchronous electrocorticographic BCI. Journal of neural engineering, 2013. 10(4): p. 046001.

132. Gangadhar, G., R. Chavarriaga, and J. del R Millán, Fast recognition of anticipation-related potentials. Biomedical Engineering, IEEE Transactions on, 2009. 56(4): p. 1257-1260.

133. Ayaz, H., et al., Assessment of cognitive neural correlates for a functional near infrared-based brain computer interface system, in Foundations of Augmented Cognition. Neuroergonomics and Operational Neuroscience, D. Schmorrow, I. Estabrooke, and M. Grootjen, Editors. 2009, Springer Berlin Heidelberg. p. 699-708.

134. Parasuraman, R. and G.F. Wilson, Putting the brain to work: Neuroergonomics past, present, and future. Human Factors: The Journal of the Human Factors and Ergonomics Society, 2008. 50(3): p. 468-474.

135. Niazi, I.K., et al., Detection of movement intention from single-trial movement-related cortical potentials. Journal of neural engineering, 2011. 8(6): p. 066009.

136. Zhang, D., et al., A Hybrid FES Rehabilitation System Based on CPG and BCI Technology for Locomotion: A Preliminary Study, in Intelligent Robotics and Applications, M. Xie, et al., Editors. 2009, Springer Berlin Heidelberg. p. 1073-1084.

137. Newton, A.T., V.L. Morgan, and J.C. Gore, Task demand modulation of steady‐state functional connectivity to primary motor cortex. Human brain mapping, 2007. 28(7): p. 663-672.

138. van den Hurk, P., et al., Online maintenance of sensory and motor representations: effects on corticospinal excitability. Journal of neurophysiology, 2007. 97(2): p. 1642-1648.

139. Ferrari, M. and V. Quaresima, A brief review on the history of human functional near-infrared spectroscopy (fNIRS) development and fields of application. Neuroimage, 2012. 63(2): p. 921-935.

140. Ayaz, H., et al., Using MazeSuite and functional near infrared spectroscopy to study learning in spatial navigation. Journal of visualized experiments: JoVE, 2011(56): p. 3443.

141. Obrig, H. and A. Villringer, Beyond the visible—imaging the human brain with light. Journal of Cerebral Blood Flow & Metabolism, 2003. 23(1): p. 1-18.

142. Ayaz, H., et al., Continuous monitoring of brain dynamics with functional near infrared spectroscopy as a tool for neuroergonomic research: empirical examples and a technological development. Frontiers in human neuroscience, 2013. 7.

143. Derosière, G., et al., NIRS-measured prefrontal cortex activity in neuroergonomics: strengths and weaknesses. Frontiers in human neuroscience, 2013. 7.

144. Ayaz, H., et al., Optical brain monitoring for operator training and mental workload assessment. Neuroimage, 2012. 59(1): p. 36-47.

145. McKendrick, R., et al., Enhancing dual-task performance with verbal and spatial working memory training: continuous monitoring of cerebral hemodynamics with NIRS. Neuroimage, 2014. 85(3): p. 1014-1026.

146. White, B.R., et al., Resting-state functional connectivity in the human brain revealed with diffuse optical tomography. Neuroimage, 2009. 47(1): p. 148-156.

147. Lu, C.-M., et al., Use of fNIRS to assess resting state functional connectivity. Journal of neuroscience methods, 2010. 186(2): p. 242-249.

148. Mesquita, R.C., M.A. Franceschini, and D.A. Boas, Resting state functional connectivity of the whole head with near-infrared spectroscopy. Biomedical optics express, 2010. 1(1): p. 324-336.

149. Xiong, J., et al., Interregional connectivity to primary motor cortex revealed using MRI resting state images. Human brain mapping, 1999. 8(2‐3): p. 151-156.

150. Zhang, H., et al., Functional connectivity as revealed by independent component analysis of resting-state fNIRS measurements. Neuroimage, 2010. 51(3): p. 1150-1161.

151. Sasai, S., et al., Frequency-specific functional connectivity in the brain during resting state revealed by NIRS. Neuroimage, 2011. 56(1): p. 252-257.

152. Medvedev, A.V., Does the resting state connectivity have hemispheric asymmetry? A near-infrared spectroscopy study. Neuroimage, 2014. 85(1): p. 400-407.

153. Fekete, T., et al., Small-world network properties in prefrontal cortex correlate with predictors of psychopathology risk in young children: a NIRS study. Neuroimage, 2014. 85(1): p. 345-353.

154. Niu, H., et al., Revealing topological organization of human brain functional networks with resting-state functional near infrared spectroscopy. PloS one, 2012. 7(9): p. e45771.

155. Ye, J.C., et al., NIRS-SPM: statistical parametric mapping for near-infrared spectroscopy. Neuroimage, 2009. 44(2): p. 428-447.

156. Cunnington, R., et al., The preparation and execution of self-initiated and externally-triggered movement: a study of event-related fMRI. Neuroimage, 2002. 15(2): p. 373-385.

157. Sweeney, K.T., et al., A methodology for validating artifact removal techniques for physiological signals. Information Technology in Biomedicine, IEEE Transactions on, 2012. 16(5): p. 918-926.

158. Ayaz, H., et al. Sliding-window motion artifact rejection for functional near-infrared spectroscopy. in Engineering in Medicine and Biology Society (EMBC), 2010 Annual International Conference of the IEEE. 2010. Buenos Aires: IEEE.

159. Miyai, I., et al., Cortical mapping of gait in humans: a near-infrared spectroscopic topography study. Neuroimage, 2001. 14(5): p. 1186-1192.

160. Suzuki, M., et al., Prefrontal and premotor cortices are involved in adapting walking and running speed on the treadmill: an optical imaging study. Neuroimage, 2004. 23(3): p. 1020-1026.

161. Batula, A.M., Y.E. Kim, and H. Ayaz, Virtual and Actual Humanoid Robot Control with Four-Class Motor-Imagery-Based Optical Brain-Computer Interface. 2017. 2017: p. 1-13.

162. Batula, A.M., et al., Comparison of Brain Activation during Motor Imagery and Motor Movement Using fNIRS. Computational Intelligence and Neuroscience,2017,(2017-5-4), 2017. 2017: p. 1-12.

163. Fisher, R.A., Frequency distribution of the values of the correlation coefficient in samples from an indefinitely large population. Biometrika, 1915. 10(4): p. 507-521.

164. Benjamini, Y. and Y. Hochberg, Controlling the false discovery rate: a practical and powerful approach to multiple testing. Journal of the Royal Statistical Society. Series B (Methodological), 1995. 57(1): p. 289-300.

165. Vogt, S., et al., Prefrontal involvement in imitation learning of hand actions: effects of practice and expertise. Neuroimage, 2007. 37(4): p. 1371-1383.

166. Zheng, D., et al., The key locus of common response inhibition network for no-go and stop signals. Cognitive Neuroscience, Journal of, 2008. 20(8): p. 1434-1442.

167. Lewis, P.A. and R.C. Miall, Distinct systems for automatic and cognitively controlled time measurement: evidence from neuroimaging. Current opinion in neurobiology, 2003. 13(2): p. 250-255.

168. Lewis, P.A. and R.C. Miall, Remembering the time: a continuous clock. Trends in cognitive sciences, 2006. 10(9): p. 401-406.

169. Bortoletto, M. and R. Cunnington, Motor timing and motor sequencing contribute differently to the preparation for voluntary movement. NeuroImage, 2010. 49(4): p. 3338-3348.

170. Sadato, N., et al., Role of the supplementary motor area and the right premotor cortex in the coordination of bimanual finger movements. The Journal of neuroscience, 1997. 17(24): p. 9667-9674.

171. Halsband, U., et al., The role of premotor cortex and the supplementary motor area in the temporal control of movement in man. Brain, 1993. 116(1): p. 243-266.

172. Papa, S., J. Artieda, and J.A. Obeso, Cortical activity preceding self‐initiated and externally triggered voluntary movement. Movement Disorders, 1991. 6(3): p. 217-224.

173. Jahanshahi, M., et al., Self-initiated versus externally triggered movements I. An investigation using measurement of regional cerebral blood flow with PET and movement-related potentials in normal and Parkinson's disease subjects. Brain, 1995. 118(4): p. 913-933.

174. Kuboyama, N., et al., The effect of maximal finger tapping on cerebral activation. Journal of physiological anthropology and applied human science, 2004. 23(4): p. 105-110.

175. Mostofsky, S.H., et al., Atypical motor and sensory cortex activation in attention-deficit/hyperactivity disorder: a functional magnetic resonance imaging study of simple sequential finger tapping. Biological psychiatry, 2006. 59(1): p. 48-56.

176. Gangadhar, G., R. Chavarriaga, and J. Millan. Anticipation based brain-computer interfacing (aBCI). in Neural Engineering, 2009. NER'09. 4th International IEEE/EMBS Conference on. 2009. IEEE.

177. Ibáñez, J., et al., An EEG-based design for the online detection of movement intention, in Advances in Computational Intelligence. 2011, Springer. p. 370-377.

178. Jäncke, L., et al., Cortical activations during paced finger-tapping applying visual and auditory pacing stimuli. Cognitive Brain Research, 2000. 10(1): p. 51-66.

179. Cramer, S.C., et al., Activation of distinct motor cortex regions during ipsilateral and contralateral finger movements. Journal of neurophysiology, 1999. 81(1): p. 383-387.

180. Allison, J., et al., Functional MRI cerebral activation and deactivation during finger movement. Neurology, 2000. 54(1): p. 135-135.

181. Porro, C.A., et al., Primary motor and sensory cortex activation during motor performance and motor imagery: a functional magnetic resonance imaging study. The Journal of neuroscience, 1996. 16(23): p. 7688-7698.

182. Batula, A.M., et al., Comparison of Brain Activation During Motor Imagery and Motor Movement Using fNIRS. Computational Intelligence and Neuroscience, 2017. 5491296.

183. Rangaprakash, D., X. Hu, and G. Deshpande, Phase Synchronization in Brain Networks Derived from Correlation between Probabilities of Recurrences in Functional MRI Data. International Journal of Neural Systems, 2013. 23(02): p. 1350003.

184. Jones, D.T., et al., Non-Stationarity in the "Resting Brain's" Modular Architecture. PLoS ONE, 2012. 7(6): p. e39731.

185. Cheng, L., et al., Modulation of functional connectivity and activation during preparation for hand movement. IIE Transactions on Occupational Ergonomics and Human Factors, 2016. 4(2-3): p. 175-187.

186. Picinbono, B., On instantaneous amplitude and phase of signals. IEEE Transactions on Signal Processing, 1997. 45(3): p. 552-560.

187. Sun, J. and M. Small, Unified framework for detecting phase synchronization in coupled time series. Physical Review E, 2009. 80(4): p. 046219.

188. Cui, X., S. Bray, and A.L. Reiss, Functional near infrared spectroscopy (NIRS) signal improvement based on negative correlation between oxygenated and deoxygenated hemoglobin dynamics. NeuroImage, 2010. 49(4): p. 3039-3046.

189. Mormann, F., et al., Mean phase coherence as a measure for phase synchronization and its application to the EEG of epilepsy patients. Physica D: Nonlinear Phenomena, 2000. 144(3–4): p. 358-369.

190. Sun, J., X. Hong, and S. Tong, Phase Synchronization Analysis of EEG Signals: An Evaluation Based on Surrogate Tests. IEEE Transactions on Biomedical Engineering, 2012. 59(8): p. 2254-2263.

191. Dum, R.P. and P.L. Strick, The origin of corticospinal projections from the premotor areas in the frontal lobe. The Journal of Neuroscience, 1991. 11(3): p. 667.

192. Picard, N. and P.L. Strick, Imaging the premotor areas. Current Opinion in Neurobiology, 2001. 11(6): p. 663-672.

193. Muir, R.B. and R.N. Lemon, Corticospinal neurons with a special role in precision grip. Brain Research, 1983. 261(2): p. 312-316.

194. Evarts, E.V., Role of Motor Cortex in Voluntary Movements in Primates, in Comprehensive Physiology. 2011, John Wiley & Sons, Inc.

195. Passingham, R., H. Perry, and F. Wilkinson, Failure to develop a precision grip in monkeys with unilateral neocortical lesions made in infancy. Brain Research, 1978. 145(2): p. 410-414.

196. Passingham, R.E., V.H. Perry, and F. Wilkinson, THE LONG-TERM EFFECTS OF REMOVAL OF SENSORIMOTOR CORTEX IN INFANT AND ADULT RHESUS MONKEYS. Brain, 1983. 106(3): p. 675.

197. Mitz, A.R., M. Godschalk, and S.P. Wise, Learning-dependent neuronal activity in the premotor cortex: activity during the acquisition of conditional motor associations. The Journal of neuroscience : the official journal of the Society for Neuroscience, 1991. 11(6): p. 1855-1872.

198. Chouinard, P.A., G. Leonard, and T. Paus, Role of the Primary Motor and Dorsal Premotor Cortices in the Anticipation of Forces during Object Lifting. The Journal of Neuroscience, 2005. 25(9): p. 2277.

199. Kuhtz-Buschbeck, J.P., H.H. Ehrsson, and H. Forssberg, Human brain activity in the control of fine static precision grip forces: an fMRI study. European Journal of Neuroscience, 2001. 14(2): p. 382-390.

200. Münchau, A., et al., Functional Connectivity of Human Premotor and Motor Cortex Explored with Repetitive Transcranial Magnetic Stimulation. The Journal of Neuroscience, 2002. 22(2): p. 554.

201. Chouinard, P.A., et al., Modulating Neural Networks With Transcranial Magnetic Stimulation Applied Over the Dorsal Premotor and Primary Motor Cortices. Journal of Neurophysiology, 2003. 90(2): p. 1071.

202. Ghez, C., W. Hening, and J. Gordon, Organization of voluntary movement. Current opinion in neurobiology, 1991. 1(4): p. 664-671.

203. Leonardi, N. and D. Van De Ville, On spurious and real fluctuations of dynamic functional connectivity during rest. NeuroImage, 2015. 104: p. 430-436.

204. Omidvarnia, A., et al., Dynamic regional phase synchrony (DRePS). Human Brain Mapping, 2016. 37(5): p. 1970-1985.

205. Hasson, U., H.C. Nusbaum, and S.L. Small, Task-dependent organization of brain regions active during rest. Proceedings of the National Academy of Sciences, 2009. 106(26): p. 10841-10846.

206. Harrison, B.J., et al., Consistency and functional specialization in the default mode brain network. Proceedings of the National Academy of Sciences, 2008. 105(28): p. 9781-9786.

207. Gao, W. and W. Lin, Frontal parietal control network regulates the anti‐correlated default and dorsal attention networks. Human brain mapping, 2012. 33(1): p. 192-202.

208. Fornito, A., et al., Competitive and cooperative dynamics of large-scale brain functional networks supporting recollection. Proceedings of the National Academy of Sciences, 2012. 109(31): p. 12788-12793.

209. Rao, H., et al., A regulation role of the prefrontal cortex in the fist-edge-palm task: Evidence from functional connectivity analysis. NeuroImage, 2008. 41(4): p. 1345-1351.

210. Koenig, T., et al., Millisecond by millisecond, year by year: normative EEG microstates and developmental stages. Neuroimage, 2002. 16(1): p. 41-48.

211. Lehmann, D., H. Ozaki, and I. Pal, EEG alpha map series: brain micro-states by space-oriented adaptive segmentation. Electroencephalography and clinical neurophysiology, 1987. 67(3): p. 271-288.

212. Van de Ville, D., J. Britz, and C.M. Michel, EEG microstate sequences in healthy humans at rest reveal scale-free dynamics. Proceedings of the National Academy of Sciences, 2010. 107(42): p. 18179-18184.

213. Ahmadlou, M. and H. Adeli, Functional community analysis of brain: A new approach for EEG-based investigation of the brain pathology. Neuroimage, 2011. 58(2): p. 401-408.

214. Michalopoulos, K., et al., Classification of EEG Single Trial Microstates Using Local Global Graphs and Discrete Hidden Markov Models. International Journal of Neural Systems, 2016. 26(06): p. 1650036.

215. Michalopoulos, K. and N. Bourbakis, Combining EEG Microstates with fMRI Structural Features for Modeling Brain Activity. International Journal of Neural Systems, 2015. 25(08): p. 1550041.

216. Warren Boling, et al., Localization of hand motor activation in Broca's pli de passage moyen. Journal of Neurosurgery, 1999. 91(6): p. 903-910.

217. Pelphrey, K.A., et al., Functional Anatomy of Biological Motion Perception in Posterior Temporal Cortex: An fMRI Study of Eye, Mouth and Hand Movements. Cerebral Cortex, 2005. 15(12): p. 1866-1876.

218. Boroojerdi, B., et al., Localization of the motor hand area using transcranial magnetic stimulation and functional magnetic resonance imaging. Clinical Neurophysiology, 1999. 110(4): p. 699-704.

219. Yupeng, R., P. Hyung-Soon, and Z. Li-Qun. Developing a whole-arm exoskeleton robot with hand opening and closing mechanism for upper limb stroke rehabilitation. in Rehabilitation Robotics, 2009. ICORR 2009. IEEE International Conference on. 2009.

220. Ho, N.S.K., et al. An EMG-driven exoskeleton hand robotic training device on chronic stroke subjects: Task training system for stroke rehabilitation. in Rehabilitation Robotics (ICORR), 2011 IEEE International Conference on. 2011.

221. Ramos-Murguialday, A., et al., Brain–machine interface in chronic stroke rehabilitation: A controlled study. Annals of Neurology, 2013. 74(1): p. 100-108.

222. Gusnard, D.A. and M.E. Raichle, Searching for a baseline: functional imaging and the resting human brain. Nature Reviews Neuroscience, 2001. 2(10): p. 685-694.

223. Broyd, S.J., et al., Default-mode brain dysfunction in mental disorders: a systematic review. Neuroscience & biobehavioral reviews, 2009. 33(3): p. 279-296.

224. Yamanishi, T., J.-Q. Liu, and H. Nishimura, Modeling Fluctuations in Default-Mode Brain Network Using a Spiking Neural Network. International Journal of Neural Systems, 2012. 22(04): p. 1250016.

225. Yan, C.-G. and Y.-F. Zang, DPARSF: a MATLAB toolbox for “pipeline” data analysis of resting-state fMRI. Frontiers in Systems Neuroscience, 2010. 4: p. 13.

226. Ashburner, J., A fast diffeomorphic image registration algorithm. NeuroImage, 2007. 38(1): p. 95-113.

227. Friston, K.J., et al., Movement ‐ related effects in fMRI time ‐ series. Magnetic Resonance in Medicine, 1996. 35(3): p. 346-355.

228. Power, J.D., et al., Functional network organization of the human brain. Neuron, 2011. 72(4): p. 665-678.

229. Shirer, W.R., et al., Decoding Subject-Driven Cognitive States with Whole-Brain Connectivity Patterns. Cerebral Cortex, 2011. 22(1): p. 158-165.

230. Lloyd, S.P., Least squares quantization in PCM. Information Theory, IEEE Transactions on, 1982. 28(2): p. 129-137.

231. Aggarwal, C.C., A. Hinneburg, and D.A. Keim, On the surprising behavior of distance metrics in high dimensional space. 2001: Springer.

232. McCullagh, P., Generalized linear models. European Journal of Operational Research, 1984. 16(3): p. 285-292.

233. O'hara, R.B. and D.J. Kotze, Do not log ‐ transform count data. Methods in Ecology and Evolution, 2010. 1(2): p. 118-122.

234. Greene, W., Functional forms for the negative binomial model for count data. Economics Letters, 2008. 99(3): p. 585-590.

235. Chin, H.C. and M.A. Quddus, Applying the random effect negative binomial model to examine traffic accident occurrence at signalized intersections. Accident Analysis & Prevention, 2003. 35(2): p. 253-259.

236. Gardner, W., E.P. Mulvey, and E.C. Shaw, Regression analyses of counts and rates: Poisson, overdispersed Poisson, and negative binomial models. Psychological bulletin, 1995. 118(3): p. 392.

237. Fair, D.A., et al., A method for using blocked and event-related fMRI data to study "resting state" functional connectivity. Neuroimage, 2007. 35(1): p. 396-405.

238. Fox, M.D., et al., Intrinsic fluctuations within cortical systems account for intertrial variability in human behavior. Neuron, 2007. 56(1): p. 171-184.

239. Cole, M.W., et al., Intrinsic and task-evoked network architectures of the human brain. Neuron, 2014. 83(1): p. 238-251.

240. Hermundstad, A.M., et al., Structural foundations of resting-state and task-based functional connectivity in the human brain. Proceedings of the National Academy of Sciences, 2013. 110(15): p. 6169-6174.

241. Delamillieure, P., et al., The resting state questionnaire: an introspective questionnaire for evaluation of inner experience during the conscious resting state. Brain research bulletin, 2010. 81(6): p. 565-573.

242. de Pasquale, F., et al., A cortical core for dynamic integration of functional networks in the resting human brain. Neuron, 2012. 74(4): p. 753-764.

243. Gu, S., et al., Controllability of structural brain networks. Nature Communications, 2015. 6.

244. Keilholz, S.D., The neural basis of time-varying resting-state functional connectivity. Brain connectivity, 2014. 4(10): p. 769-779.

245. Christoff, K., et al., Experience sampling during fMRI reveals default network and executive system contributions to mind wandering. Proceedings of the National Academy of Sciences, 2009. 106(21): p. 8719-8724.

246. Tangwiriyasakul, C., et al., Temporal evolution of event-related desynchronization in acute stroke: A pilot study. Clin. Neurophysiol., 2014. 126(6): p. 1112-1120.

247. Grefkes, C. and G.R. Fink, Reorganization of cerebral networks after stroke: New insights from neuroimaging with connectivity approaches. Brain, 2011. 134(5): p. 1264-1276.

248. Grefkes, C., et al., Cortical connectivity after subcortical stroke assessed with functional magnetic resonance imaging. Ann Neurol, 2008. 63(2): p. 236-46.

249. Loubinoux, I., et al., Correlation between cerebral reorganization and motor recovery after subcortical infarcts. NeuroImage, 2003. 20(4): p. 2166-2180.

250. Loubinoux, I., et al., Prognostic value of FMRI in recovery of hand function in subcortical stroke patients. Cereb Cortex, 2007. 17(12): p. 2980-2987.

251. Park, C.H., et al., Longitudinal changes of resting-state functional connectivity during motor recovery after stroke. Stroke, 2011. 42(5): p. 1357-62.

252. Rehme, A.K., S.B. Eickhoff, and C. Grefkes, State-dependent differences between functional and effective connectivity of the human cortical motor system. NeuroImage, 2013. 67(0): p. 237-246.

253. Xiangfei, H., S. Junfeng, and T. Shanbao, Functional Brain Networks for Sensory Maintenance in Top-Down Selective Attention to Audiovisual Inputs. IEEE Trans Neural Syst Rehabil Eng, 2013. 21(5): p. 734-743.

254. De Vico Fallani, F., et al., Brain Network Analysis From High-Resolution EEG Recordings by the Application of Theoretical Graph Indexes. IEEE Trans Neural Syst Rehabil Eng, 2008. 16(5): p. 442-452.

255. Jin, S.-H., P. Lin, and M. Hallett, Reorganization of brain functional small-world networks during finger movements. Hum Brain Mapp, 2012. 33(4): p. 861-872.

256. Sporns, O., Contributions and challenges for network models in cognitive neuroscience. Nat. Neurosci., 2014.

257. Twitchell, T.E., The restoration of motor function following hemiplegia in man. Brain, 1951. 74(4): p. 443-480.

258. Tang, A., et al., Do functional walk tests reflect cardiorespiratory fitness in sub-acute stroke? J NeuroEng Rehabil, 2006. 3(1): p. 23.

259. He, B.J., Spontaneous and task-evoked brain activity negatively interact. J. Neurosci., 2013. 33(11): p. 4672-4682.

260. Gavrilescu, M., et al., Functional connectivity estimation in fMRI data: influence of preprocessing and time course selection. Hum. Brain Mapp., 2008. 29(9): p. 1040-1052.

261. Cao, C. and S. Slobounov, Alteration of Cortical Functional Connectivity as a Result of Traumatic Brain Injury Revealed by Graph Theory, ICA, and sLORETA Analyses of EEG Signals. IEEE Trans Neural Syst Rehabil Eng, 2010. 18(1): p. 11-19.

262. Golestani, A.-M., et al., Longitudinal evaluation of resting-state FMRI after acute stroke with hemiparesis. Neurorehab Neural Re, 2013. 27(2): p. 153-163.

263. Bassett, D.S., et al., Adaptive reconfiguration of fractal small-world human brain functional networks. Proc Natl Acad Sci U S A 2006. 103(51): p. 19518-19523.

264. Wang, Y.M. and X. Jing, Unified Framework for Robust Estimation of Brain Networks From fMRI Using Temporal and Spatial Correlation Analyses. IEEE Trans. Med. Imaging, 2009. 28(8): p. 1296-1307.

265. Barrat, A., et al., The architecture of complex weighted networks. Proc Natl Acad Sci U S A, 2004. 101(11): p. 3747-3752.

266. Boccaletti, S., et al., Complex networks: Structure and dynamics. Phys Rep, 2006. 424(4–5): p. 175-308.

267. Freeman, L.C., A Set of Measures of Centrality Based on Betweenness. Sociometry, 1977. 40(1): p. 35-41.

268. Maslov, S. and K. Sneppen, Specificity and stability in topology of protein networks. Science, 2002. 296(5569): p. 910-913.

269. Gibbons, R.D., D. Hedeker, and S. DuToit, Advances in analysis of longitudinal data. Annu Rev Clin Psychol, 2010. 6: p. 79-107.

270. He, Y., Z. Chen, and A. Evans, Structural insights into aberrant topological patterns of large-scale cortical networks in Alzheimer's disease. J Neurosci, 2008. 28(18): p. 4756-4766.

271. Fallani, F.D.V., et al., Cortical functional connectivity networks in normal and spinal cord injured patients: evaluation by graph analysis. Hum Brain Mapp, 2007. 28(12): p. 1334-1346.

272. Bartolomei, F., et al., How do brain tumors alter functional connectivity? A magnetoencephalography study. Ann Neurol, 2006. 59(1): p. 128-138.

273. Ovadia-Caro, S., et al., Longitudinal effects of lesions on functional networks after stroke. J Cereb Blood Flow Metab, 2013. 33(8): p. 1279-1285.

274. Bostan, A.C., R.P. Dum, and P.L. Strick, Cerebellar networks with the cerebral cortex and basal ganglia. Trends Cogn Sci 2013. 17(5): p. 241-254.

275. Schmahmann, J.D., From movement to thought: anatomic substrates of the cerebellar contribution to cognitive processing. Hum Brain Mapp, 1996. 4(3): p. 174-198.

276. Akkal, D., R.P. Dum, and P.L. Strick, Supplementary motor area and presupplementary motor area: targets of basal ganglia and cerebellar output. J Neurosci, 2007. 27(40): p. 10659-10673.

277. van Meer, M.P., et al., Correspondence between altered functional and structural connectivity in the contralesional sensorimotor cortex after unilateral stroke in rats: a combined resting-state functional MRI and manganese-enhanced MRI study. J Cereb Blood Flow Metab, 2010. 30(10): p. 1707-1711.

278. van Meer, M.P., et al., Extent of bilateral neuronal network reorganization and functional recovery in relation to stroke severity. J Neurosci, 2012. 32(13): p. 4495-4507.

279. Rehme, A.K., et al., The role of the contralesional motor cortex for motor recovery in the early days after stroke assessed with longitudinal FMRI. Cereb cortex, 2011. 21(4): p. 756-768.

280. Weiller, C., et al., Functional reorganization of the brain in recovery from striatocapsular infarction in man. Ann Neurol, 1992. 31(5): p. 463-72.

281. Carter, A.R., et al., Resting interhemispheric functional magnetic resonance imaging connectivity predicts performance after stroke. Annals of neurology, 2010. 67(3): p. 365-375.

282. Murase, N., et al., Influence of interhemispheric interactions on motor function in chronic stroke. Annals of neurology, 2004. 55(3): p. 400-409.

283. Hummel, F.C. and L.G. Cohen, Non-invasive brain stimulation: a new strategy to improve neurorehabilitation after stroke? Lancet Neurol, 2006. 5(8): p. 708-712.

284. Fox, M.D., et al., Measuring and manipulating brain connectivity with resting state functional connectivity magnetic resonance imaging (fcMRI) and transcranial magnetic stimulation (TMS). Neuroimage, 2012. 62(4): p. 2232-2243.

285. Gu, S., et al., Controllability of structural brain networks. Nature communications, 2015. 6.

286. Werring, D.J., et al., Diffusion tensor imaging can detect and quantify corticospinal tract degeneration after stroke. Journal of Neurology, Neurosurgery & Psychiatry, 2000. 69(2): p. 269-272.

287. Urbanski, M., et al., DTI-MR tractography of white matter damage in stroke patients with neglect. Experimental brain research, 2011. 208(4): p. 491-505.

288. Park, H.-J. and K. Friston, Structural and functional brain networks: from connections to cognition. Science, 2013. 342(6158): p. 1238411.

Vita

Name: Lin Cheng

Education:

Shanghai Jiao Tong University, Shanghai, China, Sept 2010 – Sept 2017 (PhD)

Drexel University, Philadelphia, PA, United States, Sept 2012 – Dec 2017 (PhD)

Huazhong University of Science and Technology, Wuhan, China, Sept 2006 - Jun 2010 (B.Eng.)

Publications:

Cheng L, et al. "Reorganization of Motor Execution Networks During Sub-Acute Phase After Stroke"(2015),*Neural Systems and Rehabilitation Engineering, IEEE Transactions on*, vol.23, no.4, pp.713-723

Cheng L, et al. “Modulation of Functional Connectivity and Activation during Preparation for Hand Movement” (2016), IIE Transactions on Occupational Ergonomics and Human Factors. doi:10.1080/21577323.2016.1191560

Cheng L, et al. "Principal states of dynamic functional connectivity reveal the link between resting-state and task-state brain." (2017), International Journal of Neural Systems (**Accepted**).

Zhu Y, **Cheng L**, He N, et al. Comparison of Functional Connectivity Estimated from Concatenated Task-State Data from Block-Design Paradigm with That of Continuous Task[J]. Computational and Mathematical Methods in Medicine, 2017, 2017 (**Co-first author**)

Wu Z, **Cheng L**, et al. Functional Activation-Informed Structural Changes during Stroke Recovery: A Longitudinal MRI Study[J]. BioMed Research International,2017,(2017-10-24), 2017, 2017(2):1-13. (**Co-first author**)

Cheng L, et al. "Reorganization of functional brain networks during the recovery of stroke: a functional MRI study." *Engineering in Medicine and Biology Society (EMBC), 2012 Annual International Conference of the IEEE*

Cheng L, et al. “Decreased Variability of Dynamic Phase Synchronization in Brain Networks during Hand Movement.” *Engineering in Medicine and Biology Society (EMBC), 2017 Annual International Conference of the IEEE*